2017

# Mathematical and Physical Modelling of a Floating Clam-type Wave Energy Converter

Phillips, John Wilfrid

RESEARCH DEGREES WITH PLYMOUTH UNIVERSITY

# MATHEMATICAL AND PHYSICAL MODELLING OF A FLOATING CLAM-TYPE WAVE ENERGY CONVERTER

by

**JOHN WILFRID PHILLIPS**

A thesis submitted to the University of Plymouth
in partial fulfilment of the requirements for the degree of

**DOCTOR OF PHILOSOPHY**

School of Marine Science and Engineering

University of Plymouth

**September 2016**

# Abstract

**Mathematical and Physical Modelling of a Floating Clam-type Wave Energy Converter**

**John Wilfrid Phillips**

The original aim of the research project was to investigate the mechanism of power capture from sea waves and to optimise the performance of a vee-shaped floating Wave Energy Converter, the Floating Clam, patented by Francis Farley. His patent was based on the use of a pressurised bag (or 'reservoir') to hold the hinged Clam sides apart, so that, as they moved under the action of sea waves, air would be pumped into and out of a further air reservoir via a turbine/generator set, in order to extract power from the system. Such "Clam Action" would result in the lengthening of the resonant period in heave. The flexibility of the air bag supporting the Clam sides was an important design parameter. This was expected to lead to a reduction in the mass (and hence cost) of the Clam as compared with a rigid body. However, the present research has led to the conclusion that the Clam is most effective when constrained in heave and an alternative power take-off is proposed.

The theoretical investigations made use of WAMIT, an industry-standard software tool that provides an analysis based on potential flow theory where fluid viscosity is ignored. The WAMIT option of Generalised Modes has been used to model the Clam action. The hydrodynamic coefficients, calculated by WAMIT, have been curve-fitted so that the correct values are available for any chosen wave period. Two bespoke mathematical models have been developed in this work: a frequency domain model, that uses the hydrodynamic coefficients calculated by WAMIT, and a time domain model, linked to the frequency domain model in such a way as to automatically use the same hydrodynamic and hydrostatic data. In addition to modelling regular waves, the time domain model contains an approximate, but most effective method to simulate the behaviour of the Clam in irregular waves, which could be of use in future control system studies.

A comprehensive series of wave tank trials has been completed, and vital to their success has been the modification of the wave tank model to achieve very low values of power take-off stiffness through the use of constant force springs, with negligible mechanical friction in the hinge mechanism. Furthermore, the wave tank model has demonstrated its robustness and thus its suitability for use in further test programmes.

The thesis concludes with design suggestions for a full-scale device that employs a pulley/counterbalance arrangement to provide a direct connection to turbine/generator sets, giving an efficient drive with low stiffness and inherently very low friction losses. At the current stage of research, the mean annual power capture is estimated as 157.5 kW, wave to wire in a far from energetic 18 kw/m mean annual wave climate, but with scope for improvement, including through control system development.

# Acknowledgements

Grateful thanks are due to my supervisors, Professors Deborah Greaves and Alison Raby, for their continued help and encouragement throughout the six year long course of study.

I would like to acknowledge the assistance and advice received from all those whom I have met along the way, but particularly from Professor Francis Farley who influenced the starting point of my investigations, and also Dr Ming Dai, Dr Martyn Hann and Dr Adi Kurniawan who helped with theoretical aspects. A particular debt of gratitude is due to Peter Arber who enabled the Clam model to be successfully manufactured and tested.

Finally, I owe a debt of gratitude to my wife, Marylyn, and all my family for their interest and encouragement.

John W Phillips

September 2016

# Author's Declaration

At no time during the registration for the degree of Doctor of Philosophy has the author been registered for any other University award.

Work submitted for this research degree has not formed part of any other degree either at the University of Plymouth or at any other establishment.

This study was self-financed with assistance from the University of Plymouth in the form of wave tank model construction and testing.

Relevant scientific seminars and conferences were attended at which work was presented.

**Signed:** _____

**Date:** _____

## Conference proceedings and poster presentations:

**Phillips J W**, Greaves D M and Raby A C (2015) The Free Floating Clam – Performance and Potential. In: *11th European Wave and Tidal Energy Conference*, 6-11 September 2015, Nantes, France.

**Phillips J W** (2014), Free Floating Clam Wave Energy Converter, Poster Presentation. In: *1st PRIMaRE annual conference, 4-5th June 2014,* Plymouth, UK

**Word count in the main body of this thesis:** 31,400

# Contents

# List of Tables

# List of Figures

# Abbreviations

| | |
|---|---|
| **AMETS** | Atlantic Marine Energy Test Site |
| **AQWA** | A computing environment for hydrodynamic analysis |
| **AWS** | Archimedes Wave Swing |
| **CAD** | Computer Aided Design |
| **CG** | Centre of Gravity |
| **CL** | Centreline |
| **CT** | Carbon Trust |
| **DanWEC** | Danish Wave Energy Centre |
| **DFIG** | Doubly-Fed Induction Generator |
| **DoE** | Department of Energy |
| **ETSU** | Energy Technology Support Unit |
| **FORTRAN** | A general-purpose programming language, from "Formula Translation" |
| **HF** | High Frequency |
| **HMRC** | Hydraulic & Maritime Research Centre |
| **IRF** | Impulse Response Function |
| **JONSWAP** | Joint North Sea Wave Project |
| **MASK** | Manoeuvering and Seakeeping Basin, Maryland |
| **MATLAB** | A computing environment, formerly "matrix laboratory" |
| **MCT** | Marine Current Turbines |
| **MEA** | Marine Energy Accelerator |
| **MEC** | Marine Energy Challenge |
| **MILDwave** | An in-house numerical model from Ghent University |
| **MIT** | Massachusetts Institute of Technology |

| | |
|---|---|
| **MS EXCEL** | Microsoft Excel – a spread sheet programme |
| **NCEP** | National Centers for Environmental Prediction |
| **NDBC** | National Data Buoy Center |
| **NEL** | National Engineering Laboratory |
| **NOAA** | National Oceanic and Atmospheric Administration |
| **OWC** | Oscillating Water Column |
| **OWSC** | Oscillating Wave Surge Converter |
| **p/kWh** | Pence per kilowatt hour |
| **PC** | Personal Computer |
| **PTC** | A software company, formerly Parametric Technology Corporation |
| **PTO** | Power Take-Off (PTO) |
| **RAO** | Response Amplitude Operator |
| **RD&D** | Research, Development and Demonstration |
| **RHM** | Reactive Hydraulic Modulator |
| **SEA Ltd** | Systems Engineering and Assessment Ltd |
| **SHM** | Simple Harmonic Motion |
| **SPERBOY** | Sea Power Energy Recovery Buoy |
| **UK** | United Kingdom |
| **WAM** | Wave Analysis Model |
| **WAMDI** | Wave Model Development and Implementation |
| **WAMIT** | Wave Analysis MIT |
| **WEC** | Wave Energy Converter |
| **WES** | Wave Energy Scotland |
| **WW3** | WAVEWATCH III |

# Nomenclature

| | |
|---|---|
| $a$ | Wave amplitude |
| $A$ | Area |
| $A$ | Amplitude |
| $A$ | Parameter equal to $H_s^2/4\pi T_z^4$ |
| $A_{33}$ | Heave Added Mass |
| $A_{37}$ | Cross coupled (3,7) Added Mass |
| $A_{73}$ | Cross coupled (7,3) Added Mass |
| $A_{77}$ | Clam mode Added Mass |
| $A_{ij}$ | Element in the hydrodynamic added mass matrix, $A$ |
| $B$ | Parameter equal to $1/\pi T_z^4$ |
| $b$ | Damping |
| $B_{33}$ | Heave hydrodynamic damping |
| $b_{33}$ | Heave hydrodynamic damping, $B_{33}$, + externally applied heave damping, $B_{33}^E$ |
| $B_{33}^E$ | Externally applied heave damping |
| $B_{37}$ | Cross coupled (3,7) hydrodynamic damping |
| $b_{37}$ | Cross coupled (3,7) hydrodynamic damping ($= B_{37}$) |
| $B_{73}$ | Cross coupled (7,3) hydrodynamic damping |
| $b_{73}$ | Cross coupled (7,3) hydrodynamic damping ($= B_{73}$) |
| $B_{77}$ | Clam mode hydrodynamic damping |
| $b_{77}$ | PTO mode hydrodynamic damping, $B_{77}$, + externally applied PTO (=Clam mode) mode, $B_{77}^E$ |
| $B_{77}^E$ | PTO (= Clam mode) damping |
| $B_{ij}$ | Element in the hydrodynamic damping matrix, $B$ |
| $B_{ij}^E$ | Element in the external damping matrix, $B^E$ |
| $C$ | Damping |
| $c$ | Damping |
| $\mathrm{C}(s)$ | Normalising factor |
| $C_{33}$ | Heave hydrostatic coefficient |
| $c_{33}$ | Hydrostatic stiffness, $C_{33}$ + externally applied heave stiffness, $C_{33}^E$ |
| $C_{33}^E$ | Externally applied heave stiffness |

| | |
|---|---|
| $C_{37}$ | Cross coupled (3,7) hydrostatic coefficient |
| $c_{37}$ | Cross coupled (3,7) hydrostatic coefficient, $C_{37}$ |
| $C_{73}$ | Cross coupled (7,3) hydrostatic coefficient |
| $c_{73}$ | Cross coupled (7,3) hydrostatic coefficient, $C_{73}$ |
| $C_{77}$ | Clam mode hydrostatic coefficient |
| $c_{77}$ | Clam hydrostatic stiffness $C_{77}$ + externally applied Clam mode stiffness (= PTO stiffness), $C_{77}^{E}$ |
| $C_{77}^{E}$ | Clam mode stiffness (= PTO stiffness) |
| $C_D$ | Drag coefficient |
| $C_{ij}$ | Hydrostatic Coefficient - Element in the hydrostatic stiffness matrix, $C$ |
| $C_{ij}^{E}$ | Element in the external stiffness matrix, $C^E$ |
| $D$ | Duration of record |
| $D(f,\theta)$ | Angular spreading function |
| $f$ | Wave frequency |
| $f(t)$ | Excitation Impulse Response Function (IRF) |
| $F$ | PTO Force |
| $F_{CD}$ | Coulomb damping force |
| $F_{CF}$ | Coulomb friction force |
| $f_n$ | Wave frequency for index $n$ |
| $F_b$ | Buoyancy force |
| $F_S$ | Spring force |
| $F_D$ | Component of PTO force due to damping |
| $F_e(t)$ | Excitation force |
| $F_w$ | Wave force |
| $g$ | Acceleration due to gravity |
| G | Acceleration due to gravity |
| $h$ | Height of Clam side |
| $H_{1/3}$ | Significant wave height |
| $H_s$ | Significant wave height |
| $i$ | Imaginary number (= $\sqrt{-1}$) – used in complex number notation |
| $j$ | Imaginary number (= $\sqrt{-1}$) – used in complex number notation |

| | |
|---|---|
| $ImX_3$ | Imaginary part of complex heave excitation force |
| $Im\{F_e(\omega)\}$ | Imaginary part of the Excitation Force in the frequency domain. |
| $k$ | Stiffness |
| $k'$ | Stiffness |
| $k(t)$ | Radiation Impulse Response Function (IRF) |
| L | Length of Clam side |
| M | Mass |
| $m$ | Mass of the buoy |
| $m_a$ | Hydrodynamic added mass |
| $m_m$ | Mass of body |
| $m(\omega)$ | Hydrodynamic added mass |
| $m(\infty)$ | Body added mass as wave frequency tends to infinity (i.e. at zero wave period) |
| $M_{33}$ | Device mass |
| $m_{33}$ | Body mass, $M_{33}$+ heave Added Mass, $A_{33}$ |
| $m_{37}$ | Cross coupled (3,7) Added Mass ($= A_{37}$) |
| $m_{73}$ | Cross coupled (7,3) Added Mass ($= A_{73}$) |
| $m_{77}$ | Hydrodynamic added mass for PTO mode ($= A_{77}$) |
| $M_{ij}$ | Element in the mass and inertia matrix, $M$ |
| $M_{ij}^E$ | Element in the external mass and inertia matrix, $M^E$ |
| $M_n$ | n$^{th}$ spectral moment |
| $Mod_{33}$ | Modulus of Haskinds Exciting Force in Heave |
| $Mod_{77}$ | Modulus of Haskinds Exciting Force for Clam Mode |
| $n$ | Integer index |
| $n$ | Number of sample values taken of $y_i$ – an integer |
| $n_z$ | Number of times the water surface moves through its mean level in the upward direction |
| $N$ | Maximum number of steps |
| $P_{wave}$ | Power per unit width of wave crest |
| $P_m$ | Mean power absorbed by the PTO |
| $P$ | Power Capture, |
| $P_w$ | Power absorbed from the waves |

| | |
|---|---|
| $\mathrm{Period_j}$ | Wave period in seconds |
| $PSD$ | Power spectral density |
| $RAO$ | Response Amplitude Operator |
| $RAO_3$ | Heave RAO |
| $RAO_7$ | PTO RAO |
| $ReX_3$ | Real part of complex heave excitation force |
| $Re\{F_e(\omega)\}$ | Real part of the Excitation Force in the frequency domain |
| $R_q$ | Quadratic damping coefficient |
| $R(\omega)$ | Radiation damping |
| s | Spreading value |
| $S$ | Externally applied stiffness |
| $S_b$ | Hydrostatic stiffness |
| $s(t)$ | Body vertical position |
| $S(f)$ | One-dimensional wave spectrum (or 'power spectral density function') |
| $S(f,\theta)$ | Directional wave spectrum |
| $S(f_n)$ | Wave input spectrum at the wave frequency $f_n$ |
| $\mathrm{S_j}$ | Spectrum used in the frequency domain analysis |
| T | Resonant Period |
| T | Sampling interval |
| $t$ | Time |
| $T$ | Wave Period |
| $T_{1/3}$ | Significant Period |
| $T_0$ | Undamped resonant period $(= \frac{2\pi}{\omega_0})$ |
| $T_e$ | Energy Period |
| $T_n$ | Wave period for index $n$ |
| $T_z$ | Zero Crossing Period |
| $U$ | Wind speed at 19.6 m above sea level ($ms^{-1}$) |
| $U$ | Velocity |
| $u(t)$ | Body vertical velocity |
| $\dot{u}(t)$ | Body vertical acceleration |

| | |
|---|---|
| VELH | Displacement normal to the surface (+ve into the body) |
| w | Wave position |
| $W$ | Width of the WEC/buoy |
| $W_c$ | Capture Width |
| $x$ | Buoy displacement |
| $x$ | Length of spring |
| $x, y$ and $z$ | Cartesian coordinates. |
| $x_1$ , $x_2$ | Successive peaks in logarithmic decay record |
| $X_3$ | Wave excitation force in heave (mode 3) |
| $X_7$ | Wave excitation force in clam mode (mode 7) |
| $X_i$ | Exciting force in the i$^{th}$ mode |
| Y | Water level |
| $y_i$ | Water level at instant, $i$ , relative to the mean water level |
| $Z$ | Vertical distance from the Clam pivot to the line of action of the PTO ram, |
| $Z_{33}$ | Complex stiffness, heave mode |
| $Z_{37}$ | Complex stiffness, cross-coupled mode (3,7) |
| $Z_{73}$ | Complex stiffness, cross-coupled mode (7,3) |
| $Z_{77}$ | Complex stiffness, clam mode |
| $z, \dot{z}, \ddot{z}$ | Vertical displacement, velocity and acceleration of buoy |
| ZDISP | Vertical (Z-direction) displacement |
| $\Gamma$ | Gamma function |
| $\delta$ | Intermediate parameter in calculation of $\zeta$ |
| $\delta$ | Logarithmic decrement |
| $\dot{\delta}_3$ | Heave velocity |
| $\ddot{\delta}_3$ | Heave acceleration |
| $\dot{\delta}_7$ | PTO velocity |
| $\ddot{\delta}_7$ . | PTO acceleration |
| $\delta_3$ | Heave position |
| $\delta_7$ | PTO position |
| $\Delta f$ | Small frequency interval at frequency $f$ |

| | |
|---|---|
| $\Delta f_n$ | Step size in wave frequency, equivalent to step size $T_n$ in Wave period |
| $\Delta P_n$ | Incremental contribution to power capture over frequency step, $\Delta f_n$ |
| $\Delta T$ | Step size in time |
| $\zeta$ | Damping ratio |
| $\eta(t)$ | Wave Position (in relation to mean) |
| $\theta$ | Angular difference between the wave direction and the mean wind direction |
| $\theta$ | Clam semi-angle |
| $\xi_7$ | Complex PTO amplitude |
| $\xi_j$ | Displacement in the j$^{th}$ degree of freedom (or mode) caused by the force $X_i$ |
| $\pi$ | Ratio of a circle's circumference to its diameter |
| $\rho$ | Density of water |
| $\sigma$ | Root mean square value of the water level relative to the mean water level |
| $\sigma^2$ | Mean square value |
| $\sigma_{33}$ | Argument of Haskinds Exciting Force in Heave |
| $\sigma_{33}$ | Phase lag in mode 3 (heave) |
| $\sigma_{77}$ | Argument of Haskinds Exciting Force for Clam Mode |
| $\sigma_{77}$ | Phase lag in mode 7 (clam mode) |
| $\tau$ | Time before current time |
| $\varphi$ | Velocity Potential |
| $\omega$ | Wave radian frequency ($= \frac{2\pi}{Wave\ Period}$) |
| $\omega_0$ | Undamped resonant frequency |
| $\lvert\xi_3\rvert$ | Modulus of the heave amplitude |
| $\lvert\xi_7\rvert$ | Modulus of the PTO (mode 7) amplitude |

# 1 Overview

## 1.1 Introduction

Marine energy, and particularly wave energy has the potential to provide a substantial proportion of the UK and global energy requirement. For example in 1982 the realisable UK potential for wave energy was estimated to be 20% of UK electrical energy demand, some 5 GW of a total mean UK requirement of 25 GW (Shaw, 1982). Tidal stream turbine installations were estimated to be capable of providing 1.8 GW, while the Severn Barrage scheme could provide a further 2 GW, some 5% of UK demand.

In the few years prior to 1982 UK research into wave energy had received the largest share of renewables funding. In 1978 Research, Development and Demonstration (RD&D) programmes in wave energy received £5.4 M which was increased to £13.1 M by June 1981. In 1981 contracts were awarded to Edinburgh University for work on the spine structure for the 'Salter Duck' and wave tank development, to Vickers for oscillating water column development, to Sea Energy Associates for spine and mooring systems and to Sir Robert McAlpine for the Bristol Cylinder development. Unfortunately in 1982 the government decided to abandon support for wave power in favour of conventional sources. Final curtailment followed publication of "Wave Energy, ETSU R26" in March 1985 (DoE UK, 1985). Acrimony surrounded the decision and it was believed that the conclusions were based on invalid assumptions (Wilson, 2010). Although large scale funding was curtailed the ETSU report (DoE UK, 1985) suggested funding for research should continue and in particular small scale versions of both the CLAM device of SEA Ltd and the NEL Breakwater device were supported by the Department of Energy. The Edinburgh DUCK received special attention in the report since it was far and away the most efficient device tested. The methodology for assessing the various devices involved scoring the various attributes of each device in order to arrive at an overall score. On account of its complexity the DUCK scored so low in regards to its estimated availability that the engineering problems *"prevented the Consultants from carrying out their assessment"*. It is interesting to make the comparison with the Pelamis wave energy converter (WEC), also complicated and also from the Edinburgh stable. However, as will be seen from the work on the Floating

Clam reported here, a degree of complexity is required in order to achieve an acceptable level of power capture. The ETSU report (DoE UK, 1985) highlighted the potential for small scale use of wave power in particular cases such as when integrated with breakwaters. Thus continued small scale development of wave power was encouraged. Research continued in the UK, notably Edinburgh and in other countries including Norway.

Research into renewable sources of energy was initially driven by the realisation that ultimately fossil fuels would run out. However in the light of an increasing awareness of the threat of global warming RD&D into renewable technologies then received increasing UK government support and in 2005 eight off-shore devices were chosen to take part in the Carbon Trust's Marine Energy Challenge (MEC). The developers were Clearpower Technologies (WaveBob), Ocean Power Delivery (Pelamis), SeaVolt Technologies (Wave Rider), AquaEnergy (AquaBuOY), Lancaster University (PS Frog), Evelop (Wave Rotor), Embley Energy (Sperboy) and Wave Dragon. The MEC also included discrete work packages such as shoreline OWC, tidal stream, and marine energy design codes and standards to supplement the direct technology assessment. The programme was launched amid great optimism. In the launch press release of 11th February 2004 Tom Delay, Chief Executive of the Carbon Trust, commented: *"As yet no country has taken a leading position in marine energy. A relatively small investment now could make a significant impact to the UK's competitive position due to the early-stage of technology development".*

Naturally wave energy devices require test facilities, from small scale testing in a wave tank, through to sea-going prototypes. The UK is well placed to support these activities which have received appropriate government support. Of particular note in the context of wave energy development are the wave tanks at Edinburgh and Plymouth Universities. Ocean test sites include the European Marine Energy Centre (EMEC) based at Stromness in Orkney and Wave Hub Ltd in Cornwall. This latter company operates two wave energy test sites, the Pembrokeshire Demonstration Zone and Wave Hub which is off the North Coast of Cornwall. Wave Hub would be the obvious choice to test a prototype arising from the present work.

Events have shown that wave power has some way to go in becoming commercially viable. Of the eight developers that were chosen to take part in the Marine Energy Challenge, none are still active. The developers of Wave Bob and Pelamis have gone into liquidation, and an AquaBuoy prototype sank in 2007 - development appears to not to have been continued. Internet searches result in virtually no trace of Wave Rotor, while the development of both SPERBOY and Wave Dragon appears to have ceased, at least temporarily.

Nevertheless optimism as to the future of wave energy has continued. In the UK the Carbon Trust (CT) has been a major supporter of wave energy development and has helped the industry by means of a number of initiatives. Between 2003 and 2011 the CT had invested £30M in the marine energy industry. CT's Marine Energy Accelerator (MEA) programme, which ran from 2007 to 2010 was designed to achieve reductions in the cost of energy produced. The MEA aimed to gain an understanding of the potential of cost of energy reduction through targeted innovation, working with existing device concepts to develop a set of cost reductions. The MEA programme also included support for new device concepts to explore the potential for a single step change in cost of energy. The MEA report (Carbon Trust, 2011) considered that in the case of wave energy, sufficient improvements in performance, produceability, survivability, structural design etc. would come through gradual improvements in accordance with normal established "learning curves", albeit with some targeted accelerated cost reduction techniques. Both wave and tidal power energy costs were predicted to reduce from 35 or 40 p/kWh - to equivalence with offshore wind at 13 or 14 p/kWh over the fifteen year period, from 2010 to 2025. Case studies undertaken within the MEA programme included an innovative linear generator for future wave energy devices (Edinburgh University) and the development of installation and connection equipment for Pelamis to enable operations in bigger seas, and faster deployment. Checkmate Sea Energy also received funding for the promising innovative concept, Anaconda.

In addition the Marine Renewables Proving Fund was set up and managed by the Carbon Trust during 2009 to 2011 to provide financial and technical support for the demonstration

of promising wave and tidal devices. Six developers were selected for support. These were Aquamarine Power (Oyster - wave), Atlantis Resources Corporation (Atlantis - tidal), Pelamis Wave Power (Pelamis - wave), Voith Hydro Ocean Current Technologies (Voith - tidal), Hammerfest Strom UK (HS-1000 - tidal) and Marine Current Turbines (MCT – tidal). Just two of these six developers were involved in wave power and both have failed financially. The remaining four developers were in tidal power. Two of them (MCT and Atlantis) are now owned by them same company (Atlantis). ANDRITZ HYDRO Hammerfest Strom is part of ANDRITZ, which is a global and stock exchange listed technology Group with more than 17,000 employees. No reference to tidal power can be found on the Voith website. According to the information on the CT web site the scheme has proved that *"full scale marine energy devices can be installed and operated in open-sea environments"* (Carbon Trust, 2016). Thus for tidal power the technology is maturing fast and market leaders in the form of large international companies are emerging. However, in view of the fact that both of the front runners, Pelamis and Oyster have failed financially, this can hardly be said to be true for wave power.

Nevertheless, support continues for wave power development. The Scottish government, through Wave Energy Scotland (WES) (WES, 2016b) stepped in following the demise of Pelamis and Oyster by purchasing the intellectual property and some of the hardware. It is hoped that buyers will be found for what can be salvaged. In parallel, WES launched fresh initiatives to support the industry with two funding calls. The first supported innovations in Power Take-Off (PTO) technology while the second was for Novel Wave Energy Converters (WES, 2016a). These calls provided up to 100% funding to encourage innovation and enable the wave power industry to become a cost effective generator of electricity. The long term cost (50 years hence) for wave power generated electricity is put at only 2 p/kWh at present price levels (Carbon Trust, 2006). Whether this is achievable remains to be seen. However it is interesting to note that onshore wind power is now the least expensive form of electrical energy in the UK. In 2015 the price of onshore wind generated electricity was 5.53 p/kWh, which compared with 7.4 p/kWh for electricity from coal or gas (Bawden, 2015).

In the USA wave energy is receiving increased support under the “Wave Energy Prize” scheme (Anon, 2016) which is part of the US Department of Energy’s Water Power Programme. The aim is to attract next generation ideas by offering a prize purse and providing an opportunity for testing at the US’s most advanced wave-making facility, the Naval Surface Warfare Center Carderock’s Maneuvering and Seakeeping (MASK) Basin in Maryland. The assessment process began with model testing at a scale of 1:50 and a proof of concept assessment by an expert panel. As a result 11 teams have been chosen to take part in the final stage which includes wave tank trials at a scale of 1:20. Grants are given to participants towards the cost of model construction, testing etc. The developers of the most promising devices will receive prizes, a first prize of - $1,500,000, a second prize of $500,000 and a third prize of $250,000.

The writer became involved in wave energy as a spare-time interest in 1997 by providing a mathematical simulation model for Rod Youlton, the inventor of SPERBOY$^{TM}$, the floating oscillating water column WEC. In 1998 funding was secured by the University of Plymouth from The European Commission within the Non Nuclear Energy Programme JOULE III for research funding for SPERBOY, and a 1/5th size pilot device was deployed south of Plymouth Sound in 2001. Unfortunately this was irreparably damaged in a storm after only 10 days of testing. Having been involved through SPERBOY in the Marine Energy Challenge, the writer then led a study entitled 'Advanced Concrete Structural Design of the SPERBOY Wave Energy Converter’, which was supported by the Carbon Trust and the nPower Juice Fund. This showed a delivered cost of electricity of 16 p/kWh based on a 15% discount rate and a 20 year life – the standard conditions used by the CT for device assessment.

In 2010 the writer was fortunate to be accepted for a self-funded programme of research at the University of Plymouth. Initially this was to be an optimisation study of the SPERBOY type of WEC – a floating oscillating water column device. However, the opportunity presented itself to work on a promising novel concept which Francis Farley (Farley, 2011d) had patented. Thus the Floating Clam was taken as the basic concept around which this study revolves. The basis of the concept as originally conceived was to use “Clam action”

to lengthen the resonant period – as compared to that of a rigid body. In addition the Power Take-Off (PTO) was contained entirely with the structure, thus avoiding contamination and hazards from sea-borne debris etc. In the process of testing the Floating Clam it has been found that wide-band energy capture would result from restraining the Clam in heave. Tuning the heave response in the way originally conceived has in the final analysis not proved beneficial – for discussion on this point see Section 2.3.

Whether the Floating Clam will be prove to be a successful device remains to be seen. It may well join the long list of promising and not-so-promising devices. A recent study compares a total of 175 mostly unsuccessful devices (Joubert et al., 2013).

The one parameter that feeds directly into any calculation of the cost of generated electricity is the efficiency of power capture itself – and this is the main topic of interest in the present study. It will be shown that the Floating Clam is particularly efficient in this regard but that the full-scale embodiment of the technology is challenging. Whereas the device, as described in the patent is designed to employ an air turbine generator, alternative PTO methods are possible. A promising and innovative method of power take off is the Capstan Drive as discussed in the final chapter.

This document presents the reader in the first chapter with the theoretical basis on which the subsequent analyses depend. Then in Chapter 2 the wave tank models are described. Chapter 3 describes the mathematical models that have been developed to predict device behaviour and power capture performance while Chapter 4 covers the practical testing and its analysis. Chapter 5 presents an estimate of the performance that might be expected of a full scale device at a specific location - the Wave Hub test site in Cornwall Finally Chapter 6 draws conclusions and makes suggestions for further work

## 1.2 Resource

### 1.2.1 *Wave energy*

A convenient measure of the wave energy availability at a specific site is the annual average power per metre of wave front. Figure 1.1 shows the global wave energy availability, measured in kW/m (Cornett, 2008).

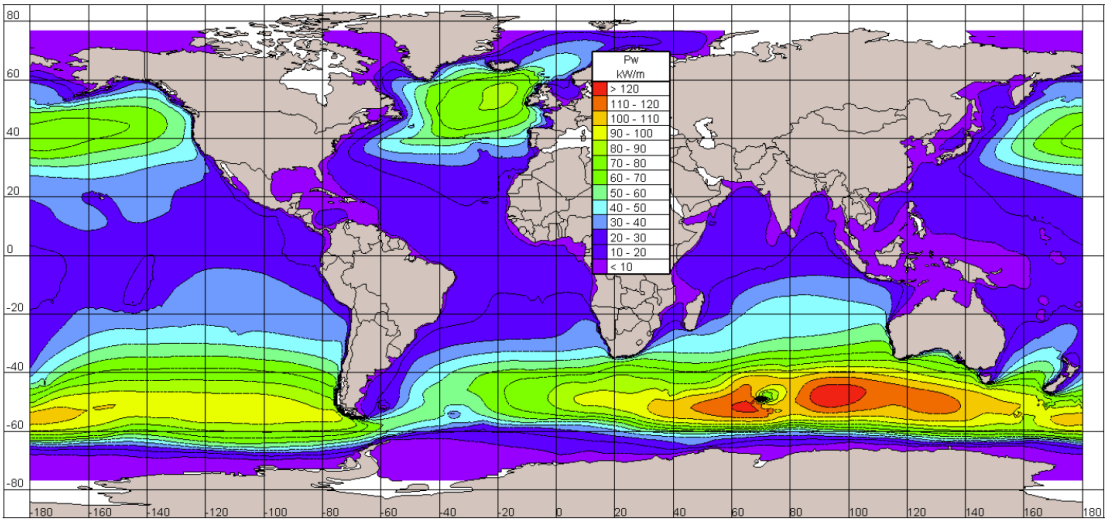


Figure 1.1: Wave Power Levels in kW/m Crest Length (Cornett, 2008)

The waves in real seas are random, varying in height, period and direction. However, for analysis purposes they can be considered to be made up of a combination of "regular" waves, each moving with simple harmonic motion. The mathematical analysis of these simple waves was solved in the early part of the 19th century (Stokes, 1847). A review of Stokes' work is contained in the paper by Craik (2005).

The profile of the water surface in a regular wave is close to being a sine wave – and in deep water it is so. For this case the power per unit width of wave crest, $P_{wave}$, is:

$$P_{wave} = \frac{\rho\, a^2 g^2 T}{8\pi} \qquad (1.1)$$

where $a$ is the wave amplitude, $T$ is the wave period, $\rho$ is the density of sea water and $g$ is the acceleration due to gravity (Mei, 2012).

As mentioned earlier, real seas are composed of random waves - clearly not regular. Such seas may also be described as “panchromatic”, being made up of waves of different periods, heights and phases. Thus a given sea state may be described by a spectral density diagram, such as that shown in Figure 1.2, taken from Shaw (1982), based on Dawson (1979), the spectral density being obtained by analysing the wave height time record.

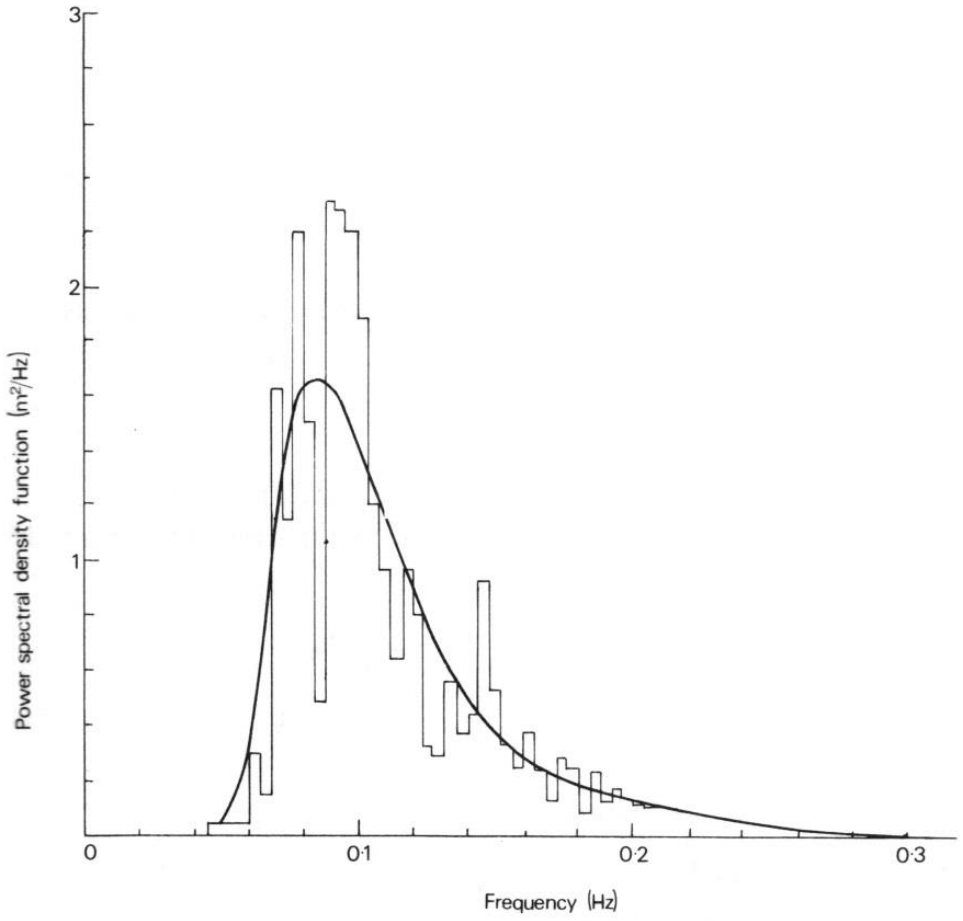


Figure 1.2: Power Spectrum of typical sea state(Shaw, 1982)

A given sea state may be characterised in a number of ways. For example, the Royal Navy uses the system invented by H. P. Douglas in 1917 where sea states 1 to 9 are each determined by observing the behaviour of the sea, noting such things as the apparent height of the waves, the extent of wave breaking and wind speed – and comparing these with a standard description of each sea state – as in Table 1.1

Table 1.1: Douglas sea states

| Sea State Code | Wave Height (meters) | Characteristics |
|---|---|---|
| 0 | 0 | Calm (glassy) |
| 1 | 0 to 0.1 | Calm (rippled) |
| 2 | 0.1 to 0.5 | Smooth (wavelets) |
| 3 | 0.5 to 1.25 | Slight |
| 4 | 1.25 to 2.5 | Moderate |
| 5 | 2.5 to 4 | Rough |
| 6 | 4 to 6 | Very rough |
| 7 | 6 to 9 | High |
| 8 | 9 to 14 | Very high |
| 9 | Over 14 | Phenomenal |

Another traditional approach, that correlates well with direct observation is to define the significant height, $H_{1/3}$, as the average height of the highest one-third of the waves with a significant period, $T_{1/3}$, being the average period of these waves. Note that this is wave height, as opposed to wave amplitude, and is the vertical distance between the trough and peak of the wave. Thus for regular waves the wave height is double the wave amplitude.

The more satisfactory way to define wave height is by first calculating the root mean square value of the water level relative to the mean water level, (Shaw, 1982):

$$\sigma = \sqrt{\frac{\sum_{i=1}^{n} y_i^2}{n}} \qquad (1.2)$$

where $y_i$ is the water level at instant $i$ relative to the mean water level and $n$ is the number of sample values taken of $y_i$.

The Significant Wave Height, $H_s$, is then defined by:

$$H_s = 4\sigma \ . \qquad (1.3)$$

One convenient definition of wave period is the Zero Crossing Period,$T_z$, defined by:

$$T_z = \frac{D}{n_z} \tag{1.4}$$

where $D$ is the duration of the record, and $n_z$ is the number of times the water surface moves through its mean level in an upward direction during time $D$.

The parameters $H_s$ and $T_z$ are not sufficient to define the behaviour of real seas and a knowledge of the spectrum of wave periods and wave height is necessary. Assuming that the time history of wave heights and periods may be considered to be a random process that is both stationary and ergodic, then a real sea may be represented by means of a Power Spectral Density Function, $S(f)$, whose mathematical definition is:-

$$S(f) = \lim_{\Delta f \to 0} \lim_{T \to 0} \frac{1}{(\Delta f)T} \int_0^T y^2(t, f, \Delta f)dt \tag{1.5}$$

where $y$ is the wave surface elevation, $T$ is the sampling interval and the function $S(f)$ is defined for the small frequency interval $\Delta f$ at frequency $f$.

Practical estimation usually entails capturing the time history of the wave height and evaluating $S(f)$ by means of a Fourier transform. . Furthermore, it may be shown that

$$\sigma^2 = \int_0^\infty S(f)df \ . \tag{1.6}$$

By defining spectral moments as follows, the relationships between a number of important parameters may be found. Thus the n$^{th}$ spectral moment $M_n$ is given by the relationship:

Spectral Moment $\quad M_n = f^n S(f)df$

where $n$ is an integer that takes a value between $-1$ and 2. (1.7)

The significant wave height, $H_s$, zero-crossing period, $T_z$, and energy period, $T_e$, are defined in terms of spectral moments by the following relationships (Shaw, 1982):

$$H_s = 4\sigma = 4\sqrt{M_0} \qquad T_z = \sqrt{M_0/M_2} \qquad \text{and} \qquad T_e = M_{-1}/M_0 \qquad (1.8)$$

The energy period, $T_e$, is such that the Power per unit width of wave becomes:

$$P_{wave} = \frac{\rho g^2}{8\pi} a^2 T = \frac{\rho g^2}{4\pi} \sigma^2 T = \frac{\rho g^2}{64\pi} H_s^2 T_e \qquad (1.9)$$

(since $\sigma^2 = a^2/2$ for a simple sine wave).

Thus the power in any given sea state may be conveniently defined by two parameters, the Significant Wave Height, $H_s$, and the Energy Period, $T_e$, albeit that the characteristics of two seas with the same significant wave heights and energy period may be quite different in terms of their spectra. However, in practice the characteristics of real seas are sufficiently similar, so that it is useful to have standardised mathematical definitions of wave spectra. A number of power spectra have been proposed, such as that due to Pierson and Moskowitz (Pierson & Moskowitz, 1964) and Bretschneider (Sarpkaya & Isaacson, 1981). The Pierson and Moskowitz spectrum contains wind speed as the basic parameter,

thus: $$S(f) = (5 \cdot 10^{-4}) f^{-5} \exp(-4.4/f^4 U^4) \quad [\, m^2/Hz] \qquad (1.10)$$

where $f$ = frequency in Hz, and $U$ = wind speed in m/s at 19.6 m above sea level

However, this can be shown to be equivalent to the spectrum used by the writer in the study that follows (Glendenning, 1964) and (Shaw, 1982), i.e.:

$$S(f) = A f^{-5} \exp(-B f^{-4}) \text{ where } A = H_s^2/4\pi T_z^4 \text{ and } B = 1/\pi T_z^4 \qquad (1.11)$$

Since much of the wave climate data is given in terms of energy period, $T_e$, rather than zero-crossing period, a conversion factor is needed. Thus, taking the definitions of $T_z$ and $T_e$ from Equation 1.8 results in the following relationship:

$$\frac{T_e}{T_z} = \frac{M_{-1}/M_0}{\sqrt{M_0/M_2}}. \qquad (1.12)$$

Applying Equation 1.12 to the definition of the Pierson-Moskowitz spectrum of Equation 1.11 results in the ratio of $T_e$to $T_z$ given by Equation 1.13:

$$\frac{T_e}{T_z} = 1.20265 \qquad (1.13)$$

It should be noted that this ratio is different from the normally accepted ratio of 1.12 (Shaw, 1982). Wave spectra will differ from location to location and clearly 1.12 is not always the most appropriate figure. For example, a figure of 1.206 results from applying the relationship of Equation 1.12 to the Bretschneider spectrum (Cahill & Lewis, 2014). Furthermore, a study carried out using measured data for locations off the north coast of Cornwall suggest the use of Equation 1.14 (South West of England Regional Development Agency, 2004):

$$T_e = 1.162\, T_z + 0.3285 \text{ s} \qquad (1.14)$$

Thus from equation 1.14 a sea state where the zero-crossing period is 8 s, will have an energy period of 9.62 s, which equates to a ratio $T_e/T_z$ of 1.203.

The annual wave climate at a particular location may be characterised by means of a scatter diagram showing the frequency of occurrence of individual sea states, as shown in Figure 1.3, and which has a mean power of around 50 kW/m (Dawson, 1979).

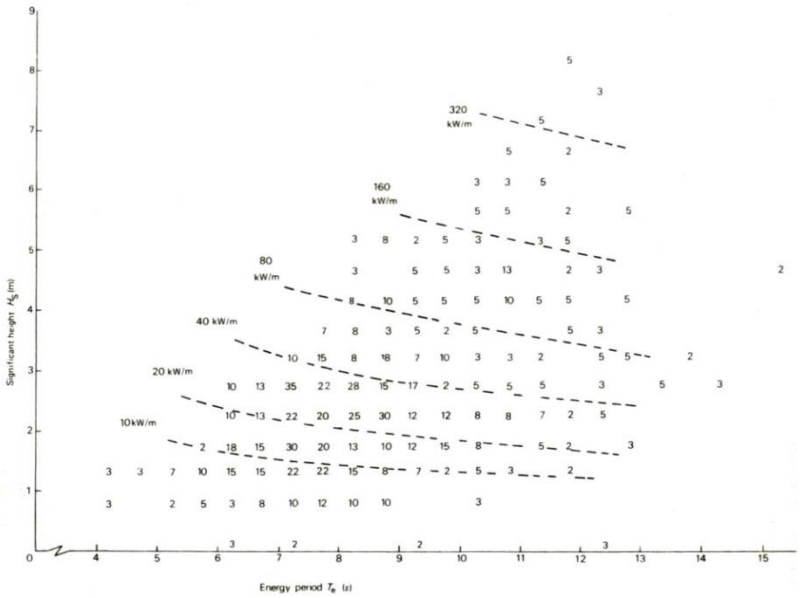


Figure 1.3: South Uist Scatter diagram 1976/77 (occurrence in parts per thousand) (Dawson, 1979)

### 1.2.2 *Wave direction*

Much of the available data giving the energy content of the waves, such as that contained in Figure 1.3 does not include wave direction. The Floating Clam being studied here, is sensitive to wave direction. However even where the WEC itself is not sensitive to wave direction, the positioning of the individual units within a wave farm will need to be considered in the light of the prevailing wave direction.

In studying wave direction data it becomes apparent that in many locations the wave direction although varying, is contained within an arc of up to around 80°, due to the particular properties of the location such as the prevailing wind and the position of open sea. Due to the physics of refraction the waves will tend to approach a shallow coast normally (Mei, 2012). Thus a WEC that is sensitive to wave direction may nevertheless perform well at these locations. For example Figure 1.4 shows the wave power angular distribution off the coast of Galicia, at a point where the water depth is in the region of 200 m (Iglesias & Carballo, 2011). The various segments are colour coded to indicate power available and the wave direction is indicated graphically. It can be seen that virtually all the wave energy comes within an arc of less than 90°, with the majority coming from the North-Westerly direction.

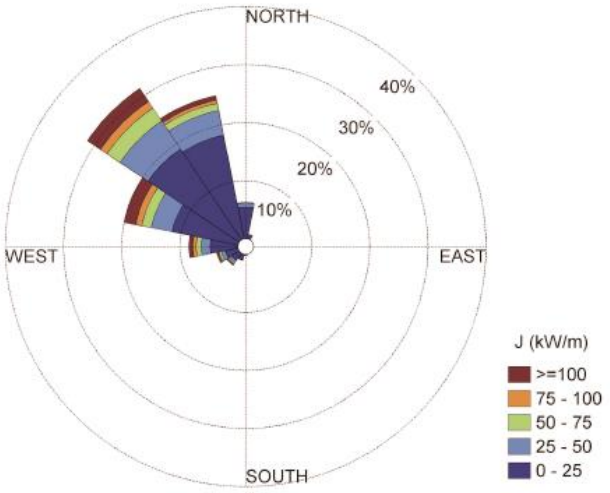


Figure 1.4: Wave Power Rose at the offshore buoy (Iglesias & Carballo, 2011)

Figure 1.5 tells a similar story for the Wave Hub test site, off the Cornish coast (Saulnier, Maisondieu, et al., 2011)

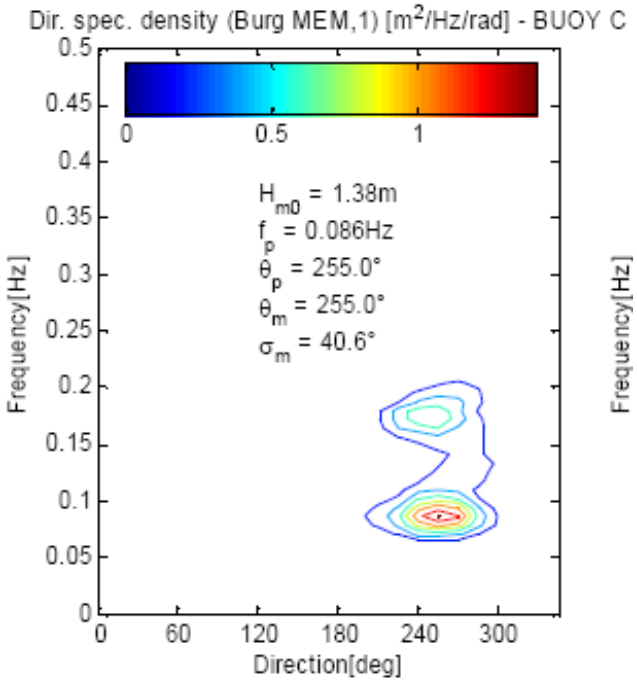


Figure 1.5: Directional Spectra at the Wave Hub Test site (Saulnier, Maisondieu, et al., 2011)

Figure 1.6 is taken from a presentation given by the marine energy researcher at Aquamarine Power, the developers of Oyster (Henry, 2010). The Oyster WEC is deployed in shallow water and is sensitive to wave direction.

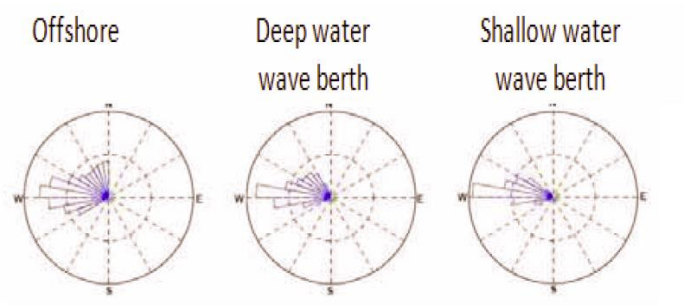


Figure 1.6: Tightening of directional spectra due to shoaling (Henry, 2010)

During the Oyster development the concept of “wave resource evaluation” or “Exploitable Wave Power” has been defined as “the net power crossing a line orthogonal to the mean wave direction” (Henry, 2010).

### 1.2.3 *Length of wave crest and Wave spreading*

The mechanisms that govern the ability of the wave energy converter (WEC) to harvest or “capture” energy are discussed in Section1.5.1. However, the theoretical analysis of energy capture normally starts from the assumption that the wave front is infinitely long and straight. However, it is clear that this is not the case and that the wave crests will have a finite length. It is found that short crested waves may be simulated by superimposing plane waves of differing incident angles, i.e. by a “spread” of wave directions.

One of the most commonly used directional spreading functions is the frequency dependent cosine power function (Saulnier, Prevosto, et al., 2011), such that:

$$S(f,\theta) = S(f)D(f,\theta) \tag{1.15}$$

where $S(f)$ is the one-dimensional wave spectrum (or ‘spectral density function’)

$S(f,\theta)$ is the directional wave spectrum, and

$D(f,\theta)$ is the angular spreading function, given by:

$$D(f,\theta) = \mathrm{C}(s)cos^{2s}\left(\frac{\theta}{2}\right) \tag{1.16}$$

where $\mathrm{C}(s)$ is a normalising factor, such that

$$\int_{-\pi}^{\pi} D(f,\theta)d\theta = 1. \quad (1.17)$$

Thus:
$$\mathrm{C}(s) = \frac{2^{2s-1}\Gamma^2(s+1)}{\pi\Gamma(2s+1)} \quad (1.18)$$

where $\Gamma$ is the Gamma function, $f$ is the wave frequency and $\theta$ is the angular difference between the wave direction and the mean wind direction (= in effect the mean wave direction).

The ocean wave basin at Plymouth (see Section 4.2) may be programmed to produce waves in accordance with the above definition, with $s$ being one of the input parameters,

### 1.2.4 *Short period component of wave spectra*

A case has been made for building a wave power converter for the short period component of the available wave energy spectrum (Farley, 2012). Based on data from the American wave buoy at Shumagin, it is shown that the 4 s wave is likely to be present all the time, whereas the energetic 10 s waves are absent for a significant part of the year. The problem is that the energy contained in these shorter waves is of an order of magnitude less than the longer ones. Although the case is made (Farley, 2012) for the likely economics of the device itself (on the basis that many small machines might cost no more than fewer, but larger and more expensive ones), the connection costs, maintenance costs and many other factors could make such a scheme uneconomic.

### 1.2.5 *Bimodal spectra*

In some locations the wave spectra has two peaks rather than the single peak more usually described. A study based on three data buoy locations has been carried out (Mackay, 2011). Data from the National Data Buoy Center (NDBC) buoys numbered 44014, 46042 and 51001 were used. This shows how ‘bimodal’ spectra may be approximated by 3-, 4- and 6-parameter JONSWAP spectra. The 4-parameter JONSWAP spectrum is shown to provide a good compromise between accuracy of description and the number of parameters used. By matching the wave spectral shape at a small number of sea states within the geographical area of interest it is possible by interpolation to accurately describe

the wave spectra across the site. This particular study (Mackay, 2011) considers only omnidirectional spectra and ignores directionality.

### 1.2.6 *Practical resource measurement*

Various methods are used to measure ocean waves. The most straightforward method involves the use of wave measurement buoys that simply float on the top of the wave and thus provide a measure of the wave position as a function of time. Rather as a cork floats on water, the lighter and more buoyant the buoy is, the better.

The measurement of a resource such as a potential wave farm site may be estimated from knowledge of historical wind speeds and their direction – and the local topography. Such estimates would be compared, for validation purposes, with such wave measurement buoy data as was available – a process known as 'hindcasting'.

A more recent development concerns the use of land-based radar for resource measurement, which has a clear advantage over the use of buoys (Wyatt, 2011). Estimates may be made of wave power, its directional characteristics and spatial and temporal variability. Data is obtained (Wyatt, 2011) from two different radars and compared with buoy data. Data from the Pisces HF radar in the Celtic Sea is used to show evidence of spatial variations in directionality of the power resource and the results demonstrate that HF radar can be used to both measure the resource and provide useful monitoring data during power extraction, device installation, testing and operations. HF wave measurements are being made at Wave Hub (see next section).

### 1.2.7 *Wave resource at test sites*

***Spain***

The energy resource in the seas off the Galacia coast in NW Spain has been studied, with the aim of identifying promising areas for the deployment of wave farms (Iglesias & Carballo, 2011). Measurements from one offshore data collection buoy were taken as the base data for the study. This data was then split into 104 separately defined wave patterns or "bins". Each pattern defined a wave state in terms of significant wave height, energy period, mean direction and frequency of occurrence. This is essentially the same

technique as the “scatter diagram” technique (see Figure 1.3), but with the added parameter of wave direction. The study used the SWAN coastal wave model to compute the wave resource over a large coastal area for each of 104 combinations of wave height and period. This enabled the inshore areas of high wave energy resource to be identified and characterized, the technique being validated by reference to an inshore data collection buoy. The study showed the potential for this methodology to provide WEC designers with wave climate data for specific locations.

***Cornwall – Wave Hub***

Wave Hub Ltd operate the Wave Hub test site where full sized prototype devices may be tested. Now owned by the Department for Business, Innovation and Skills, the project was originally developed by the South West of England Regional Development Agency. Up to four device developers are able to connect their arrays into the Wave Hub, which allows them to transmit and sell their renewable electricity to the UK's electricity distribution grid. Each developer is able to locate their devices in one quarter of the 3 by 1 km rectangle allocated to the Wave Hub, and there is capacity to deliver up to a total of 20 MW of power into the local distribution network (Wave Hub Ltd, 2016).

A study, aiming to predict the effect of global warming on the wave energy resource at the Wave Hub test site, has been carried out by Reeve et al. (2011). Tentative conclusions show that over a 100 year span (comparing 1961-2000 with 2061-2100) wave power will increase by between 2% and 3%. Of particular interest is the use of the WAVEWATCH III (WW3) - a third generation wave model developed at NOAA/NCEP in the spirit of the WAM model (see next paragraph). The model does not require the pre-defined shape of wave energy spectrum; and since the modelling is capable of generating wave climate data over the entire computational domain this method can be applied to choosing an optimal site for a wave farm, in terms of available wave power and/or energy yield.

The WAM model (WAMDI Group, 1988) is commercially available software that provides predictions of the shape and magnitude of wave spectra based on wind input, water depth and other location-specific data - avoiding ad-hoc assumptions of spectral shape. It is

regarded as superior to earlier models in requiring less empirically derived data, although some tuning is required for the white-capping dissipation function. The model was calibrated against fetch-limited wave growth data (WAMDI Group, 1988).

A further study (Saulnier, Maisondieu, et al., 2011) covers the characterisation of the Wave Hub test site, and shows how the deployment of four buoys in a close array contributes to the understanding of oceanographic processes, which includes key aspects of uncertainty and spatio-temporal variability. The local wave energy resource is assessed through time-domain and frequency-domain analysis, and preliminary results are presented, which have been obtained from the processing of the extended data, which also includes wind and tidal information.

***Denmark***

Estimates have been made of the year-round wave climate at the Danish Wave Energy Centre (DanWEC) test site at Hanstholm (Margheritini et al., 2011). Use is made of data from wave measurement buoys and mathematical modelling that computes the wave climate variation throughout the area of interest. In this case the numerical computation is carried out by the computer model MILDwave (Universiteit Ghent, 2016).

***Ireland***

The Sustainable Energy Authority of Ireland is developing the Atlantic Marine Energy Test Site (AMETS), a grid-connected test area for the deployment of full scale Wave Energy Converters (WECs) near Belmullet, Co. Mayo, Ireland (Cahill & Lewis, 2011). In common with the practice employed at other test sites, data is provided by two wave buoys – one positioned at a deep-water location (100m depth) and the other further inshore (50m depth), in order to characterise the wave resource at the site. There is no attempt at modelling the spatial variability of the resource, but comparison of the measurements from the two wave buoys indicates a considerable level of homogeneity over the site. The resource at the quarter scale site at Galway Bay is compared with the resource at AMETS and the degree of scalability between the two sites is assessed. Also, estimates of annual energy capture of the Pelamis WEC are presented.

## 1.3 Hydrodynamic analysis

The behaviour of an incompressible fluid may be described by the Navier-Stokes equations. These equations govern the motion of a viscous fluid subject only to the assumptions of constant density and a Newtonian stress-strain relationship (Newman, 1977). The Navier-Stokes equations, written in full and in Cartesian coordinates are:

$$\frac{\partial u}{\partial t} + \mathrm{u}\frac{\partial u}{\partial x} + \mathrm{v}\frac{\partial u}{\partial y} + \mathrm{w}\frac{\partial u}{\partial z} = -\frac{1}{\rho}\frac{\partial p}{\partial x} + \frac{\mu}{\rho}\nabla^2 u + \frac{1}{\rho}F_x$$

$$\frac{\partial v}{\partial t} + \mathrm{u}\frac{\partial v}{\partial x} + \mathrm{v}\frac{\partial v}{\partial y} + \mathrm{w}\frac{\partial v}{\partial z} = -\frac{1}{\rho}\frac{\partial p}{\partial y} + \frac{\mu}{\rho}\nabla^2 v + \frac{1}{\rho}F_y \qquad (1.19)$$

$$\frac{\partial w}{\partial t} + \mathrm{u}\frac{\partial w}{\partial x} + \mathrm{v}\frac{\partial w}{\partial y} + \mathrm{w}\frac{\partial w}{\partial z} = -\frac{1}{\rho}\frac{\partial p}{\partial x} + \frac{\mu}{\rho}\nabla^2 w + \frac{1}{\rho}F_z$$

where $x, y, \mathrm{and}\ z$ are the Cartesian coordinates of a point in the fluid and $u, v, \mathrm{and}\ w$ are the corresponding velocities of the fluid. Fluid density is $\rho$, viscosity is $\mu$ and $t$ is time. $F_x, F_y, F_z$ are the external forces acting the fluid.

The Continuity Equation is also required:

$$\frac{\partial u}{\partial x} + \frac{\partial v}{\partial y} + \frac{\partial w}{\partial z} = 0 \qquad (1.20)$$

The Navier-Stokes equations are difficult to solve as they form a coupled system of nonlinear partial differential equations which may be solved analytically only for some very simple geometrical configurations. However, by making the assumption of an inviscid fluid the equations become much simpler and easier to solve. This results in the discovery that the velocity field may be represented by the gradient of a scalar function, the Velocity Potential, $\varphi$. The fluid is said to be “irrotational” (Newman, 1977).

In the case of large objects, such as ships and wave energy converters (WEC) the effect of fluid viscosity on the overall flow pattern is slight. The viscous forces in the main body of fluid are small, so that in these areas the assumption of an inviscid, irrotational fluid becomes valid (Newman, 1977). The effect of viscous forces, such as skin friction may then be included in the analysis as additional terms in the equations of motion etc.

Historically this approach has proved successful but with the advent of powerful computers more advanced methods that solve the complete Navier Stokes equation are being used. Recent research carried out at the University of Plymouth has demonstrated the use of such methods to assess the survivability of a WEC in severe waves (Ransley, 2015).

With the assumption of zero viscosity it can be shown that the velocity profiles within the fluid satisfy the Laplace Equation (Equation1.21), and, as in the case of the Clam, a good understanding of the dynamics of the WEC may be gained through this simplification.

$$\frac{\partial^2 \varphi}{\partial x^2} + \frac{\partial^2 \varphi}{\partial y^2} + \frac{\partial^2 \varphi}{\partial z^2} = 0 \qquad (1.21)$$

where $\varphi$ is the Velocity Potential and $x, y \text{ and } z$ are the Cartesian coordinates.

The important conclusion to be drawn from this relationship is that the fluid motion depends only on the velocity of the fluid at its boundaries and may be completely described by the fluid velocity normal to the surface – and the geometry of the surface.

In the case of a stationary surface the fluid velocity normal to the surface is zero – although the flow may be along the surface. However, in the case of a free surface, such as a sea wave, the velocity of the boundary is unknown. In this case, knowledge of the pressure on the free surface leads to a solution using Bernoulli's equation (Newman, 1977, Section 4.3).

An introduction to the theory of water waves, using basic level calculus, is provided by the book, "Water Waves" (Barber & Ghey, 1969), which has the merit of helping the reader understand the fundamental concepts, including the derivation of the Laplace Equation without the need of advanced mathematics. More recent textbooks, such as "Water Wave Mechanics for Engineers and Scientists" (Dean & Dalrymple, 1991) cover the derivation of the Laplace Equation and the solution of hydrodynamic problems through more advance techniques including vector analysis.

## 1.4 Analysis tools

### 1.4.1 *AQWA and WAMIT*

Two commercially available numerical analysis tools have been investigated here for application to the Clam: WAMIT (WAMIT, 2012) and AQWA (Ansys, 2010). Both analyse the hydrodynamics of fixed and floating bodies, and wave makers, based on the use of the Velocity Potential, $\varphi$, as described in the previous section. Both use the boundary-value method to compute the results for points on a user-specified mesh. Virtually identical results are obtained from these tools in terms of the basic analysis, using the same mesh geometry. However their development has followed different paths.

WAMIT consists, in effect, of a toolbox of analysis methods of varying degrees of sophistication, including the very useful ability to "patch in" sections of the surface from a menu of geometric shapes. Additionally there is the technique of using "generalised modes" that facilitates the analysis of a range of problems; particularly those involving flexible bodies, where the body flexure affects the hydrodynamic behaviour of the system. The WAMIT package itself has no graphics capability, but may be used in conjunction with a graphics package – MultiSurf (AeroHydro, 2012).

All versions of WAMIT earlier than version 6 were based strictly on the low-order panel method, where the geometric form of the submerged body surface is defined by flat quadrilateral elements and the solutions for the velocity potential and/or source strength are assumed constant on each panel. WAMIT Version 6 has been extended to include a complementary higher-order panel method based on a continuous B-spline representation for the velocity potential, and several alternative schemes for defining the body surface including explicit analytic formulae. The order of the B-splines is controlled by user-specified input parameters.

AQWA on the other hand is less sophisticated in regard to the mathematical methods on which it is based, being equivalent to the "low order" WAMIT methodology. Meshing is based on two simple shapes, the plane triangle and quadrilateral, and curved surfaces are modelled by refining the mesh. Although WAMIT has an advanced capability that can

model curvature accurately, AQWA has a sophisticated graphical front end, the Ansys Workbench, which enables the user to visually build the model. AQWA also uses non-diffracting surface that allow visualisation of the parts of the model above the water surface. The term “non-diffracting” is used (by AQWA) to describe elements that are not part of the hydrodynamic calculations. Also much use is made of “Morison elements” that allow hydrodynamically small objects to be included, such as mooring lines.

Morison’s Formula (Newman, 1977) assumes that the total wave force is the sum of inertia forces and viscous forces, i.e.:

$$Force = (added\ mass + body\ mass) \times acceleration + viscous forces \qquad (1.22)$$

Viscous forces usually take the form, $\frac{1}{2}\rho A C_D U|U|$, where $\rho$ is the water density, $A$, is representative area, $U$ is the body velocity relative to the fluid, and $C_D$ is an appropriate drag coefficient.

It should be noted that Morison’s Formula is semi-empirical and depends on the use of factors based on model tests and takes no account of the force on the body due to radiated waves. In AQWA it is only used on tubular elements, and is particularly useful in modelling mooring lines, and in adding viscous drag to a moving object or one subjected to currents.

In addition, through a mathematical technique that uses the Convolution Integral, AQWA turns a frequency domain solution into a time domain simulation that can be displayed as an animation.

Because AQWA is a commercial package designed to support the shipping and off-shore industry it contains the ability to model a moving object. It is able to model slow-drift and extreme wave conditions and enables the user to study transient effects such as line breakage (through the use of “Convolution”).

Although neither package, WAMIT or AQWA, is as straightforward as could be wished, WAMIT is the application that best fits the needs of the current programme, since the method of “generalised modes” is ideally suited to modelling the Clam action.

WAMIT's use of text files allows easy interface with other PC applications. However the absence of a built-in graphical interface, such as provided by AQWA means that it is not as easy to detect errors. Successful use depends on the skill and diligence of the user.

### 1.4.2 *Excel spreadsheet*

MS EXCEL is particularly useful in analysing data from wave tank trials. All the files generated during the wave tank testing are text files. This means that the files can be readily input into the EXCEL spreadsheets.

### 1.4.3 *Mathcad*

Mathcad (PTC, 2014) has been used for this project. It provides a similar capability to other mathematical analysis packages such as MATLAB (Mathworks, 2014) and Maple (Maplesoft, 2014).

### 1.4.4 *Time domain model*

VisSim (Visual Solutions, 2014) has been used in this project for time domain modelling. It provides a similar capability to MATLAB/Simulink (Mathworks, 2014), but is easy to use and fast. The Clam has been modelled in the time domain using a regular wave input and perfect agreement with the frequency domain models has been achieved. The simulation has also been extended to provide a time domain model employing a random input and taking account of the various non-linear elements (e.g. drag and Coulomb friction). VisSim is also capable of being modified to incorporate the mathematically correct "convolution integral" approach.

## 1.5 Power capture and control

### 1.5.1 *Mechanism of power capture*

Power Capture is, as the name implies, the power harvested by the Wave Energy Converter (WEC) and is clearly dependent on the power in the sea state of interest. As discussed in Section 1.2.1 the wave power per unit width of wave front, $P_{wave}$, may be computed from Equation 1.9, given the significant wave height, $H_s$, and energy period, $T_e$.

A measure that can be used to compare WECs is the Capture Width, $W_C$, which is found by dividing the Power Capture, $P$, by the power in the incoming wave:

Thus:
$$W_c = \frac{P}{P_{wave}} . \qquad (1.23)$$

Power capture clearly depends on the response of the Wave Energy Converter (WEC) to incoming waves. Most WECs absorb energy from the sea by resonating with periods at, or close to that of the sea waves. This mode of power capture relies on the WEC being a good wave maker. As Falnes (2002) explains, energy is taken from the wave by a process that involves cancelling the wave action as it passes the wave energy converter (WEC). When maximum energy is absorbed the sea behind the converter is perfectly calm and all the energy in the incoming wave is absorbed. Since the system may be considered (as a good approximation) to be linear, the pattern of waves is the sum of the unaffected incoming wave plus the wave system generated by the WEC.

The greatest transfer of energy occurs when the motion of the WEC has a particular phase and amplitude relation with the incoming wave. Referring to Figure 1.7, it can be seen that the amplitudes of the radiated wave (curves b and c) have to be half the amplitude of the incoming wave (curve a). Additionally, the radiated wave has to have the right phase relationship with the incoming wave, such that the crests of the wave radiating towards the right (curves b and c) coincide with the troughs of the incident wave (curve a).

Figure 1.7d shows an ideal case where all the wave energy is absorbed. However, where there is only one mode of oscillation (e.g. a heaving absorber) the resulting wave

corresponds to the superposition of waves a and b. Note that the wave radiated towards the left and the resulting wave transmitted towards the right both have an amplitude equal to half of the amplitude of the incident wave. Since wave energy is proportional to the square of the wave amplitude this means that 25% of the incident wave energy is reflected towards the left, and also 25% of it is transmitted towards the right. The remaining 50% is absorbed by the WEC, the theoretical maximum.

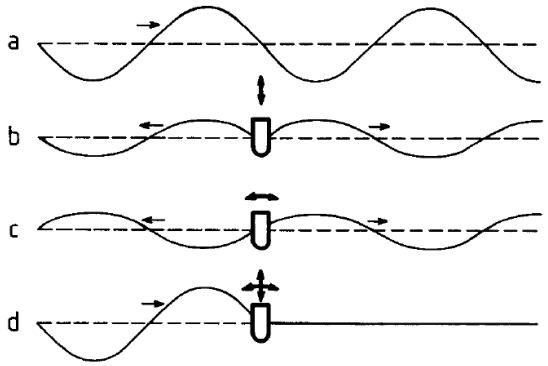


Figure 1.7: Modes of energy absorption (Falnes, 2002)

### 1.5.2 *Resonance*

The optimal phase condition for the WEC is when it is in resonance with the waves (Falnes, 2005). Thus its natural resonant period should be the same as the wave period. In a practical device it is difficult to maintain this relationship as the wave period changes with sea state, and also to some extent, from one wave to the next. A measure of the ability of the device to pick up energy when operating away from maximum resonance is its bandwidth. It is found that physically large WECs have broad bandwidths, such as SPERBOY™ (Phillips & Rainey, 2005). However, the drawback of a large WEC lies in the cost of materials, length of construction time and increased difficulties of deployment.

A smaller WEC will have a narrower bandwidth. But in this case the energy transfer may be improved in two ways: firstly by actively changing the resonant period (i.e. by “tuning”), and secondly by applying some form of phase control in order to obtain the optimum phase condition. A method that has been well researched is to achieve phase control by latching. However, before looking at latching, the performance of point absorbers is discussed.

Figure 1.8 shows the circular wave pattern radiating from a heaving point absorber, and interfering destructively with an incident plane wave. The maximum energy which may be absorbed by a heaving axisymmetric body equals the wave energy transported by an incident wave front of width equal to the wavelength, $\lambda$, divided by $2\pi$, i.e. the maximum capture width. This also applies to a device that is small in relation to the wavelength as well as to an axisymmetric absorber of any size. Thus while the capture width of a small device might be several times its physical width, for a large device the reverse may apply. For a point absorber resonating in two axes, the theoretical maximum capture width is $\lambda/\pi$ (Falnes, 2002).

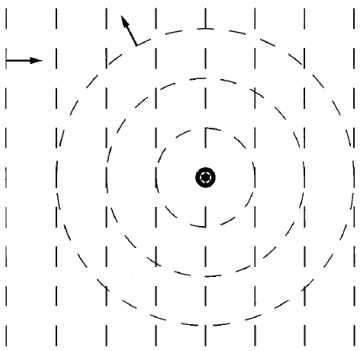

Figure 1.8: Destructive wave patterns for a heaving point absorber (Falnes, 2002)

A well-known result for a wave energy converter is that for maximum power capture, the power take-off (PTO) damping should equal the wave radiation damping (McIver, 2002) (Falnes, 2002) – when considering a linear system undergoing simple harmonic motion (SHM) and operating at its resonant frequency.

### 1.5.3 *Measurement of Added Mass and Wave Radiation Damping*

A buoy, bobbing up and down in the water, behaves like a typical damped oscillating system. In still water, if the buoy is first displaced vertically from its equilibrium position then released it will behave like a damped oscillator, as described in any textbook on the subject, (e.g. Schwarzenbach & Gill, 1992).

The motion of the buoy (to a first approximation) is subject to the following equation, which relates to a spring-mass-damper system with no external force applied:

$$m\frac{d^2x}{dt^2} + c\frac{dx}{dt} + kx = 0 \qquad (1.24)$$

where $x$ is the displacement of the buoy and $m$ is its mass, $c$ is the damping and $k$ is the stiffness of the system.

The mass, m, may be measured simply by weighing the buoy – when out of the water. However, it is found that the apparent mass is greater when the motion of the buoy is observed in water, when oscillating with Simple Harmonic Motion (SHM). This is because the dynamic system includes the water that is set in motion as the buoy oscillates. The increase of mass is known as Added Mass and varies with the frequency of oscillation. Thus the value of mass, m, for the oscillating buoy may be determined by examining the dynamic behaviour of the buoy.

An alternative form of the above second-order differential equation is:

$$\frac{d^2x}{dt^2} + 2\zeta\omega_0\frac{dx}{dt} + \omega_0^2 x = 0 \qquad (1.25)$$

where $x$ is displacement, $\omega_0$ is the undamped angular frequency and $\zeta$ is the damping ratio (a constant).

The value of the damping ratio $\zeta$ determines the behaviour of the system. A damped harmonic oscillator can be:

*Overdamped* ($\zeta > 1$): The system returns to equilibrium without oscillating. Larger values of the damping ratio $\zeta$ return to equilibrium slower.

*Critically damped* ($\zeta = 1$): The system returns to equilibrium without oscillating.

*Underdamped* ($0 < \zeta < 1$): The system oscillates (at reduced frequency compared to the *undamped* case) with the amplitude gradually decreasing to zero.

*Undamped* ($\zeta = 0$): The system oscillates at its natural resonant frequency ($\omega_o$).

By comparing the equation 1.24 with equation 1.25, we can see that:

$$\omega_0^2 = \frac{k}{m} \quad \text{and} \quad c = \frac{2\,\zeta\,\omega_0}{m} \tag{1.26}$$

A wave power buoy will normally fall into the under-damped category as shown by Figure 1.9, where the oscillations are seen to die away with time.

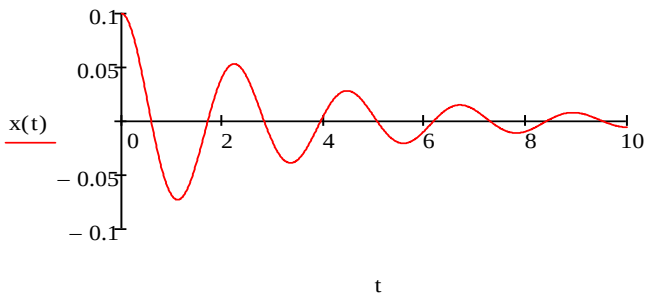


Figure 1.9: Under-Damped Oscillations

The experimental determination of the magnitude of the damping uses the logarithmic decrement method. As the oscillation dies away, each successive peak is related the one before it, by a constant ratio known as the logarithmic decrement, see Figure 1.10.

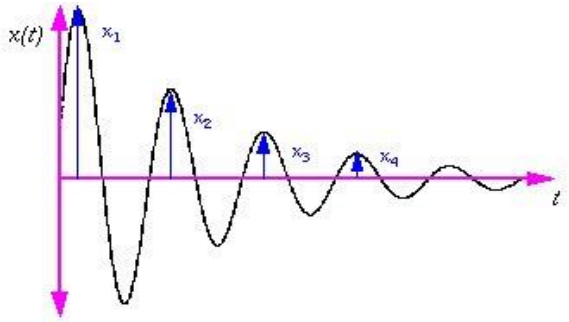


Figure 1.10: Under-Damped Oscillations – Logarithmic Decrement

The damping ratio, $\zeta$, is related to the logarithmic decrement, $\delta$, for under-damped vibrations by:

$$\zeta = \frac{\delta}{\sqrt{(2\pi)^2 + \delta^2}} \qquad \text{where} \qquad \delta \triangleq \ln \frac{x_1}{x_2}. \tag{1.27}$$

### 1.5.4 *Reactive control*

"Optimum" or "reactive" control seeks to maximise the energy capture by returning some energy to the sea during part of the oscillatory cycle and re-capturing it during a later part of the cycle. To optimally apply this strategy it is necessary to measure the waves and/or the WEC's oscillatory motion, and thus predict the wave pattern some seconds into the future.

A similar strategy is "latching phase control" - see Figure 1.11. This is employed where the wave periods are longer than the WEC's natural period. A Clamping mechanism stops the motion at the instant of extreme excursion. Further motion is then permitted after a certain time (about one quarter of the natural period) before the next maximum of the wave exciting force. For a heaving buoy of natural period shorter than the wave period this force is approximately in phase with the wave elevation of the incident wave (Falnes, 2002).

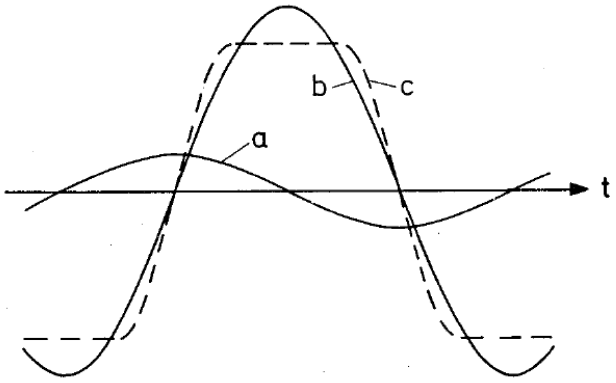


Figure 1.11: Resonance and phase control (Falnes, 2005)

Referring to Figure 1.11, the curves indicate incident wave elevation and vertical displacement of a heaving body as functions of time.

Curve a shows the elevation of the water surface due to the incident wave. This would also represent the vertical position of a body with negligible mass. For a body of diameter very small compared to the wavelength, curve a also represents the wave's heave exciting force on the body.

Curve b shows the vertical displacement of heaving body whose mass is such that its natural period is equal to the wave period (resonance).

Curve c shows the vertical displacement of a body with smaller mass, and hence shorter natural period, which would normally not keep in phase with the incoming wave. Phase control is then obtained by keeping the body in a fixed vertical position for a certain time.

Figure 1.12 show the results of a simulation study (Falnes, 2005). The curves show the wave energy (in joules) accumulated during 5 seconds for three cases, i.e. no control (lower broken curve), latching phase control (solid curve) and full, theoretically ideal optimum control (broken wavy curve). The practical limitation of amplitude is ignored, For the last case it is seen that relatively large amounts of energy have to be returned to the sea during two intervals of each oscillation cycle. The result is that the energy absorbed is about twice the absorbed energy under latching phase control, and this latter energy is about four times as much as that without any control (Falnes, 2005).

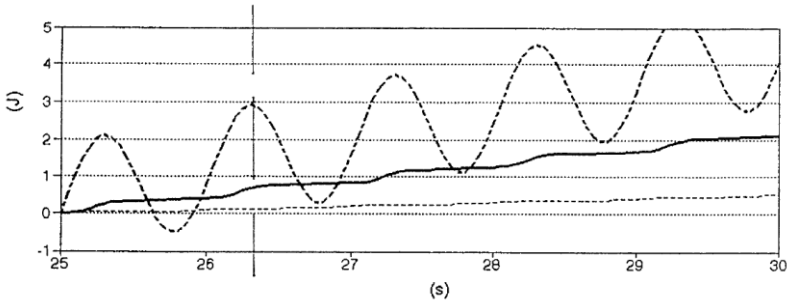


Figure 1.12: Phase and Latching Control – a comparison (Falnes, 2005)

For real sea waves the time intervals between crests and troughs vary in a random manner. With operation of a latching-controlled WEC in such random waves the point of release is determined by a control system that uses signals from sensors measuring the wave position or the wave exciting force in order to make a prediction of the wave force at a future time. The decision to unlatch the WEC should be taken at least one quarter of the WEC's natural period before the next extreme of the wave force (Falnes, 2005).

### 1.5.5 *Power Take-Off (PTO) and associated control systems*

The possible technical solutions for the PTO and its control systems clearly depend on the type of WEC under consideration. In reviewing the literature it appears that among the multiplicity of concepts, there is more commonality in control methodology than in hardware.

The least efficient, but possibly the easiest control methodology to implement, is the type of control based on resonance (see Section 1.5.2) and which can be described as impedance matching. This is almost the only option available to oscillating water column (OWC) devices, where the movement of the water column pumps air through a turbine/generator set. A practical solution is to match the characteristics of the turbine and the resonant period of oscillation of the WEC to the wave resource, as has been proposed for the SPERBOY$^{TM}$ WEC (Phillips & Rainey, 2005). A certain degree of reactive control may be possible, dependent on the characteristics of the turbine, and this has been the object of recent research at Plymouth (Freeman, 2011). It is seen that the most appropriate control system will be dependent on the type of WEC and its PTO. Practical considerations such as the stall characteristics of an air turbine and the behaviour of the WEC in heavy seas influence the choice of control system. Reactive control where power is input to the WEC during part of the wave cycle provides greater overall power capture than simple impedance matching (Freeman, 2011). Normally the turbine is designed to rotate in the same direction irrespective of the direction of air flow, which reciprocates. Suitable turbine types include the Wells turbine and the impulse turbine. Among the WEC design options are those where the WEC is incorporated into a fixed structure such as a breakwater. Here it is possible to maximise power capture by for example controlling the speed of the turbine and by controlling the resonance of the system. Where the turbine communicates with a closed air chamber, the resonant period may be altered by actively modifying its pressure and/or volume, as proposed for a breakwater to be installed off the Italian La Spezia coast. (Filianoti, P & Camporeale, S M, 2005). A similar scheme is to be installed in a caisson forming the head of the new Douro breakwater near Porto, Portugal. The PTO comprises a

Wells turbine and a variable speed generator whose optimum speed is computed for each sea state. (Gato et al., 2005).

PTO systems based on the use of hydraulic machinery are proposed by many developers. These commonly include hydraulic rams, hydraulic motors and accumulators. One such application is shown in Figure 1.13. This particular system has been modelled by using hydrodynamic coefficients based on linear theory within a non-linear time domain analysis. A simplified one-dimensional (heave) model has been developed to include the convolution integral approach (Falcão, 2005). The PTO and the same modelling approach may be developed to include phase control by latching (Falcão, 2007).

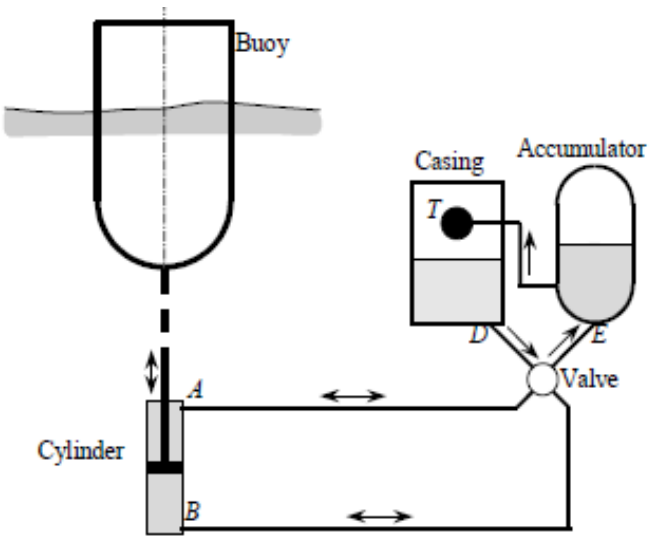


Figure 1.13: Heaving Point Absorber with Hydraulic PTO (Falcão, 2005)

Studies of a heaving point absorber WEC equipped with hydraulic energy storage and a variable speed generator Doubly-Fed Induction Generator (DFIG) have been carried out with the aid of a generic wave-to-wire dynamic model. The emphasis was on developing a control strategy for the intermediate (hydraulic) energy stage and the generator (Kiprakis & Wallace, 2005). The electrical engineering aspects were fully examined but the control philosophy appears little more advanced than that of impedance and resonance matching.

A theoretical framework has been devised to analyse the behaviour and energy collection potential of a wave energy converter operating in random waves under latching control. Applying the analysis to a heaving buoy demonstrates the effectiveness of latching, and the method is readily applicable to other types of WEC (Babarit & Clément, 2005).

Control methods and performance figures for a heaving point absorber have been investigated where the WEC takes the form of a semi-submerged sphere. This has demonstrated the significant increase of absorbed wave power due to phase control. The difference between optimum reactive control and sub-optimum latching control was less significant. Unfortunately the experimental work was flawed by excessive friction levels in the test set-up (Torkel & Falnes, 2005).

MacTaggart Scott have developed an infinitely variable reactive control system that offers increased energy capture for wave power devices that use a hydraulic PTO. This they call a “Reactive Hydraulic Modulator (RHM)”. MacTaggart Scott are considering the use of seawater as the working medium. Also claimed is that active control may be used to smooth wave farm output and ‘detune’ the device, thus allowing continued generation in higher sea states (Skinner & Scott, 2010).

Not all devices employ a PTO control system that falls into one of the above categories. A case in point is the Oyster WEC, which is an Oscillating wave surge converter (OWSC), where the enhanced horizontal fluid particle movement of waves in the near shore coastal zone is exploited (Whittaker & Folley, 2012). Oyster does not follow the conventional wisdom of Section 1.5.2, it “couples with incoming waves without being highly tuned” and aims to optimise the wave torque (Whittaker et al., 2007).

A further PTO system concept is the use of a compact array of small buoys that are not resonated. The theoretical potential of the compact array have been compared with that of a large buoy of equal volume, and shown to be superior (Mei, 2012).

## 1.6 Sea keeping

By their very nature, wave energy devices need to be sited in areas of high wave energy, and thus a floating WEC will need to be sufficiently stable in rough seas. Normal, well established criteria may be used to calculate such parameters as the centre of gravity, centre of buoyancy and metacentric height (Francis, 1962). The natural periods of pitch and roll should also be predicted. If these are not relevant to the energy capture, then the periods should be of the order of 30 seconds – long enough to avoid resonance in storm conditions but short enough to give a satisfactory level of static stability.

In this connection it is necessary to consider how the sea-keeping ability of the device affects its maintainability – methods of altering its response when undergoing maintenance may have to be considered. It should be noted that as well as calculating the hydrodynamic characteristics of a floating body, AQWA also computes its static stability.

Wave tank testing, incorporating correctly scaled models is essential to assess the behaviour of a device in storm conditions, since the assumption of linearity breaks down in this case. In addition, wave tank testing may show up aspects that have not been previously considered.

## 1.7 Wave energy converters – a comparison

As explained in Section 1.1, wave energy research in the UK was actively pursued in the 1970s although there was a decision to cease funding in favour of the nuclear industry in the 1980s. However, due to threat of global warming and the need to find renewable energy sources, wave energy is again receiving government attention and support.

There are now well over 170 individual devices that have been proposed to extract energy from sea waves (Joubert et al., 2013). Many of these have been patented and tested in an ad hoc fashion. Some have been built, tested and subjected to scientific scrutiny, but as yet there are no clear winners since the viability of a WEC depends on its energy collection efficiency measured in pence per kW-hour (or similar) having taken all factors into consideration, i.e. cost of construction, energy capture performance, maintenance, etc.

There are a number of fundamentally different ways of extracting energy from the sea (Phillips, 2008), the main ones being listed below. Examples of each type are given, although many more could be quoted.

- Articulated pontoons – Cockerell Raft, McCabe Wave Pump, Pelamis

  Here the PTO utilises the rotary motion of, and torque applied to the hinges that join the floating pontoons. The McCabe Wave Pump is designed to produce high pressure water for desalination. The Pelamis' hinges take the form of hydraulic rams that allow movement in any direction.

- Oscillating Water Column (OWC) – Limpet, SPERBOY™

  Typically OWCs embody a duct whose lower end is below the sea surface. The duct then continues to a level above the surface where it feeds into a turbo-generator set. The wave action causes air to be pumped through the turbine. OWCs may be shore mounted as in the case of Limpet or incorporated into a floating structure such as SPERBOY™.

- Heaving Buoy – AquaBuoy, SPERBOY™, Ocean Power Technologies (OPT)

  As the name implies, a heaving buoy rises and falls with the wave action. They usually have an axisymmetric structure and are classed as point absorbers. The range of possible PTOs is wide. AquaBuoy, although not now being developed, was tethered directly to the ocean floor via an ingenious "hose pump" that pumped water as it was alternately stretched and relaxed. The OPT device incorporates a reaction plate placed below the buoy and is thus in relatively still water.

- Over-topping – Wave Dragon

  Wave action causes water to flow up a ramp and over the edge where it is collected and used to drive low-head turbine/generator sets. Wave Dragon incorporates arms that gather waves from an area much wider than the entry to the ramp.

- Float-operated – Wave Star, Manchester Bobber

  Float operated devices are usually based on the principle of a hinged arm with a float at its extremity, e.g. Wave Star which uses a multiplicity of such floats. The Manchester Bobber embodies floats arranged in a matrix pattern each float being suspended by cable in such a way as to drive a drum forming part of the PTO mechanism.

- Hinged paddle – Oyster

  Deployed close to shore, the Oyster consist of one large flap hinged at the

sea bed, such that wave action causes it to oscillate back and forth. Power is absorbed via hydraulic rams attached to the flap.

- Others – PS Frog, Salter's Duck, Bristol Cylinder, Anaconda

  PS Frog – a buoyant paddle with a ballasted mass within it.

  Salter's Duck – a buoyant duck-shaped body that oscillates around a spine. The PTO may take a number of forms including by internal gyroscopic action. Hydrodynamically very efficient.

  Bristol Cylinder – a cylindrically shaped and buoyant body tethered below the sea surface. The tethers are connected to subsea PTO units.

  Anaconda – a submerged rubber tube that carries a bulge wave as the wave passed along it.

In most cases the performance of the WEC depends on resonance. However this is not true for the overtopping device, and has limited applicability to the hinged paddle. In addition, Mei (2012) demonstrates mathematically that a large, compact array of buoys (e.g. the Manchester Bobber) has a wide band response that does not rely on resonance for energy extraction.

There are many reasons why the most efficient device, in terms of energy extraction, may not provide the most economical solution as measured by p/kWh taken over its full life. Often the actual performance is less than that predicted by analyses that assume an ideal, frictionless fluid – and it is these optimistic predictions that are given by WAMIT or AQWA. The cost of maintenance is also a major factor. Thus a simple and robust device could prove to be a better solution than a more efficient, but more complicated one. Hinged devices may seem simple, but the loads on the associated mechanisms can be very high and bearing failure is a potential problem – the articulated pontoon falls into this category. Oyster avoids the problem to a great extent by allowing the paddle to move freely in storm conditions. It is believed that this is not an option for Pelamis and that active control is needed to prevent structural failure. Bearing failure has been a problem for Pelamis – although now overcome.

A more recent development is the approach taken by AWS (AWS, 2012) who, after two unsuccessful development projects, AWS-I and AWS-II, chose to resurrect a concept pioneered in the 1980s by the Energy Systems Group, of Coventry's Lanchester

Polytechnic, (Bellamy, 1985) but not followed up at that time due to lack of government support. This device, the AWS-III, shown in Figure 1.14, uses the deformation of the floating bodies to extract energy from the waves – an idea that is common to some of the recent, more promising developments, namely the Anaconda (Farley et al., 2012; Chaplin et al., 2012), the Distensible Buoy (Farley, 2010), the Free-Floating Clam (Farley, 2011d) and the free-floating axi-symmetric Clam (or “Squid) (Farley, 2011b).

Unfortunately while writing-up this thesis both Pelamis, and Oyster have failed commercially. Furthermore it appears that AWS have moved away from developing AWS-III and have obtained support through Wave Energy Scotland’s call for Novel Wave Energy Converters (WES, 2016a). Apart from the AWS-III device, the other, deformable body devices are at the early stage of theoretical assessment and small-scale tank testing. This is true of the concept chosen for the current investigation, namely the Free-Floating Clam.

Figure 1.14: 1:9 Scale model of the AWS-III under test on Loch Ness, June 2010

In the hunt for the concept that will succeed it is perhaps instructive to speculate as to the reasons for the failure of Pelamis and Oyster. Since the development of these devices received significant government support one can only assume that the commercial case for

both of them was not sufficiently attractive to a private investor, i.e. a large public company and possibly also to an energy supplier who would require a system that would provide electrical power at a sufficiently low cost. Pelamis would appear to be too complicated, and full of expensive hydraulic machinery that would be subject to large oscillating loads. Oyster seemed to be a good workman-like device, but with two failings. Firstly, dependent on the nature of the sea bed its attachment could be difficult, particularly as it needs to resist continuously oscillating loads. Secondly, in comparison with moored devices the possible deployment locations are limited since it must be installed in sufficiently shallow water. Potential sites could be limited since if close to the shoreline, it would provide a potentially significant hazard to small boats, swimmers, etc.

The conclusion is then that the ultimate prize will go to the developers of a WEC that is not only efficient in terms of harvesting wave power in the hydrodynamic sense, but also employs a simple and robust PTO. It should also be capable of adaption to a wide range of locations.

# 2 Device Development and Physical Modelling

## 2.1 Introduction

During the course of the study several physical models have been trialled. The purpose of this section of the report is to describe these physical models and their construction, together with the reasons for the various changes. Details of the trials and their analysis are dealt with in Chapter 4 while the development of the mathematical models is covered in Chapter 3.

However, before looking the physical models it is useful to consider how the present study would fit into the overall development of a wave energy converter – through to full scale deployment.

## 2.2 Development pathway

In bringing a new device to the point of full scale commercial deployment it is clear that the project needs to progress in a logical manner. Hence it is desirable that the development moves forward in phases, where progress to each phase depends on the satisfactory outcome of the previous phase. The Hydraulic & Maritime Research Centre (HMRC) have put forward a protocol for the development of wave energy converters (WECs) that has been generally accepted by the industry (Holmes et al., 2007). The five phases are:

1. Validation Model - Fundamental Testing in Regular & Random Waves
2. Design Model - Testing in Realistic Sea Conditions
3. Process Model - Testing in Conditions Representative of Deployment Site
4. Prototype Model - Large Scale Pilot Plant at Sea
5. Demonstration Model - Pre-production prototype

The process is very much orientated around the model scale. Phases 1 and 2 typically employ models of say 1:25 or 1:50. The phase 3 model would be 1:6 or 1:10 and phase 4 and 5 employ full scale devices. The mathematical modelling becomes more detailed as the project proceeds.

What appears to be missing in the HMRC description of the process is an important activity – that of preparing a feasibility study and updating it as the project progresses. This is a vital task in ensuring the success of a commercial venture by identifying the best way forward and the development paths to avoid. The process of preparing a feasibility study is a well-documented activity where all aspects of the venture are considered.

Before even embarking on a programme such as the HMRC protocol it is clearly a good idea to establish whether a particular device has potential – at least as a concept – and this is where the present study fits in. During the course of study the Clam's energy capture performance has been assessed. Practical testing, that is at a level broadly consistent with HMRC's phase1 activity has been carried out and a parallel theoretical study has been undertaken. The study concludes by describing the main features of a design for a full size WEC moored at the Wave Hub test site and predicts its annual energy capture (see Chapter 5).

Future development of the Clam (outside the scope of the present study) would follow the HMRC protocol from stage 1 – supported by a comprehensive feasibility study.

## 2.3 Description of device

The device chosen for the study is the wedge-shaped Free Floating Clam (Farley, 2011d), shown in Figure 2.1.

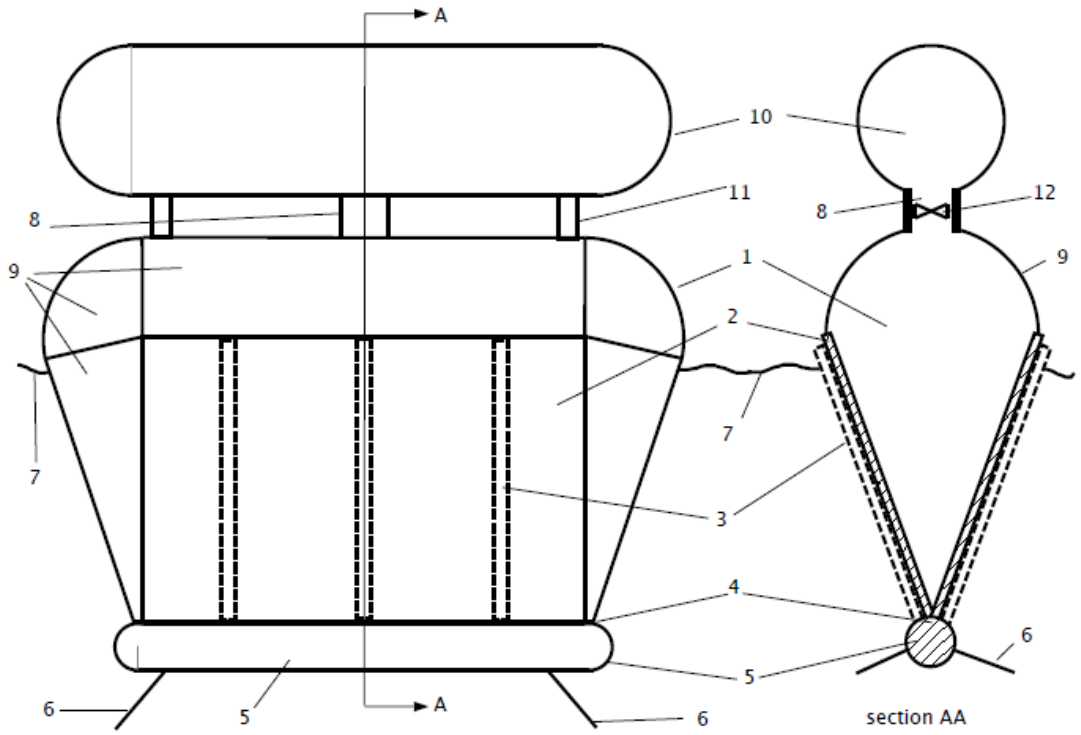


1 Clam, 2 face plate, 3 ribs, 4 flexible joint, 5 ballast, 6 mooring, 7 sea level,
8 interconnection, 9 fabric, 10 upper vessel, 11 support, 12 turbine

Figure 2.1: Free Floating Clam (Farley, 2011c)

The free floating Clam (patent application GB 1102910.5)(Farley, 2011d) is anchored with its wide faces parallel to the wave fronts, typically 40 m wide. The front and rear plates are flexibly connected at the bottom and held apart by the air pressure between them. At the top and sides, the Clam is closed by inextensible polymer-coated fabric. The opening and shutting of the Clam pumps air through a turbine into and out of a second pressure vessel also made of polymer-coated fabric.

The patent describes the way in which the resonant period in heave may be lengthened by employing “Clam action” and the compressibility of the air contained within the structure. If the device moves down the pressure outside the Clam rises and the closing force increases. This reduces the displacement as the Clam closes with the result that the Clam sinks further than it would if the sides were fixed. The internal air pressure rises to the point where the Clam angle is stabilised, and the result is that the vertical buoyancy restoring force – or rather the vertical spring effect due to buoyancy - is reduced and the natural period in heave is accordingly lengthened. The heave period is thus controlled by the volume of air enclosed by the Clam and the second pressure vessel.

While this behaviour does occur, its effect is not as pronounced as simple theory would suggest. In fact it will be seen later (Chapter 3) that the most promising configuration for the Clam does not use this effect, since it has been found both by mathematical and physical modelling that constraining the Clam in heave results in greater power capture. That being said, the Initial and Mark I models were constructed specifically to verify that the heave resonance would vary in the way suggested.

## 2.4 Initial Clam model

An initial test of the Clam behaviour was carried out using a large cylindrical container of internal diameter 600 mm, filled with water to a depth of approx. 450 mm. The Clam was formed from two pieces of plywood (270 mm wide by 385 mm high), resting on a piece of ballasted copper tube, as shown in Figure 2.2. The air-spring was simulated by a steel compression spring, and the assembly was made watertight by being placed in a bag, improvised from discarded polythene packing material. Water pressure held the whole assembly together in a very effective manner. The vertical position of the device was estimated by marking a centimetre scale on the side of the Clam and using its position in relation to the water level as the indicator.

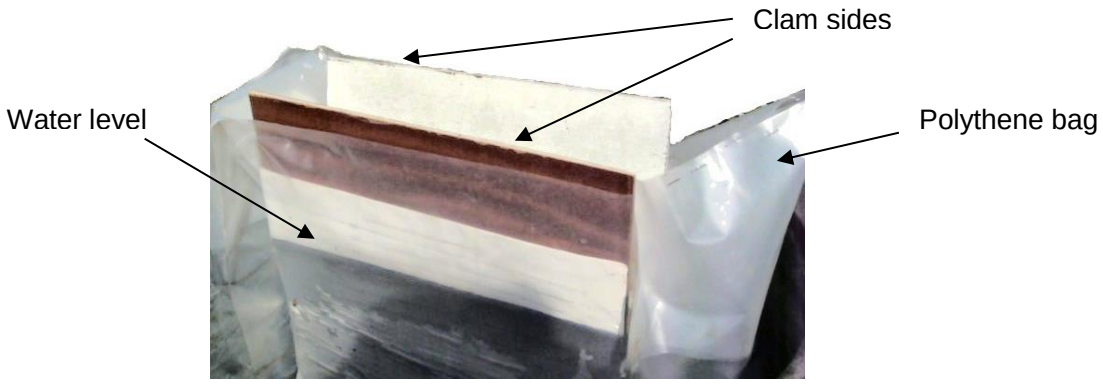


Figure 2.2: Initial Clam Model

By adjusting the mass of the assembly and moving the spring to different distances from the pivot it was possible to observe the behaviour of the device. The spring was replaced by a rigid prop to show the response with no Clam action.

The measured resonant periods were compared with those calculated by the theory of Section 3.2. Table 2.1 shows the results.

Table 2.1: Calculated and Measured Resonant Periods

| Test Ident | | Total Mass, incl. "Added Mass", kg | Predicted Period, sec | Measured Period, sec |
|---|---|---|---|---|
| 2_1_a | (sprung) | 1.451 | 0.68 | 0.8 |
| 2_1_b | (rigid) | | 0.62 | 0.62 |
| 2_2_a | (sprung) | 1.814 | 0.77 | 0.82 |
| 2_2_b | (rigid) | | 0.69 | 0.62 |
| 2_3_a | (sprung) | 2.177 | 0.89 | 0.84 |
| 2_3_b | (rigid) | | 0.73 | 0.75 |
| 2_4_a | (sprung) | 2.540 | 1.12 | 0.89 |
| 2_4_b | (rigid) | | 0.78 | 0.78 |

These initial tests demonstrated that the resonant period could be changed by Clam action. The response with no Clam action (i.e. the rigid Clam) matched the calculated value reasonably well if a hydrodynamic added mass of 0.6 times the actual mass was included.

The resonant period with Clam action was not so well predicted, but matched best if the measured spring rate of 2.25 N/mm was assumed. Clearly further analysis and carefully instrumented tests were needed.

## 2.5 Mark I wave tank model

The Mark I wave tank model was constructed to the sketch shown in Figure 2.3. The width of the Clam was 350 mm.

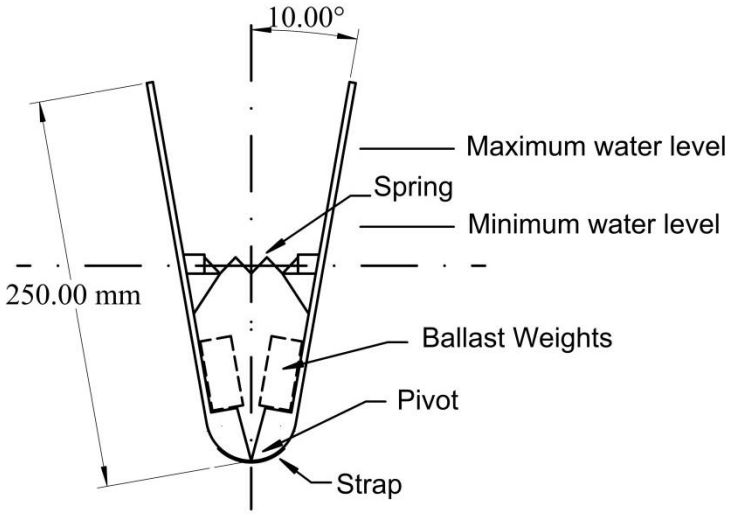


Figure 2.3: Mark I Wave Tank Model – Cross Section

The thinking behind the change in geometry from the simple Clam was to avoid the drag that would be introduced by the ballast mass suspended beneath the buoy, and to provide space for equipment in a full-size embodiment of the Clam. The ballast mass was contained within the WEC, in order keep drag to a minimum. A very useful feature of the design was that there was still sufficient buoyancy to avoid sinking even with the Clam closed.

However, during testing it was found that the pitch resonance period was too short and too close to the heave resonance, resulting what appeared to be unacceptable motions when subjected to a wave input.

The design was hastily modified in line with Figure 2.4.

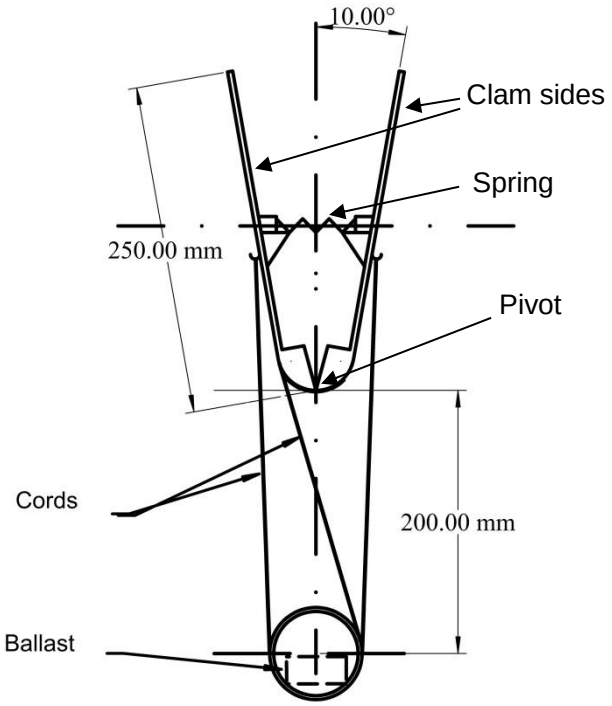


Figure 2.4: Mark I Wave Tank Model with keel

The additional structure consisted of a clear plastic tube into which the ballast weights were placed, the tube itself being suspended from the upper part of the buoy by cross-braced cords, designed to provide a rigid connection.

The model then behaved very well in terms of its sea-keeping behaviour in both heave and pitch. The roll resonance was however found to be a problem – being close to the heave resonance. In the full-scale device this is likely to be unacceptable, but could be avoided by ensuring by design that undesirable resonances were well separated from those resonances needed for good energy capture performance.

A series of still water response tests were also carried out, with the model behaviour being similar to that of the initial tests.

## 2.6 Mark I wave tank model with bag

The intention behind the wave tank testing carried out at the University of Plymouth at an early stage in the project was to demonstrate the ability of the Clam to collect power from sea waves and if possible, to make quantitative measurements of power capture. Francis Farley suggested that this could be achieved by physical modelling of the system including the pressurised bag. Hence the Mark I model was modified by enclosing it with a polythene bag, as shown in Figure 2.5.

Figure 2.5: Mark I Wave Tank Model plus bag in Plymouth Laboratory

Although the stage was reached where a model, with enclosing bag was trialled, see Figure 2.5, little useful data was obtained. There were three main problems:

- Air compressibility effects difficult to scale correctly,
- Losses in connecting pipework,
- Practical difficulties in making a leak-tight system.

These are further discussed below.

### 2.6.1 *Air compressibility*

In order to model the springing effect of the air within the bag it was necessary to connect a large external reservoir via a flexible tube, as can be seen in the photograph (Figure 2.5). The size of the reservoir was dictated by the need to correctly scale the effect of air compressibility in the model. The laws of model scaling require that pressure scales as the scale factor – in this case by a factor of 100. Ideally one would need to scale ambient

pressure by a factor of 100. This is physically impractical hence the need to add the external reservoir. Order of magnitude calculations recently carried out indicate that a volume of the order of 0.6 $m^3$ would have been needed. Although the scaling implications were not fully understood at the time of the test, the reservoir had a volume close to this value.

### 2.6.2 *Losses in connecting pipework*

The intention was to measure the power capture by observing the pressure drop across an orifice plate, placed in the line to the reservoir. In order to restrict the significant losses to the orifice plate itself the size of the connecting tubing should have been larger than the size chosen. However it was considered that providing a sufficiently large tube to overcome the problem of losses would result in a situation where the motion of the device would be unacceptably compromised, since the internal air pressure in the tube would render it insufficiently flexible. Hence the proposal to use an alternative method of simulating the PTO, as described in Section 2.7.4.

### 2.6.3 *Building a leak-tight system*

Building a leak-tight system was the third area of difficulty, which no doubt could be overcome with care and the development of suitable manufacturing techniques.

It was decided to build on the experience with the early Clam, by continuing with the use of polythene sheet. The University has a manual heat sealing press that was used to make the bag shown in the photograph (Figure 2.5). Joining the tube to the bag was a difficult design problem that was however very successfully overcome in some test samples. Providing the same degree of sealing on the wave tank model itself was more difficult and resulted in a minor leak that was however cured to a satisfactory extent with Sellotape.

In addition, during testing it was found that there was a slight leak at the base of the model, thought to be via pin-holes caused by rough handling. However, the most severe problem resulted from leaks in the large air reservoir, which was not sufficiently air-tight. The lesson to be learnt is to aim for a 100% leak-tight system and check it out at each stage while it is being constructed.

## 2.7 Design and construction of Mark IIa wave tank model

### 2.7.1 *Main assembly*

Figure 2.6 shows the basic geometry of the Mark IIa wave tank model, which is constructed almost entirely from acrylic (Perspex).

The hinged sides are made from 15 mm thick acrylic sheet, the thickness being chosen to provide sufficient depth for screw fixings and to avoid the need for additional stiffening. As can be seen from the picture (Figure 2.7) the device is not enclosed. The Clam sides are kept apart by the Power Take-Off ram(s) rather than by employing the air pressure inside a fully enclosing bag. The model scale is 1:50, the width of the Clam being 40 m at full size.

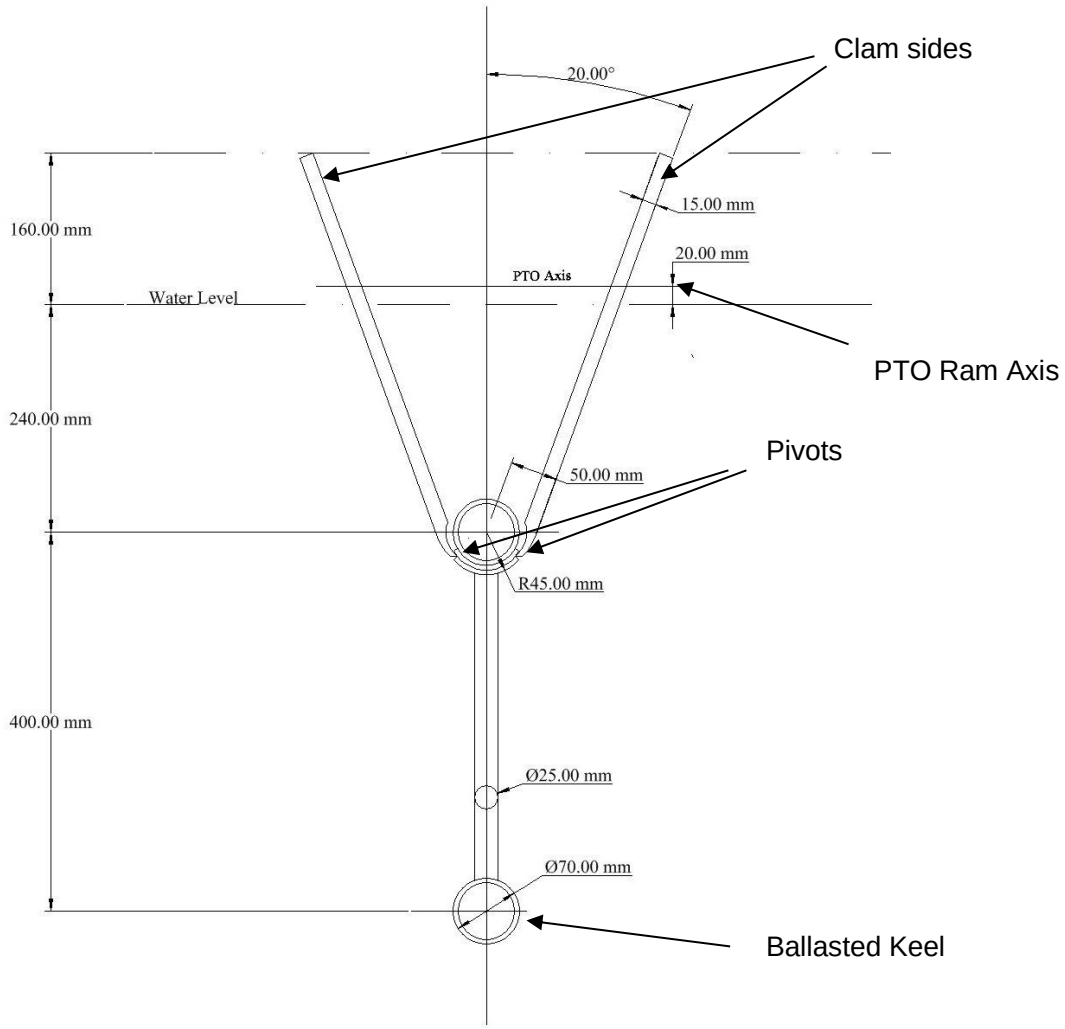


Figure 2.6: Basic Geometry of Mark IIa Wave Tank Model

Figure 2.7 shows the Mark IIa Wave Tank Model ready for testing. The small white spheres are the targets for the Qualysis motion capture system that logs the Clam's position in six degrees of freedom.

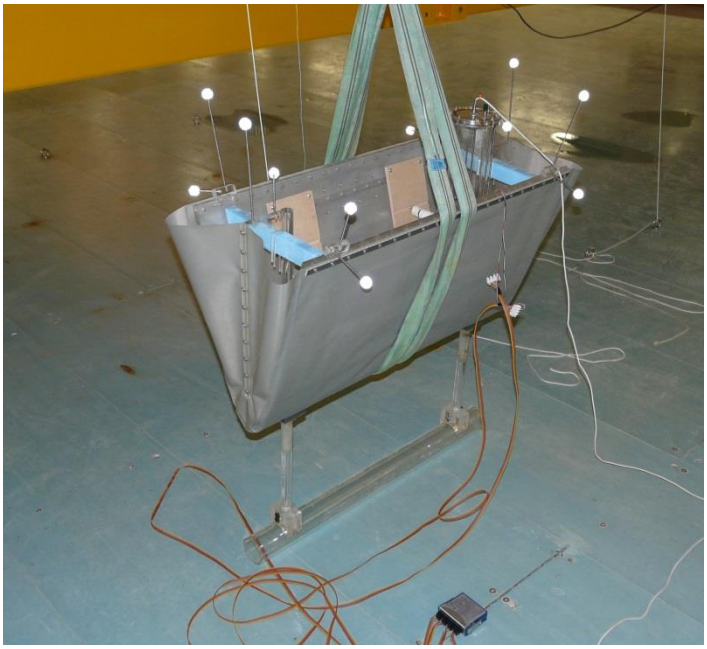

Figure 2.7: Mark IIa Wave Tank Model ready for testing

Figure 2.8 shows the parts of the Clam assembly that are constructed from acrylic sheet and tube. The Computer Aided Design (CAD) tool, SolidWorks was used to provide both the manufacturing drawings and the perspective view shown here. The two vertical members are part of the main body assembly and serve to support the Qualysis targets that provide data on the position of the main structure, which includes the keel.

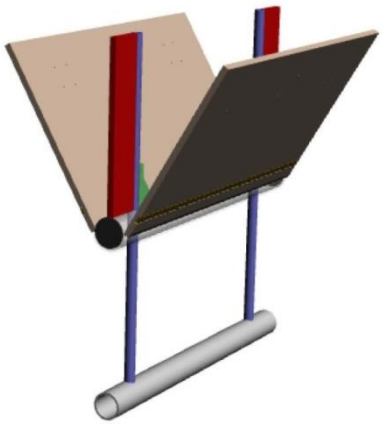

Figure 2.8: CAD model of Mark IIa Wave Tank Model

### 2.7.2 *Flexible bag*

Figure 2.9 shows the bag after it had been tailored to the Clam by Griffon Hoverworks Ltd. The Clam is shown in the inverted position prior to having the ballasted keel assembly fitted. The bag is made from a grey-green coloured material which consists of a thermoplastic coating on a nylon basecloth (weldable), thick coating on one side and a 'lick' coat on the other. The weight of the material of the bag is approximately 250 gm/$m^2$ and its thickness is 0.6 mm.

Figure 2.9: Flexible bag for Clam

### 2.7.3 *Hinge*

Figure 2.10 shows the hinge diagrammatically. The entire width of the Clam side is shaped to form a knife edge pivot. A strap completes the assembly – again this runs the whole width of the Clam side and is constructed of the same material as the bag. Water pressure holds the Clam side against the main structure.

The hinge has been found to perform its function well. It moves freely and appears friction-free.

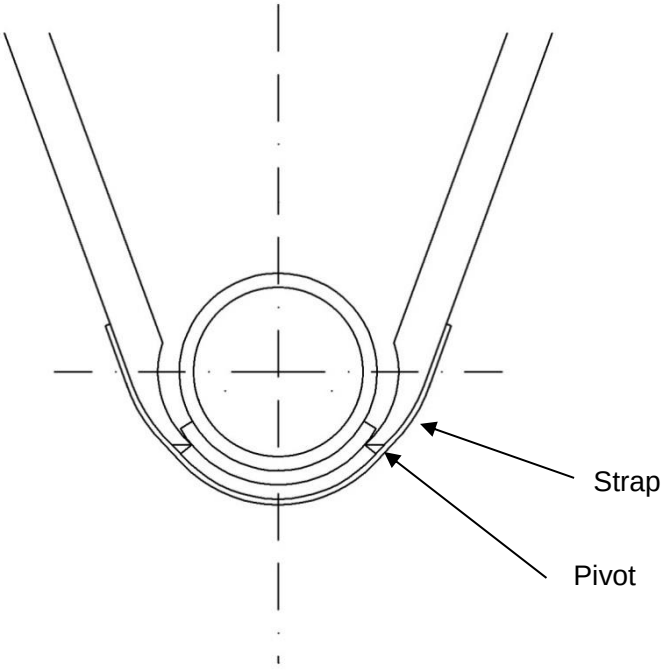


Figure 2.10: Hinge Assembly

### 2.7.4 *Power Take-Off (PTO)*

Figure 2.11 shows the principle of operation of the Power Take-Off (PTO). The miniature hydraulic ram, constructed from a bicycle pump holds the Clam sides apart.

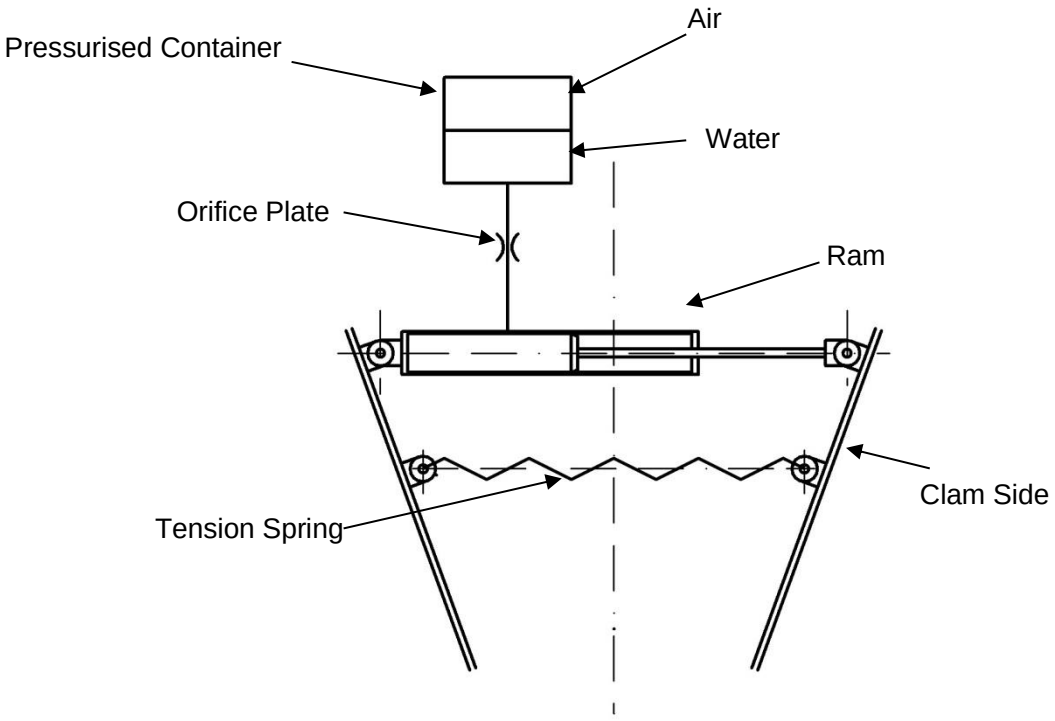


Figure 2.11: Power Take-Off Schematic

The whole system is pressurised by the air pressure in the container such that the piston seal in the ram maintains near leak-free contact.

The orifice plate in the hydraulic line provides the PTO damping while the PTO stiffness is provided by the compressibility of the air in the reservoir and by the tension spring.

The compressive load in the ram is measured by load cells. Since the hinge friction may be assumed to be negligible - and the tension spring is friction-free – the result is that all the damping in the PTO (whether due to the orifice or seal friction) is measured and used in the calculation of power capture.

Much of the testing was carried out with two PTO assemblies in the Clam model, see Figure 2.12 . However testing on the final day of the first set of trials employed a single PTO assembly.

Figure 2.13 contains a photograph of one of the PTO assemblies. Figure 2.14 shows the PTO minus the reservoir and orifice plate, while Figure 2.15 shows the plate itself. Figure 2.16 shows the instrumented strut that replaces the PTO for tests where Clam action is prevented.

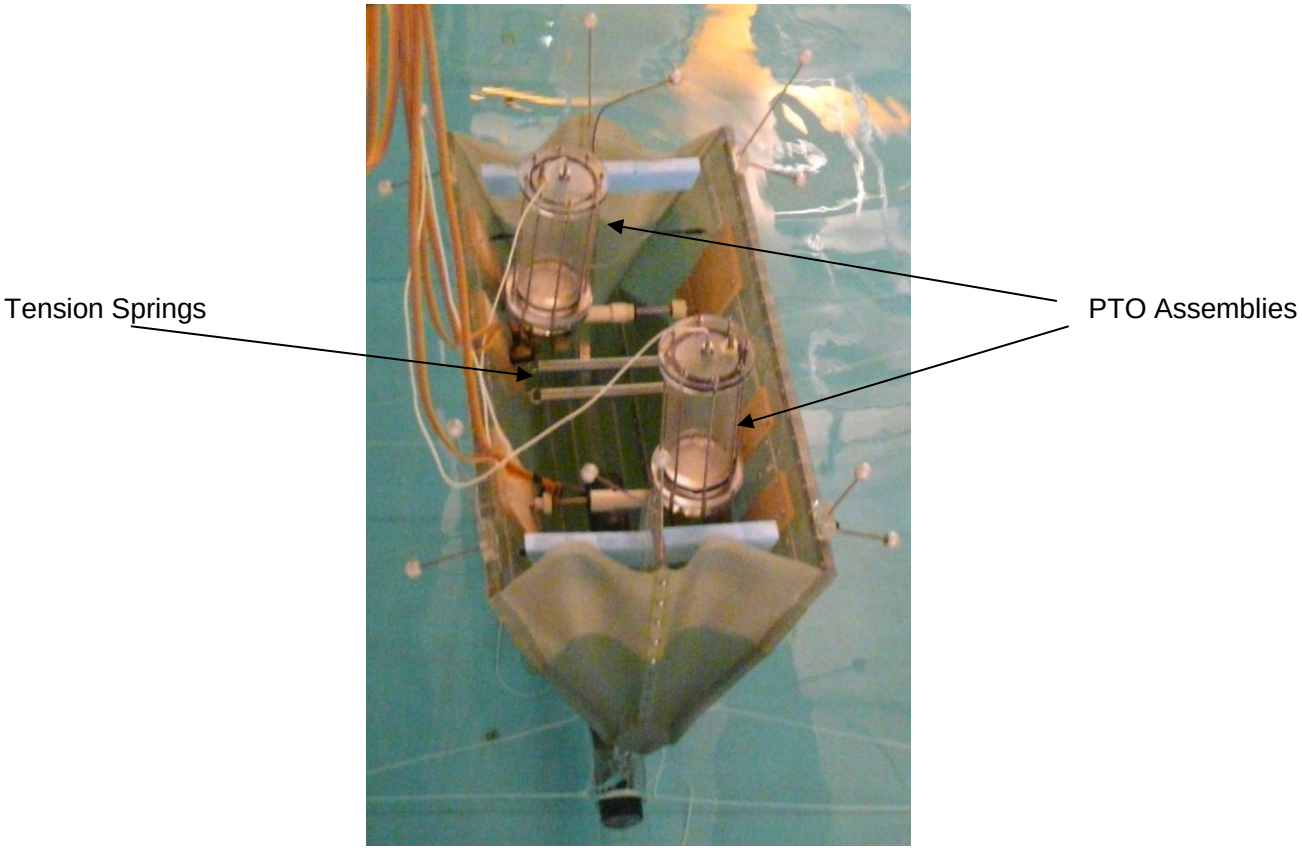


Figure 2.12: Clam Model - floating

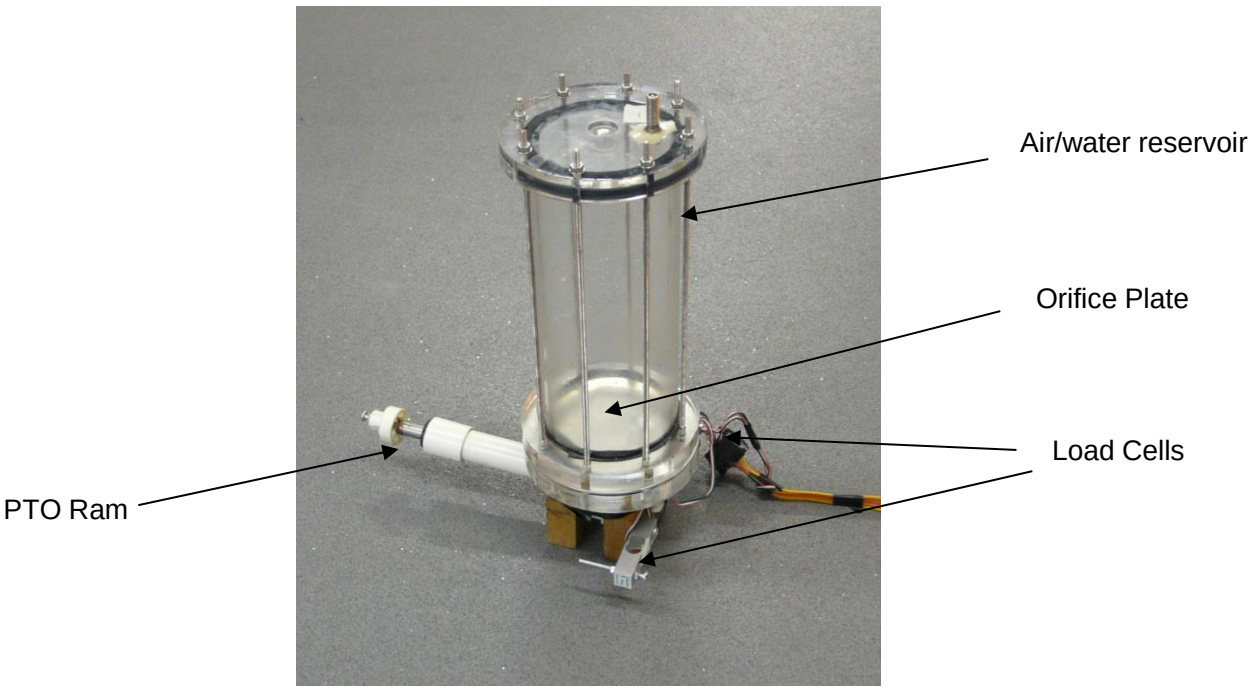


Figure 2.13: Power Take-Off Assembly

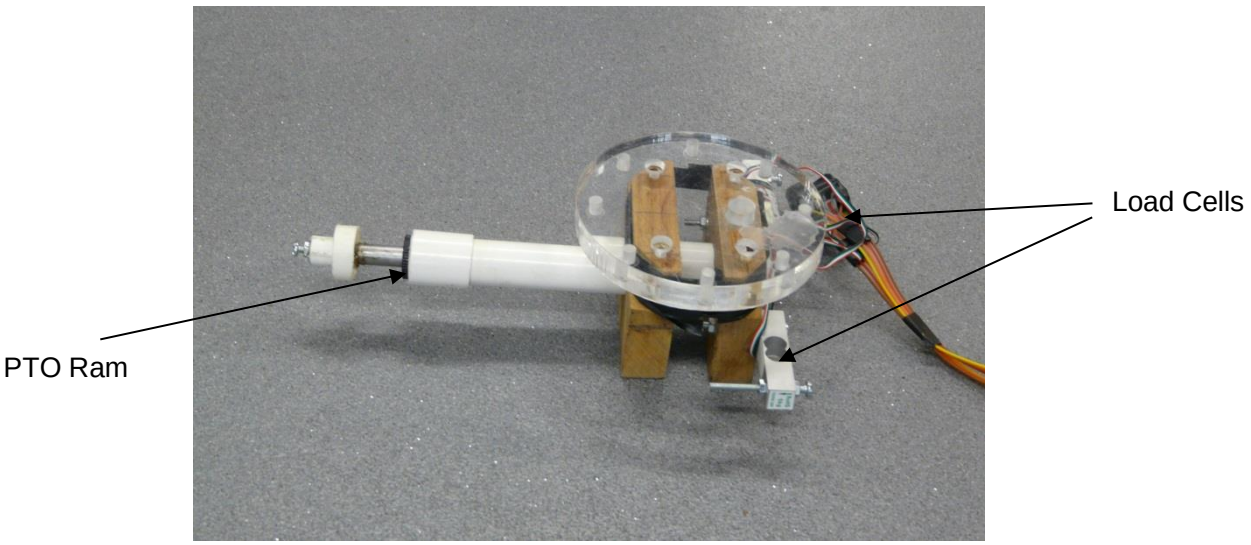


Figure 2.14: Power Take-Off Base Assembly

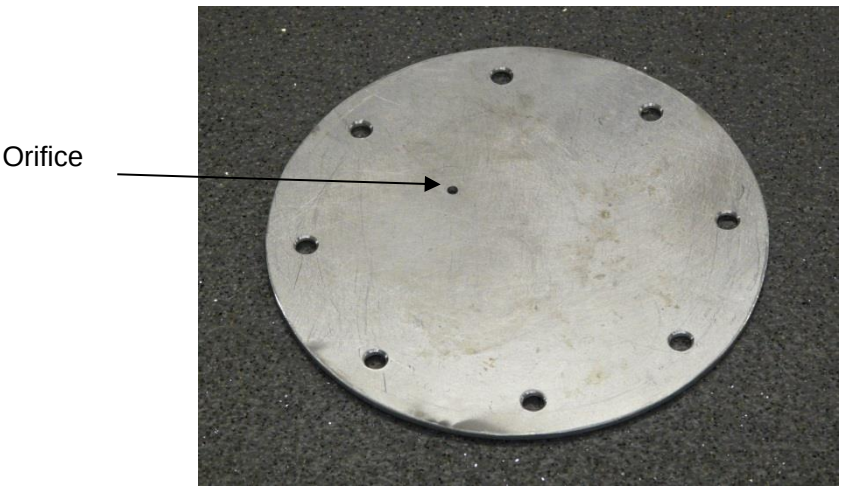


Figure 2.15: Orifice Plate

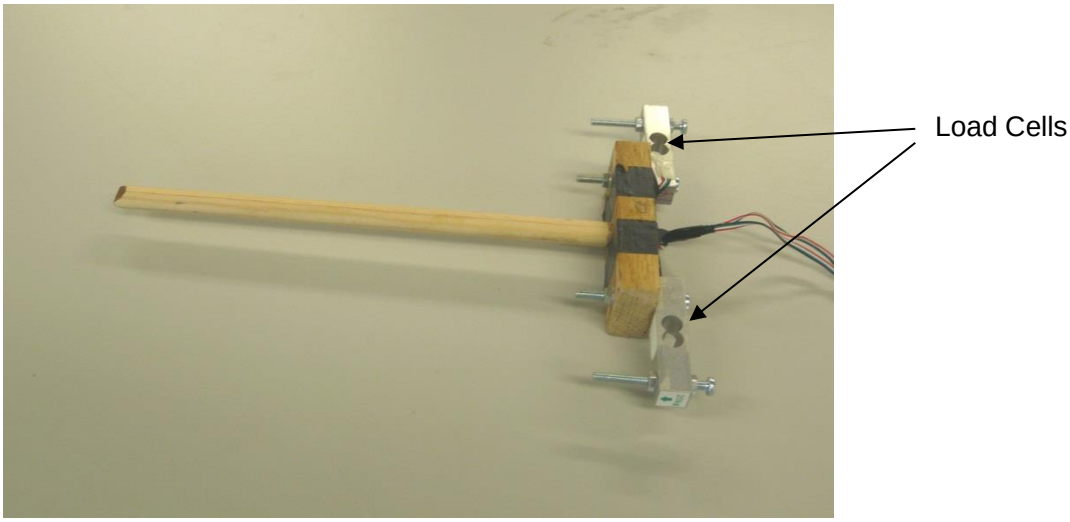


Figure 2.16: Strut

### 2.7.5 *Ballast*

The Clam model is ballasted by adding a number of cylindrical lead ballast weights, see Figure 2.17.

Figure 2.17: Ballast Weights for Clam

There were 7 weights – see Table 2.2

Table 2.2: Ballast Weights for Mark IIa Model

| Weight Identification | Mass, kg |
|---|---|
| A | 4.645 |
| B | 4.657 |
| C | 4.555 |
| D | 4.701 |
| E | 4.701 |
| F | 2.315 |
| G | 2.359 |

These weights may be placed in two positions – in the keel and in the cradle, as shown in Figure 2.18.

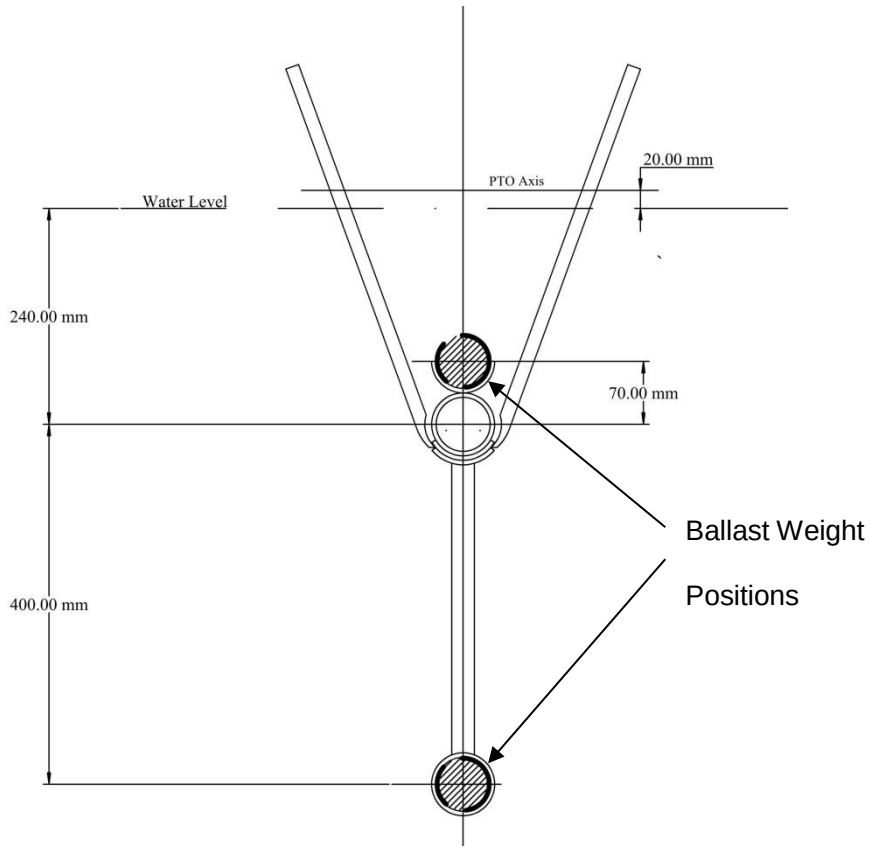


Figure 2.18: Ballast Weight Positions

2.7.6 *Mass properties:*

Prior to carrying out the trials the expected mass properties were calculated for each of two test configurations as shown in Table 2.3. Configuration 1 relates to the free-floating WEC where heave motion is not restrained. Configuration 2 applies to the case where heave motion is restrained. In this case the WEC is tethered to the floor of the wave tank and the reduction in the overall mass allows the WEC's buoyancy to keep the tether taut.

Table 2.3: Calculated Mass Properties of the Mark IIa Model

| Parameter | Configuration 1 – free floating | Configuration 2 – heave restrained |
|---|---|---|
| Ballast in Cradle, kg | 10 | 0 |
| Ballast in Keel, kg | 15 | 0 |
| Total Model Weight, kg | 43.33 | 18.33 |
| CG posn below CL of upper tube, mm | 79 | 140 |
| CG posn below waterline, mm | 319 | 100 |
| Moment of Inertia about CG, kg $m^2$ , Roll | 5.99 | 0.732 |
| Moment of Inertia about CG, kg $m^2$ , Pitch | 3.22 | 3.499 |
| Moment of Inertia about CG, kg $m^2$ , Yaw | 2.4 | 1.03 |

Having calculated the expected mass properties (as given in Table 2.3), measured mass properties for the equivalent configurations are given in Table 2.4. It can be seen that they agree closely, namely 43.34 kg versus 43.33 kg for the free floating configuration and 20.08 kg versus 18.33 kg for the heave restrained configuration. The actual model weights for individual tests varied depending on the precise configuration, such as the number and position of ballast weights chosen, the number of PTO assemblies used and the quantity of water in the reservoir(s). However, account has been taken of these variations in the analysis of the trials.

Table 2.4: Measured Mass Properties of the Mark IIa Model

| Parameter | Configuration 1 – free floating<br>PTO replaced by fixed length prop | Configuration 2 – fixed in heave<br>PTO replaced by fixed length prop |
|---|---|---|
| Ballast in Cradle, kg | 4.701 | 0 |
| Ballast in Keel, kg | 18.558 | 0 |
| Total Ballast Weight, kg | 23.259 | 0 |
| Weight of wooden prop, kg | 0.2 | 0.2 |
| Weight of Model without Ballast or PTOs, kg | 19.88 | 19.88 |
| Total Model Weight, kg | 43.34 | 20.08 |

## 2.8 Mark IIb wave tank model

### 2.8.1 *Description of modification*

Wave tank testing of the Mark IIa model indicated the need to reduce the friction levels in the PTO. Consequently a scheme was devised whereby the hydrostatic forces on the Clam sides were balanced by tension springs as shown in Figure 2.19. The springs were essentially friction-free and allowed the PTO ram to operate at a lower force level, thus reducing the ram friction since the load on the piston seal was reduced.

The modification involved a pair of cantilevered arms and associated springs. Two alternative types of springs were incorporated:

- Coil springs (Figure 2.19) – Mark IIb_1, and
- Constant force springs (Figure 2.20) – Mark IIb_2.

The constant force springs were of particular significance, since mathematical modelling indicated that the smaller the PTO stiffness, the greater would be the power capture. In addition the constant force springs accommodated the full range of movement, whilst the choice of coil springs was determined by the required force levels and stroke. In consequence the PTO stiffness when using the coil springs was far from optimal.

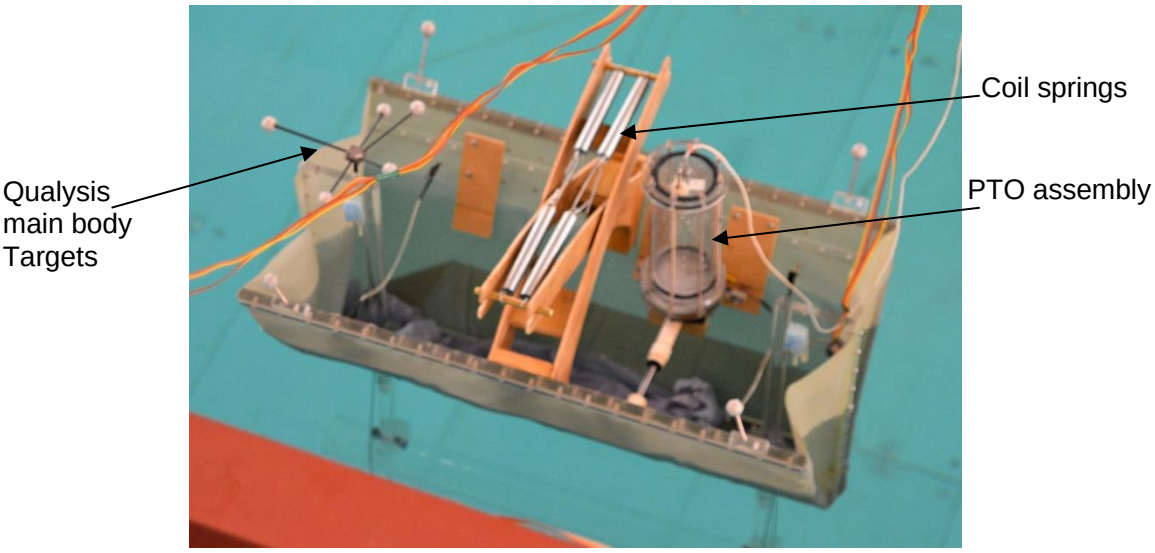


Figure 2.19: Mark IIb_1, Model with coil springs fitted

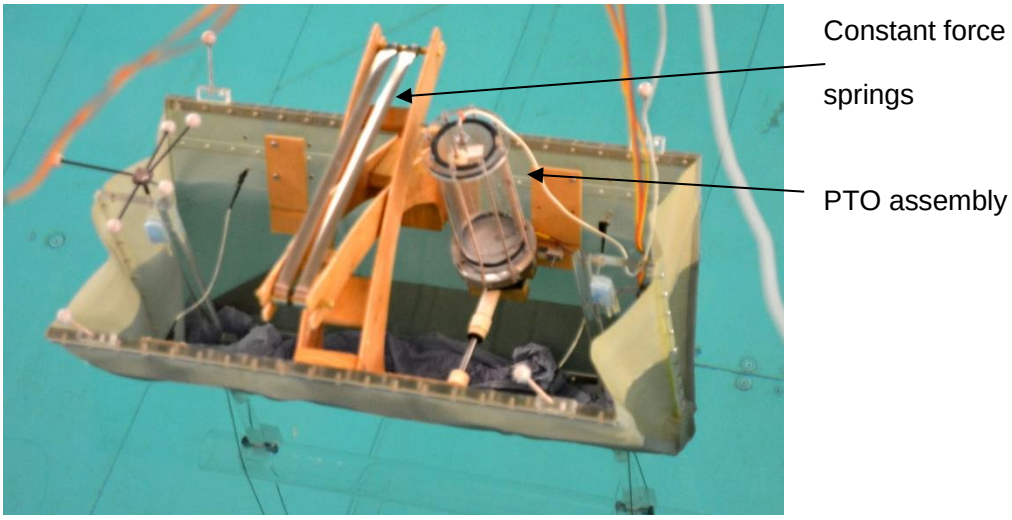


Figure 2.20: Mark IIb_2, Model with constant force springs fitted

# 3 Mathematical Modelling

## 3.1 General

In order to gain an insight into the behaviour of the Clam, Francis Farley developed a series of single degree of freedom (i.e. 1D in heave) models, programmed in Visual Basic (VBA) within a spreadsheet (Farley, 2011a) using the theory presented in a confidential note (Farley, 2011d). A simplified analysis following (Farley, 2011d) that predicts the resonant period, is presented in Section3.2.1.

It should be noted that the effect of viscous drag on the performance of the Clam has not been included in the theoretical analyses. Drag would normally be expected to reduce the power capture of the device. However, the practical tests reported in Chapter 4 demonstrate good agreement with theoretical predictions even though viscous drag has been ignored.

## 3.2 Resonant period and heave stability

### 3.2.1 *Resonant period*

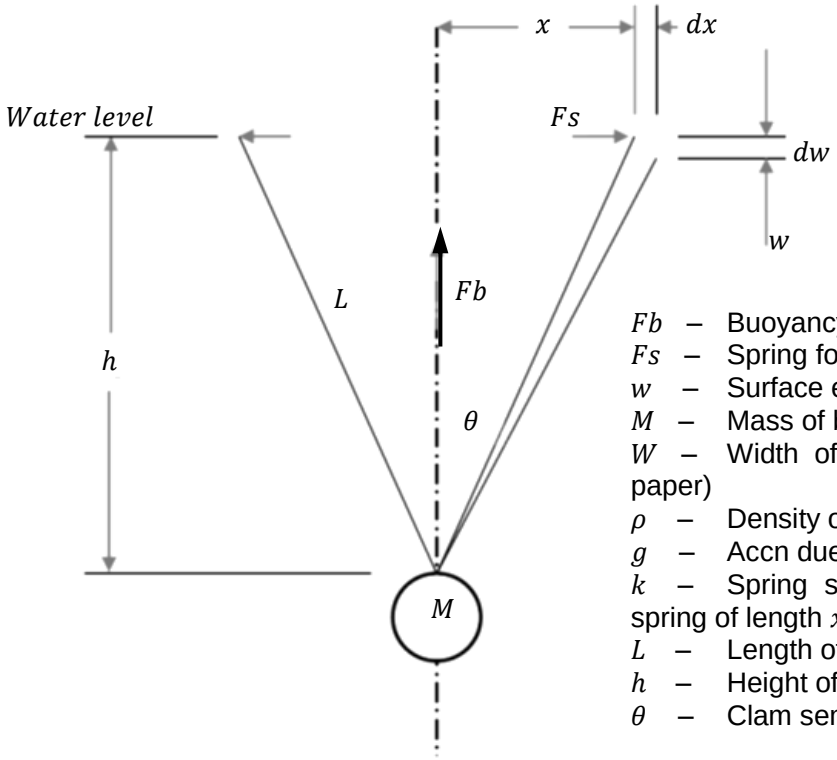


Figure 3.1: Clam Geometry

Consider first the situation where the wave surface rises by a small amount, $dw$, and there is no vertical movement of buoy. The water pressure acting on the clam increases and as a consequence the spring force increases. The increase in spring force, $dFs$, is given by:

$$dFs = k\,dx \tag{3.1}$$

where $k$ is the spring's stiffness and $dx$ is its change in length.

The increase of spring force, $dFs$, can be found by equating the moment due to the increase of water pressure, $Mp$, with the moment due to the spring, $Ms$. Thus:

$$\mathrm{Mp} = Ms \tag{3.2}$$

where $Mp = W\rho gL^2 dw/2$ and $Ms = hdFs = L\cos\theta\, dFs$.

Thus, from equations (3.1) and (3.2), the following relationship may be obtained:

$$\frac{dx}{dw} = \frac{W\rho gL}{2k\cos\theta} \tag{3.3}$$

The change in buoyancy force acting on the device, as the water surface rises, is found by considering the volume of water displaced. The increase of volume due to water rising is $2Wxdw$, and the decrease due to the Clam closing is $2hWdx/2$. Thus the increase in buoyancy force, $dFb$, is given by:

$$dFb = \rho gW\,(2xdw - hdx). \tag{3.4}$$

Substitute for $dx$ from (3.3):

$$dFb = \rho gW\left(2xdw - \frac{hW\rho gL}{2k\cos\theta}\,dw\right). \tag{3.5}$$

Thus:

$$dFb = \rho\, g\, W\left(2\,x\, - \frac{W\,\rho\, g\, L^2}{2\,k}\right) dw, \tag{3.6}$$

since $h = L\cos\theta$.

This equation gives the change of buoyancy force when the water level changes by $dw$. However the relationship is equally valid for the situation where the water level is constant and the buoy moves by the same amount, i.e. by $dw$.

Thus using $z$ to infer vertical motion, and using Newton's 2nd law of motion (Accn = force/mass) we can say that:

$$\frac{d^2z}{dt^2} = -\rho g W \left(2\,x - \frac{W\rho g L^2}{2k}\right)\frac{z}{M}. \qquad (3.7)$$

This is the well-known simple harmonic equation, from which it can be found that the natural period of resonance, $T$, is given by:

$$T = 2\,\pi \sqrt{\frac{M}{\rho\, g\, W(2\,x - \frac{\rho\, g\, W\, L^2}{2\,k})}}\ . \qquad (3.8)$$

It is important to note that the spring coefficient, $k$, applies to a spring of length, $x$. Thus in a lab experiment where use is made of a single spring of coefficient, $k'$, then:

$$k = 2k' \qquad (3.9)$$

### 3.2.2 *Heave stability*

Referring to equation 3.8, it can be seen that the denominator of the expression under the square root sign becomes negative when:

$$\frac{\rho\, g\, W\, L^2}{2\,k} = 2\,x\,. \qquad (3.10)$$

This corresponds to an infinite Natural Period, i.e. the point at which the buoy becomes unstable in heave, i.e. when:

$$k < \frac{\rho\, g\, W\, L^2}{4\,x}\ . \qquad (3.11)$$

## 3.3 AQWA/WAMIT verification

Obtaining the same or similar solution to a problem through the use of more than one technique (or analysis package) is a standard engineering technique in providing confidence in the solution. Since AQWA and WAMIT make the same simplifying assumption of zero viscosity and the same mathematical technique, it is to be expected that each would give the same solution when presented with the same device geometry.

Having successfully compared WAMIT and AQWA results for some simple shapes it was then decided to use the geometry of the wave tank model to complete the exercise. All the hydrodynamic analyses were carried out using the full scale geometry (rather than the scaled dimensions) as it has been found that this provides a more reliable computation. Figure 3.2 shows the geometry chosen for the analysis.

When using AQWA Workbench, the geometric data for the surface elements are computed automatically within the software application. Provided the model is represented correctly on the computer screen, the mathematical definition of the model has a good chance of being correct. The WAMIT package itself has no graphics capability, but may be used in conjunction with a graphics package – MultiSurf (AeroHydro, 2012). In the present instance however it was decided to build the model using a spreadsheet to compute the geometric data. In order to reduce the scope for error, the model was simplified by omitting the uprights that connect the keel to the wedge. Two versions of the AWQA model were constructed – one with and one without the uprights.

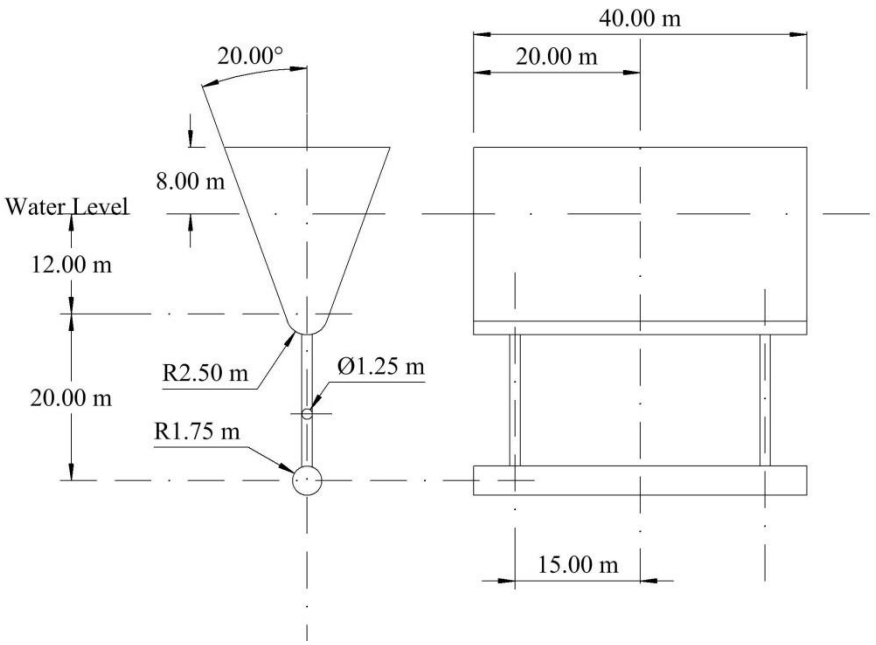


Figure 3.2: Wave Tank Model Geometry for Hydrodynamic Analyses

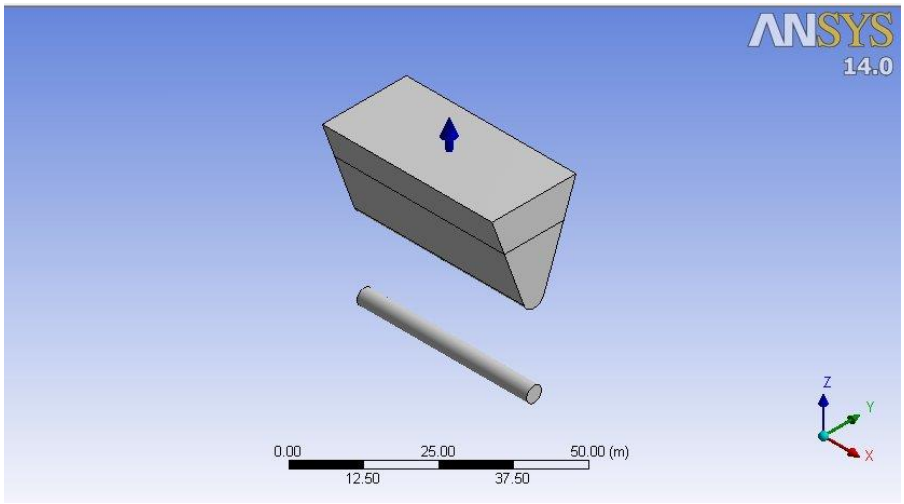


Figure 3.3: AQWA Wave Tank Model – without uprights

Figure 3.3 is a screen shot from the Ansys/AQWA modelling package. As can be seen the uprights have been omitted in order to make the model entirely comparable with the WAMIT model.

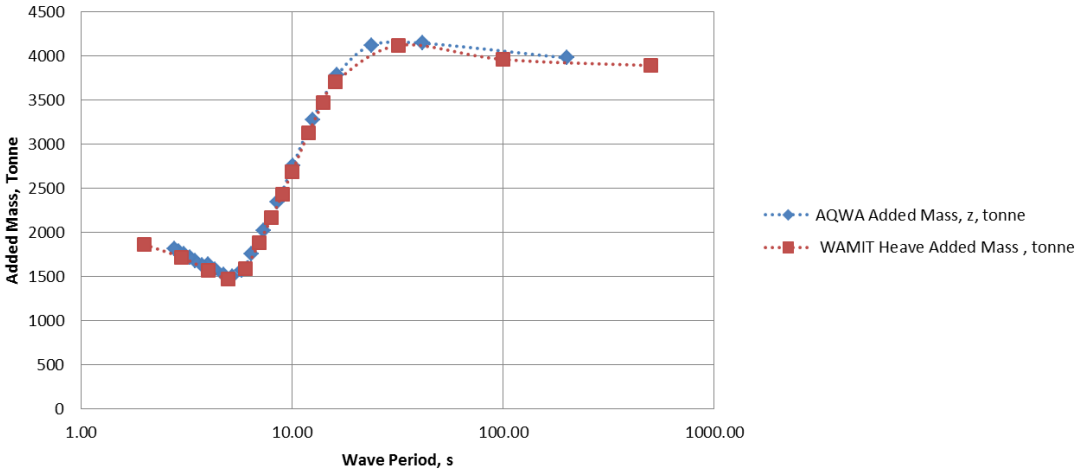


Figure 3.4: AQWA/WAMIT Heave Added Mass Comparison

Figure 3.4 shows heave added mass, while Figure 3.5 shows hydrodynamic damping, both versus wave period. Close agreement between the two modelling tools, AQWA and WAMIT can been seen, thus verifying the mathematical analysis. It should be noted that all the subsequent analysis and performance predictions presented in this document use the same geometrical representation.

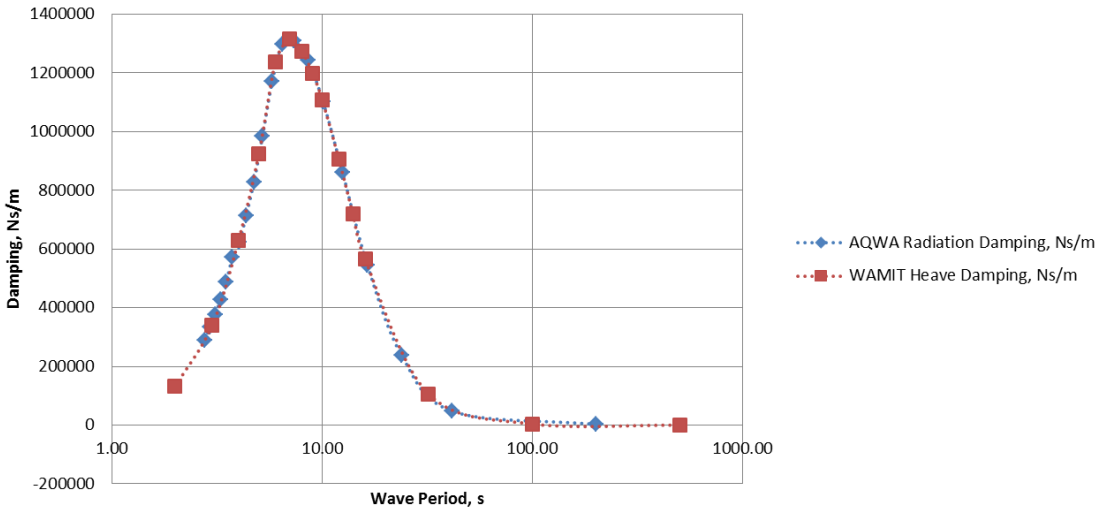


Figure 3.5: AQWA/WAMIT Heave Radiation Damping Comparison

As a final check on the validity of this approach Figure 3.3 and Figure 3.6 present a comparison of the AQWA model of the Clam, with and without the uprights. The Added

Mass and Radiation Damping comparisons are shown in Figure 3.7 and Figure 3.8. The differences between the two AQWA models are seen to be negligible – so much so that the plot for the AQWA model without uprights is obscured by the 'with uprights' plot. The plots are to all intents and purposes identical, thus demonstrating that leaving out the uprights in the WAMIT model is legitimate.

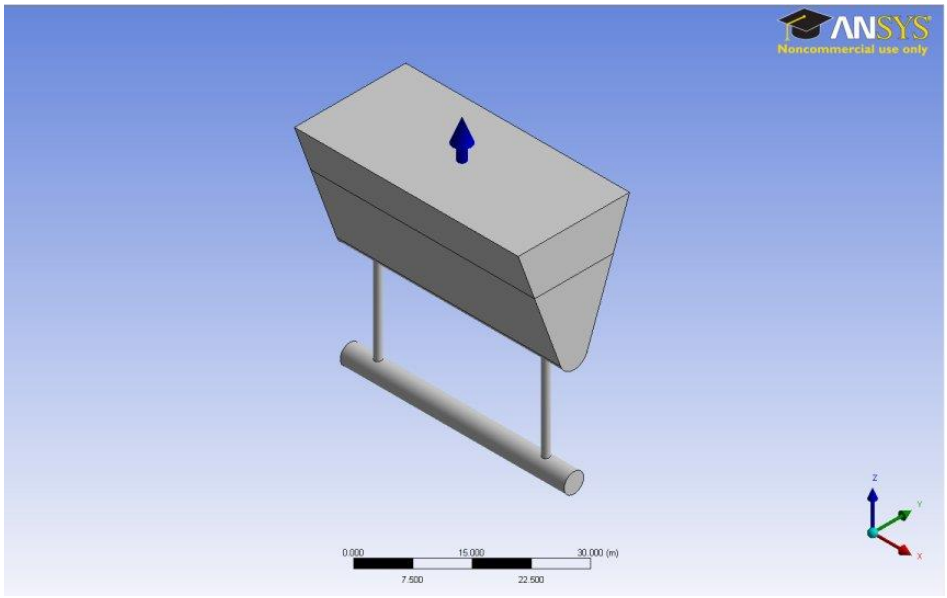


Figure 3.6: AQWA Wave Tank Model – with uprights

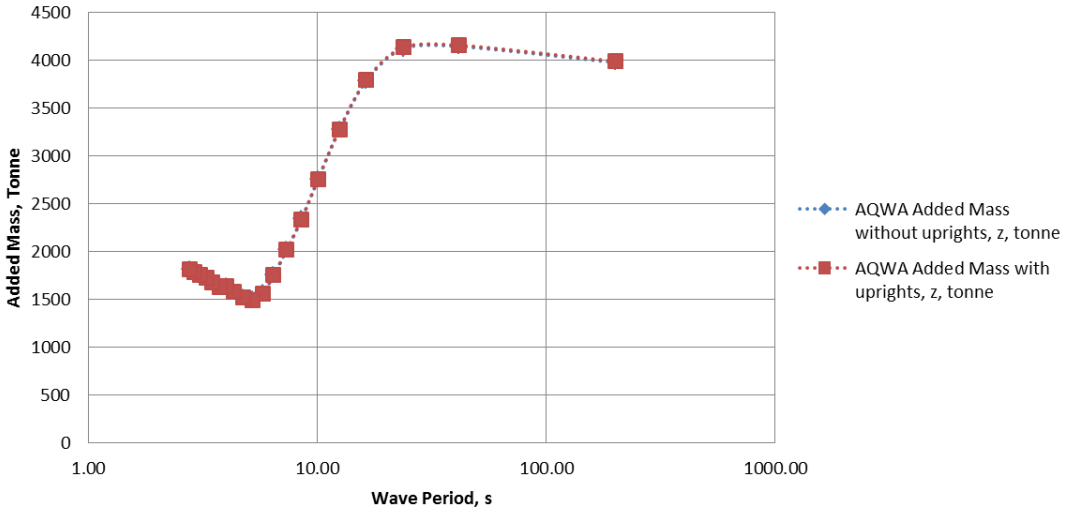


Figure 3.7: AQWA Wave Tank Model comparison – Added Mass

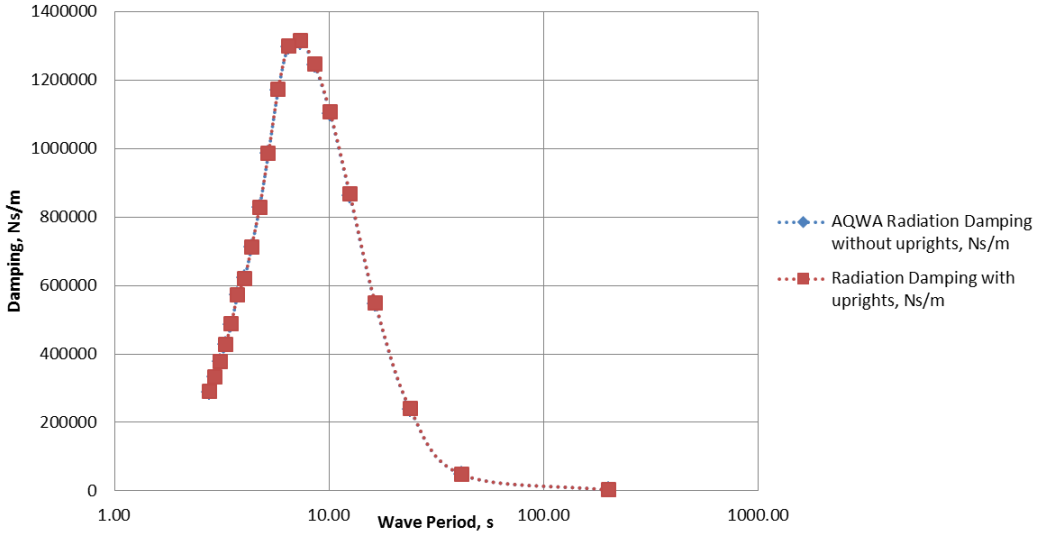


Figure 3.8: AQWA Wave Tank Model comparison – Radiation Damping

## 3.4 Generalised Mode applied to Clam action

As has been explained earlier (see Section 1.4.1) WAMIT allows a “deformable body” to be analysed using “Generalized Body Modes”. The method is explained in the WAMIT User Guide (WAMIT 2012), and Newman (Newman, 1994).

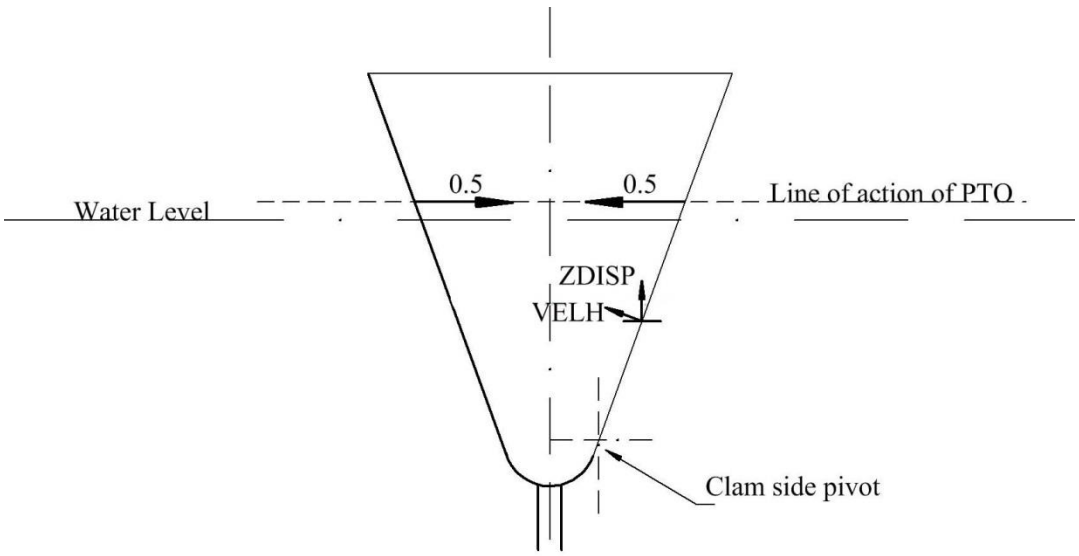


Figure 3.9: Definition of Mode 7

The two sides of the Clam move towards and away from each other, being hinged at their lower ends. This hinged action is the only ‘generalised mode’ and therefore becomes mode 7, the first 6 modes being the conventional rigid body modes. Modes 1 to 3 describe translational motion in the x, y, z (surge, sway and heave) axes respectively and rotation about the x, y, and z axes (roll, pitch and yaw) is described by modes 4, 5 and 6. Mode 7 is known as the Clam mode and is defined by the movement of the PTO ram, as shown in Figure 3.9 - the positive direction of movement being shown by the arrows. Note that the models used in this thesis utilise modes 3 and 7, alone i.e. mode 3, heave, and mode 7, the Clam mode.

By defining the mode in terms of the movement of the PTO ram the result is that the mode 7 force and displacement are identically the same as the PTO force and displacement. Consequently the values of PTO stiffness and damping may be applied to the Clam mode (mode 7) without modification.

The quantities, VELH and ZDISP, need to be computed at all relevant panel vertices in relation to a 'unit displacement' (i.e. a displacement of unity) of the PTO ram, the positive direction of these quantities being shown in Figure 3.9. VELH is the displacement normal to the surface (+ve into the body) and ZDISP is the vertical (Z-direction) displacement. Accordingly the FORTRAN code to compute VELH and ZDISP is incorporated into the FORTRAN subroutine NEWMODES (actually 'newmodes.f'). To complete the model preparation a '.dll' file needs to be compiled.

Computing VELH and ZDISP at each panel vertex is not straightforward, since the Clam pivot is not in line with the outer surface of the Clam. The trigonometric formulae to compute for VELH and ZDISP were thus coded and included in the NEWMODES subroutine. As a precaution the computation was carefully checked using a CAD package.

As previously mentioned, a spreadsheet was used to produce the geometric data file for WAMIT, using the most basic type of element, namely the flat quadrilateral panel, as specified in the WAMIT control files as the "Low Order" panel method.

Although WAMIT should allow the origin to be positioned below the water surface, it was found necessary to put the origin for the axis system on the waterline. The geometric data initially took the vertex of the Clam as a datum. However, this produced results that were clearly in error when attempting to incorporate the Clam mode. After some experimentation with a different analysis option (i.e. the pre-processor program DEFMOD), the most satisfactory approach proved to be the use of the NEWMODES option to model the Clam mode, with the axes origin at the waterline.

Preliminary testing of the model produced results that appeared at first sight to be incorrect - and in fact proved to be so. The model predicted the behaviour shown in Figure 3.10, and discussed more fully below. The concern was that the NEWMODES approach did not correctly compute the hydrostatic coefficients and it was suspected that this was due to the fact that the NEWMODES program code does not completely compute the coefficients when the surface stretches. The mathematics behind this is described in the WAMIT User

Guide (WAMIT, 2012), Chapter 9, 2012) and by (Newman, 1994). Thus the hydrostatic coefficient, $C_{ij}$ , may be calculated by equation 3.12 which is reproduced from the WAMIT User Guide (WAMIT, 2012), equation 9.11.

$$C_{ij} = \rho g \iint_{S_b} n_j (w_i + zD_i) dS \tag{3.12}$$

where $C_{ij}$ is the force component for generalised mode '$i$' due to unit displacement of the body in mode '$j$'.

For definitions of the other parameters refer to (WAMIT, 2012) and (Newman, 1994).

The User Guide (WAMIT, 2012) states that the first term within the brackets is calculated within WAMIT if "newmodes.dll" is used, while the second term, involving the Divergence of the surface displacement vector, is not. Advice was taken from the WAMIT developers who explained that this second part only applies when the surface is stretched. Although the Clam surface is in effect "stretched" as the Clam moves, they advised that this is a minor effect and may be ignored.

A typical, but erroneous output from the WAMIT/NEWMODES analysis is shown in Figure 3.10. Firstly, the PTO response shows a dip near to the resonant peak of the heave motion which was not expected. Secondly it would be expected that the heave amplitude would become equal to the wave amplitude for long period waves – and this did not occur.

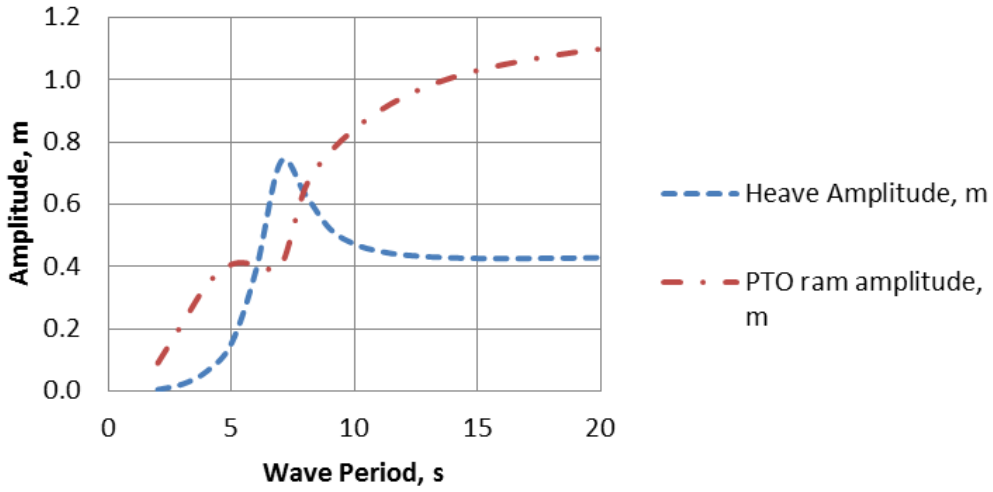


Figure 3.10: Incorrectly predicted Clam response

When the model was physically tested in the wave tank it became clear that the analysis was indeed incorrect. The most likely source was an error in the calculation of the hydrostatic coefficients, $C_{ij}$ , within the WAMIT-supplied NEWMODES program code.

An alternative method of calculating the hydrostatic coefficients was then devised, resulting in response predictions in line with model tests and expectations, as shown in Figure 3.11, which is based on the analysis of Trial 2, see Table 4.1.

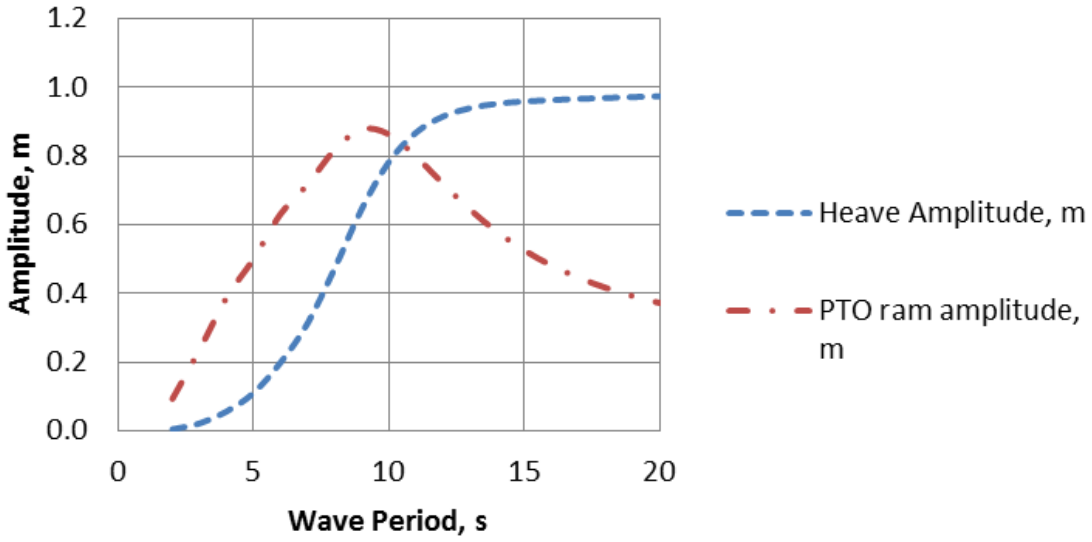


Figure 3.11: Improved prediction of Clam response

The method of calculating the hydrostatic coefficients is now described, taking as an example the Cross Coupled Hydrostatic Coefficient, $C_{73}$. This is given by the change in PTO/Clam force (i.e. mode 7) due to a unit heave displacement of the device (i.e. mode 3). Thus:

$$C_{73} = \frac{dF}{dh} \tag{3.13}$$

where $F$ is the PTO load and $h$ is the vertical distance from the Clam pivot to the waterline.

It can readily be shown that $F$ is given by:

$$F = \frac{\rho g W h^3}{6 Z cos^2\theta} \tag{3.14}$$

where $\rho$ is density of water, $g$ is the acceleration due to gravity, $Z$ is the vertical distance from the Clam pivot to the line of action of the PTO ram, $W$ is the width of the WEC and $\theta$ is the Clam semi-angle

Thus:

$$C_{73} = \frac{\rho g W h^2}{2 Z cos^2\theta} \tag{3.15}$$

A similar approach was used to calculate values for all the hydrostatic coefficients.

## 3.5 WAMIT analysis

WAMIT modelling followed the methodology and examples given in the user manual (WAMIT, 2012), using the flat lower order quadrilateral surface element throughout the analysis. The model input included data files to specify the calculation options, control the progress of the computation and specify the required output data files. Also required were files to define the model geometry and externally applied stiffness and damping.

The geometric input data was computed using a spreadsheet, verified by the method described in Section 3.3. The output data contained the calculated response to the various wave input data, and also included data files of hydrodynamic coefficients.

As will be described in Section 3.6, the hydrodynamic coefficients were curve-fitted for use in the frequency domain model, thus allowing the model behaviour to be assessed at any particular wave period.

For full details of the WAMIT analysis, reference should be made to Appendix B.

## 3.6 Frequency domain model

The development of the modelling suite moved to the use of a mathematical package, Mathcad (PTC, 2014) to carry out further frequency domain modelling, the main reason being to facilitate the efficient production of performance curves – to study the effect of changes to PTO stiffness and damping and also look at the effect of restraining the device in heave.

Once the hydrodynamic coefficients were known, then quantities such as the heave and Clam response and power capture could be calculated by straightforward linear algebraic equations. Thus the approach taken in the Mathcad modelling was to curve-fit the hydrodynamic data, using cubic splines, so that accurate figures for the data might be computed for any chosen wave period.

A particular advantage of this approach is that the output data may be plotted as smooth curves, and any particular point of interest, such as a resonant peak may be identified. Table 3.1 lists the hydrodynamic parameters that are curve-fitted.

Table 3.1: Hydrodynamic Parameters that are Curve Fitted

| Parameter | Description | Parameter | Description |
|---|---|---|---|
| $A_{33}$ | Heave Added Mass | $\sigma_{33}$ | Argument of Haskinds Exciting Force in Heave |
| $B_{33}$ | Heave Damping | $Mod_{33}$ | Modulus of Haskinds Exciting Force in Heave |
| $M_{33}$ | Device Mass | $\sigma_{77}$ | Argument of Haskinds Exciting Force for Clam Mode |
| $A_{77}$ | Clam Added Mass | $Mod_{77}$ | Modulus of Haskinds Exciting Force for Clam Mode |
| $B_{77}$ | Clam (Added) Damping | | |
| $A_{37}$ | Cross Coupled (3,7) Added Mass | | |
| $B_{37}$ | Cross Coupled (3,7) Damping | | |
| $A_{73}$ | Cross Coupled (7,3) Added Mass | | |
| $B_{73}$ | Cross Coupled (7,3) Damping | | |

Table 3.2 lists the hydrostatic parameters that are constant, i.e. not a function of wave period:

Table 3.2: Hydrostatic Parameters

| Parameter | Description | Parameter | Description |
|---|---|---|---|
| $C_{33}$ | Heave Hydrostatic Coefficient | $C_{37}$ | Cross Coupled (3,7) Hydrostatic Coefficient |
| $C_{77}$ | Clam Hydrostatic Coefficient | $C_{73}$ | Cross Coupled (7,3) Hydrostatic Coefficient |

The following data is input to the calculation:

Table 3.3: Input Data

| Parameter | Description | Parameter | Description |
|---|---|---|---|
| $M_{33}$ | Device Mass | | |
| $B_{33}^{E}$ | Externally Applied Heave Damping | $B_{77}^{E}$ | PTO Damping |
| $C_{33}^{E}$ | Externally Applied Heave Stiffness | $C_{77}^{E}$ | PTO Stiffness |

Note that the parameters are appropriately scaled within the Mathcad model, in accordance with the scaling factors in the User Manual (WAMIT, 2012), such that the calculations are carried out in real units. This is good engineering practice and through dimensional analysis proves to be most helpful in tracing errors.

Equation 3.16 describes the equation of motion that WAMIT solves - see the WAMIT User Guide, Section 3.4.

$$\sum_{j=1}^{7}\left[-\omega^2\left(M_{ij}+M_{ij}^{E}+A_{ij}\right)+i\omega\left(B_{ij}+B_{ij}^{E}\right)+\left(C_{ij}+C_{ij}^{E}\right)\right]\xi_j = X_i \qquad (3.16)$$

where $\xi_j$ is the displacement in the j[th] degree of freedom caused by the force $X_i$.

This is implemented in the frequency domain model for just two degrees of freedom i.e. heave (mode 3) and the Clam or PTO mode (mode 7). Equations 3.17 to 3.26 show the process.

$$X_{33} = Mod_{33}(cos(\sigma_{33}) + jsin\,(\sigma_{33})) \qquad (3.17)$$

$$X_{77} = Mod_{77}(cos(\sigma_{77}) + jsin\,(\sigma_{77})) \qquad (3.18)$$

$$Z_{33} = -\omega^2(M_{33}+A_{33}) + j\omega(B_{33}+B_{33}^{E}) + (C_{33}+C_{33}^{E}) \qquad (3.19)$$

$$Z_{37} = -\omega^2 A_{37} + j\omega B_{37} + C_{37} \qquad (3.20)$$

$$Z_{73} = -\omega^2 A_{73} + j\omega B_{73} + C_{73} \qquad (3.21)$$

$$Z_{77} = -\omega^2 A_{77} + j\omega(B_{77}+B_{77}^{E}) + (C_{77}+C_{77}^{E}) \qquad (3.22)$$

where $\omega$ is the wave radian frequency $\left(=\frac{2\pi}{Wave\ Period}\right)$, and (3.23)

$Z_{33}, Z_{37}, Z_{73}$ and $Z_{77}$ are complex stiffnesses.

Expanding this in matrix form for the two degrees of freedom under consideration (i.e. modes 3 and 7), gives:

$$\begin{bmatrix} Z_{33} & Z_{37} \\ Z_{73} & Z_{77} \end{bmatrix} . \begin{bmatrix} \xi_3 \\ \xi_7 \end{bmatrix} = \begin{bmatrix} X_{33} \\ X_{77} \end{bmatrix} \quad (3.24)$$

Or $$[Z].[\xi] = [X] \quad (3.25)$$

The displacements $[\xi]$ are solved by inverting $[Z]$ and pre-multiplying equation 3.25, so that:

$$[\xi] = [Z]^{-1}.[X] \quad (3.26)$$

$\xi_3$ and $\xi_7$ are the heave and Clam complex displacements that contain the amplitude and phase information for modes 3 (heave) and 7 (Clam). Thus the heave and Clam amplitudes may be readily computed.

As a check on the accuracy of calculation, the heave and Clam amplitudes calculated by the frequency domain model and by WAMIT were compared at a chosen wave period. Table 3.4 shows the result, and as can be seen the figures are the same, which is expected, since the calculation in the frequency domain model uses WAMIT data and the same mathematical formulae. This demonstrated that the conversion to the frequency domain model had been carried out correctly and was error-free.

Table 3.4: Comparison of WAMIT and Mathcad frequency domain model outputs

| | **Heave amplitude (mode 3), m** | **Clam amplitude (mode 7), m** |
|---|---|---|
| WAMIT output at 6 s period | 0.20149 | 0.65948 |
| Mathcad frequency domain model output at 6 s period | 0.20149 | 0.65948 |

The power capture is calculated within the Mathcad frequency domain model using equation 3.27:

$$P = \frac{1}{2} B_{77}^{E} \, |\xi_7|^2 \omega^2 \, . \tag{3.27}$$

where $P$ is the Power Capture, $B_{77}^{E}$ is the PTO damping, $\xi_7$ is the complex PTO (= Clam) amplitude and $\omega$ is the radian wave frequency.

Note that much use is made of the acronym RAO or Response Amplitude Operator (RAO). This dimensionless quantity relates the amplitude of the chosen parameter to the wave amplitude as indicated by equation 3.28:

$$RAO_3 = \frac{|\xi_3|}{a} \quad \text{and} \; RAO_7 = \frac{|\xi_7|}{a} \, , \tag{3.28}$$

where $RAO_3$ is the heave RAO, $RAO_7$ is the Clam or PTO RAO, $|\xi_3|$ and $|\xi_7|$ are the moduli of the heave and PTO amplitudes and $a$ is the wave amplitude.

Thus equation 3.27 may be re-written:

$$P = \frac{1}{2} B_{77}^{E} {RAO_7}^2 \, a^2 \, \omega^2 \, . \tag{3.29}$$

Using Mathcad to host the frequency domain model had several advantages over the use of the WAMIT model alone. Due having curve-fitted the hydrodynamic data, the Clam's behaviour could be predicted for any selected wave period – or range of wave periods. In addition the computing time was shorter and output files suitable for input to the time domain model could be generated easily. One further significant practical advantage was that the frequency domain model could be used after the WAMIT licence period had expired.

## 3.7 Free floating Clam - regular input

The performance of the free floating device was assessed by adjusting the PTO damping and stiffness in order to maximise the power capture at each wave period – except that the damping was increased at the longer wave periods in order to keep the Clam RAO within a practical range of 2 or less, see Table 3.5 and Figure 3.12. The line marked "1/2 Power in 40 m wave front" indicates the likely maximum power capture envelope based on the theory presented in Section 1.5.1.

Table 3.5: PTO stiffness and damping, chosen to maximise power capture

| Period, s | PTO Stiffness, N/m | PTO Damping, Ns/m | Clam RAO | Heave RAO | Power, kW |
|---|---|---|---|---|---|
| 4 | 1.90E+05 | 8.00E+05 | 0.514 | 0.131 | 261 |
| 6 | 4.00E+05 | 3.90E+06 | 0.349 | 0.358 | 260 |
| 8 | 1.00E+06 | 1.25E+07 | 0.291 | 1.182 | 326 |
| 10 | 6.50E+06 | 7.00E+06 | 0.54 | 1.968 | 402 |
| 12 | 4.50E+06 | 1.30E+06 | 1.994 | 3.76 | 708 |
| 14 | 3.60E+06 | 1.50E+06 | 2.044 | 3.076 | 631 |
| 16 | 3.00E+06 | 1.60E+06 | 1.922 | 2.257 | 455 |
| 20 | 3.00E+06 | 1.90E+06 | 2 | 2.697 | 375 |

Additionally Figure 3.13 shows the power capture performance of the WEC if the PTO damping and stiffness are not varied. Two cases are shown, based on the optimised damping and stiffness for an 8 second and a 12 second period wave. In these cases the plots demonstrate the type of performance typical of a WEC which captures most power at its resonant frequency and where tuning is needed to align its response to the input wave period.

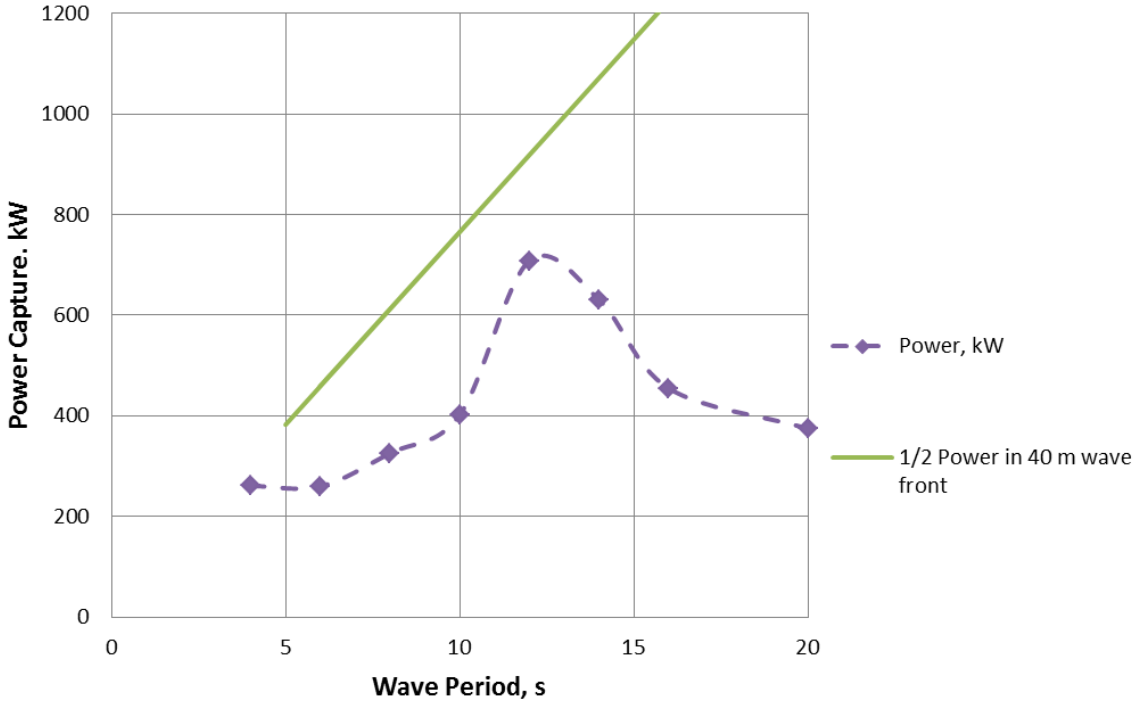


Figure 3.12: Power Capture for Free Floating device - 1

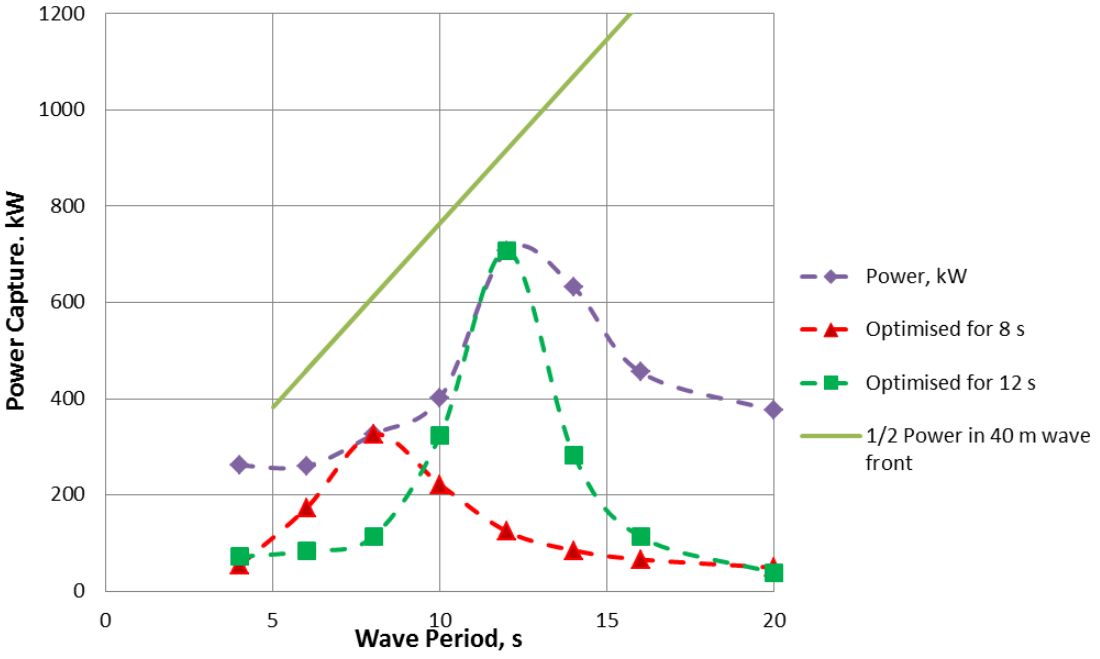


Figure 3.13: Power Capture for Free Floating device - 2

## 3.8 Heave restrained Clam - regular input

Having assessed the behaviour of the Clam as a free floating device it was decided to examine its behaviour when restrained in heave. In practice this would be achieved by tethering the device directly to the ocean floor and providing sufficient buoyancy to maintain tension in the tethers. This allows lower values of PTO stiffness to be used. As in the free floating configuration the performance of the device was assessed by adjusting the PTO damping and stiffness in order to maximise the power capture at each wave period. Also, as before, the damping was increased at the longer wave periods in order to keep the Clam RAO within a practical range of 2 or less (see Table 3.6 and Figure 3.14).

Additionally, as with the free-floating Clam, its power capture performance has been calculated for two cases where the PTO damping and stiffness are not varied, i.e. taking parameters that have been optimised for an 8 second and a 12 second period wave.

It can be seen that the response is quite different from that of the free floating device as it tends to follow the ½ power line – at least for the shorter wave periods. The limiting factor is the range of movement available at the PTO.

Table 3.6: Power Capture – model restrained in heave

| Period, s | PTO Stiffness, N/m | PTO Damping, Ns/m | Clam RAO | Power, kW |
|---|---|---|---|---|
| 4 | 2.00E+05 | 4.00E+05 | 0.794 | 311 |
| 6 | 2.00E+05 | 6.00E+05 | 1.05 | 362 |
| 8 | 2.00E+05 | 4.50E+05 | 1.858 | 479 |
| 10 | 1.50E+05 | 1.00E+06 | 1.85 | 673 |
| 12 | 1.50E+05 | 1.40E+06 | 1.99 | 761 |
| 14 | 1.50E+05 | 1.90E+06 | 1.97 | 746 |
| 16 | 1.50E+05 | 2.30E+06 | 2.02 | 724 |
| 20 | 1.50E+05 | 3.20E+06 | 2 | 634 |

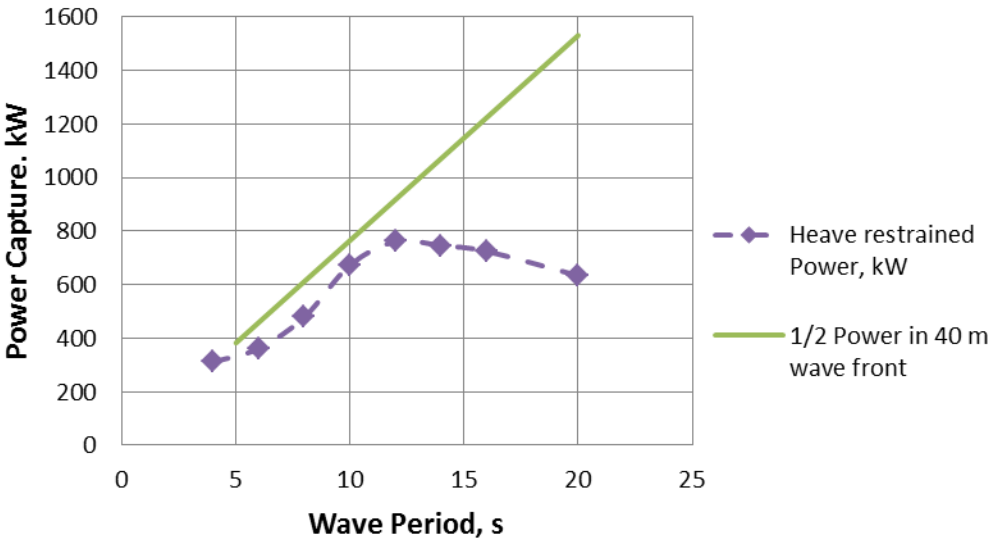


Figure 3.14: Power Capture – model restrained in heave - 1

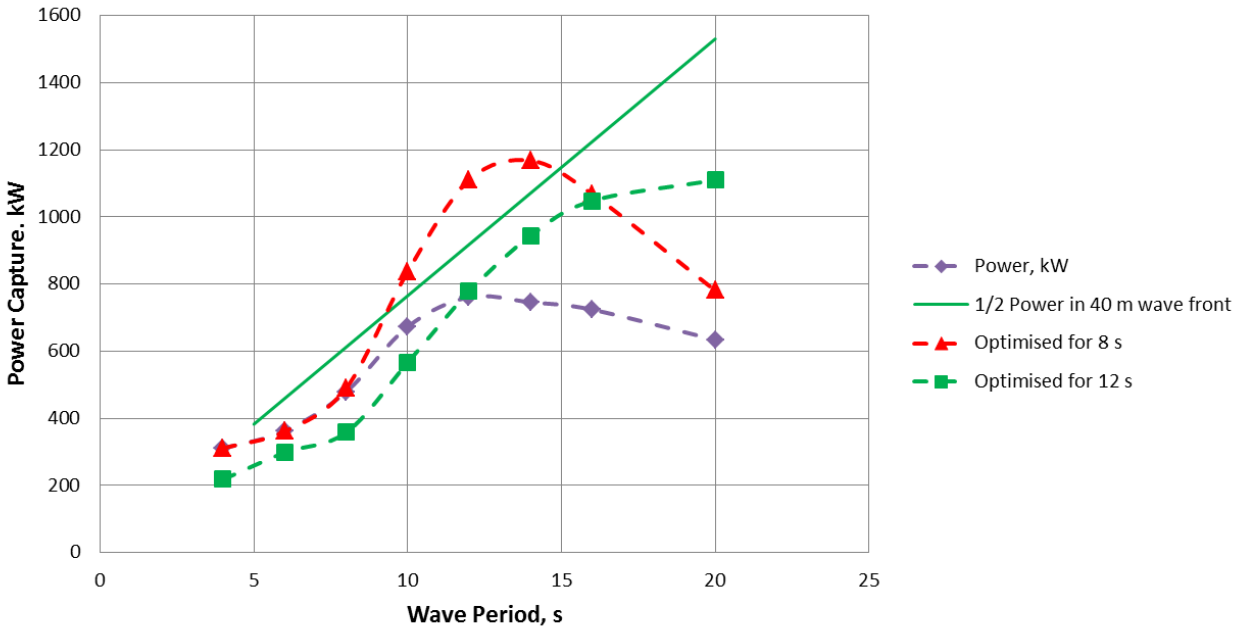


Figure 3.15: Power Capture for model restrained in heave – 2

## 3.9 Free floating versus heave restrained configurations

It is useful to compare the two configurations, free floating versus heave restrained, based on the analysis presented above. Figure 3.16 shows the comparison which indicates that the heave restrained configuration is superior.

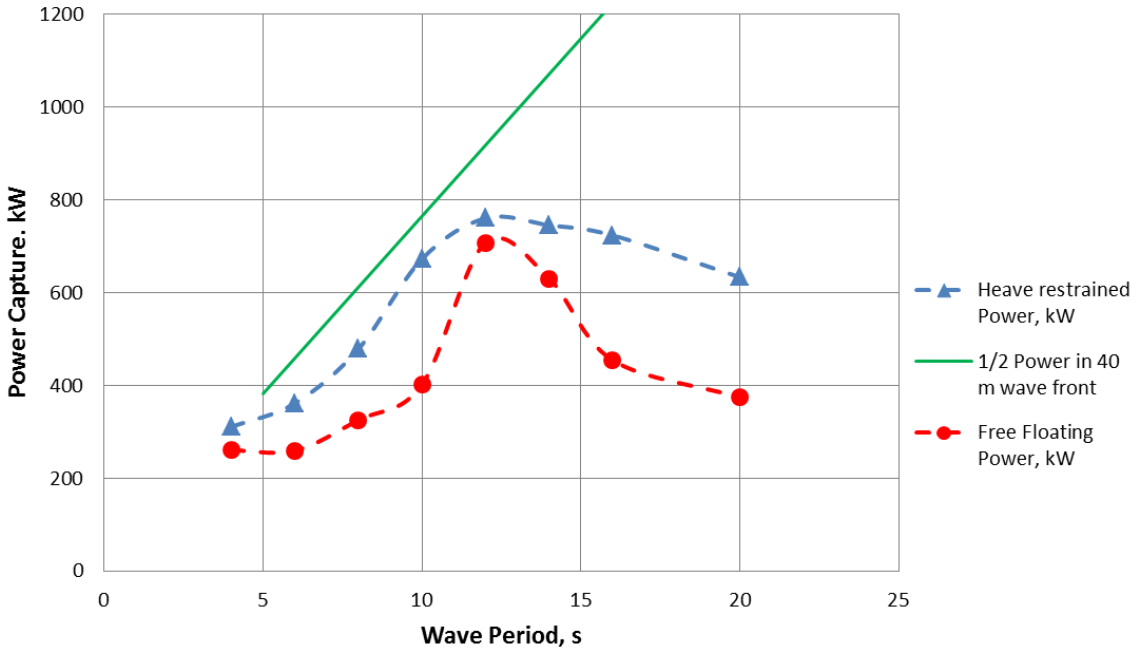


Figure 3.16: Power Capture Comparison – free floating versus heave mode

## 3.10 Performance with random input

Random or panchromatic seas are defined by three factors – the Energy Period, $T_e$ , the Significant Wave Height, $H_s$ , and the Power Spectral Density Function, $S(f)$.

A discrete analysis is performed in the following manner, using the index, $n$, within a Mathcad spread sheet. $N$ is the maximum number of steps – 800 in the present case. The step size $\Delta T$ was taken as 0.02 s, starting at 4 s, thus covering wave periods from 4 to 20 seconds.

The value of the wave input spectrum $S(f_n)$ at wave period $T_n$ is calculated using equation 1.11. However this uses the wave frequency $f_n$ in place of $T_n$ , and the Zero

Crossing Period, $T_z$ , rather than the Energy Period, $T_e$ , so the following adjustments are made:

$$f_n = \frac{1}{T_n} \tag{3.30}$$

where

$$n = 0 \; to \; N \tag{3.31}$$

and

$$T_z = \frac{T_e}{1.20265} \tag{3.32}$$

The Power $P_n$ at each wave period, $T_n$ , is calculated from equation 3.27.

At each step the incremental contribution to the power capture $\Delta P_n$ is obtained from the following equation:

$$\Delta P_n = 2P_n \, S(f_n)\Delta f_n \tag{3.33}$$

where

$$\Delta f_n = \frac{\Delta T}{\left(T_n(T_n + \Delta T)\right)} \tag{3.34}$$

The total power capture is found from equation 3.35:

$$P = \sum_{n=0}^{N} \frac{\Delta P_n}{a^2} \tag{3.35}$$

where the wave amplitude, $a$, is usually taken as unity, i.e. 1 m, but if a different figure is chosen, then this is allowed for in equation 3.35.

As an example, consider the configuration described in Table 3.6, optimised for a 10 second wave period, i.e. where the PTO stiffness is 0.15 MN/m and the PTO damping is 1 MNs/m. If the Energy Period $T_e$ is taken as 10 seconds and the Significant Wave Height $H_s$ as 2 m, the computed mean power capture is then $335 \, kW$. The incident wave power

over a 40 m wave front is 765 kW (Equation 1.9), and following the logic adopted throughout this document, a figure of 382 kW (i.e. half of 765 kW) may be considered a practical maximum. 335 kW is 0.88 of 382 kW – a good result.

Note that the performance data throughout this report are based on the use of fresh water, which has a density of 1000 kg/m$^3$, as opposed to sea water with a density of 1025 kg/m$^3$. The only exception is the analysis of Appendix D, where the Clam's performance at Wave Hub is estimated.

## 3.11 Time domain model description

### 3.11.1 *General*

Time domain modelling of the Clam employs the VisSim continuous systems modelling tool to provide a time domain simulation of the motion of the device. A number of numerical integration techniques are available within VisSim. However, the Runge Kutta 4$^{th}$ order integration option has been used for all the simulations, generally with a time step of 0.05 s. In common with all the mathematical modelling carried out on this project, full scale values of all parameters are used. The model is restricted to modelling just the Heave and the Clam motion.

A block diagram is constructed, using the PC monitor, with arithmetic and logical functions being implemented by interconnecting the relevant basic level blocks, such as add, multiply, etc. Other blocks are used to provide inputs, such as ramps, sine, steps etc. A range of output blocks provide on-screen plots and output to text files. Compound Blocks, containing these basic level block diagrams are employed to organise the model into a manageable form on the screen. Compound blocks may be placed within further higher level Compound Blocks. Figure 3.17 shows the block diagram at the highest level.

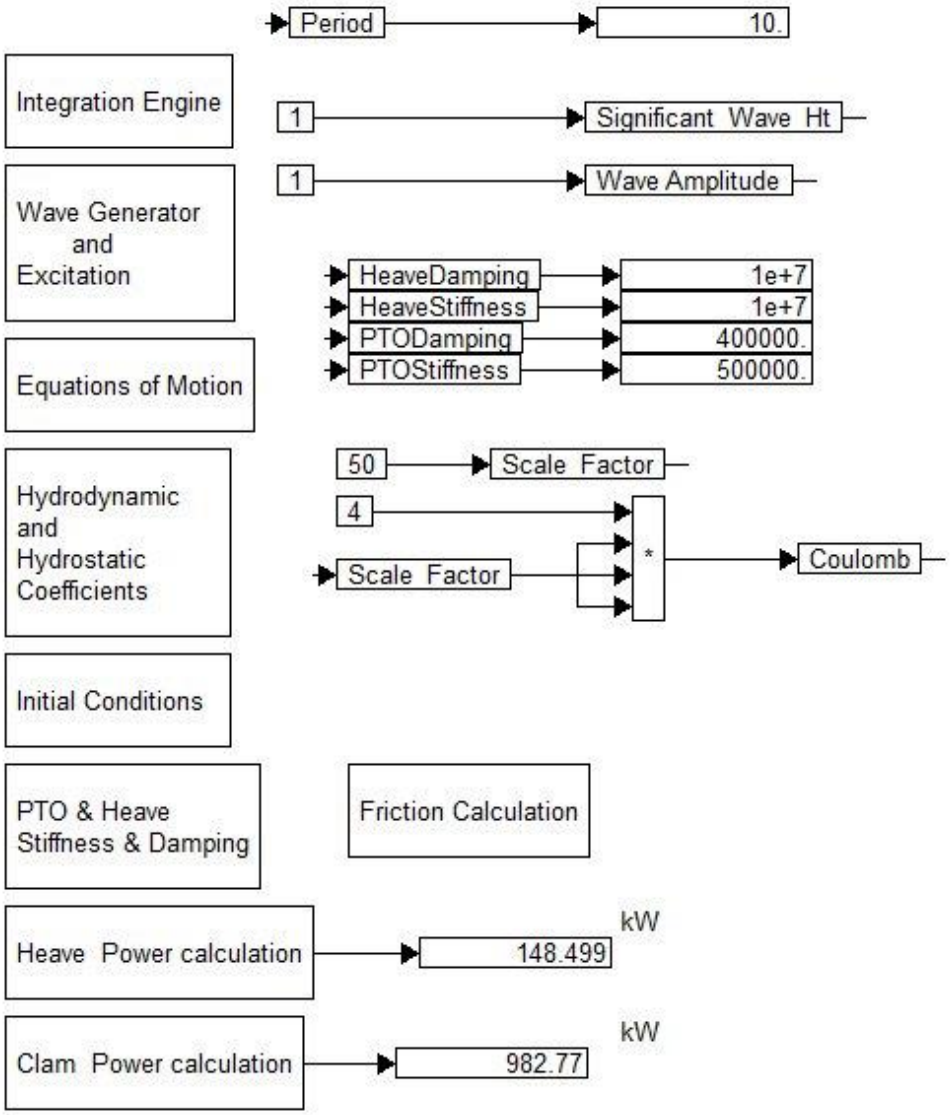


Figure 3.17: Time domain model - Top level Block Diagram

The algorithms within each high level block are described in the following sections.

### 3.11.2 *PTO and Heave Stiffness & Damping*

This block simply inputs the chosen values of externally applied PTO and Heave damping and stiffness as listed in Table 3.7.

Table 3.7: Stiffness and damping parameters for input to the time domain model.

| Parameter | Description | Parameter | Description |
|---|---|---|---|
| $B_{33}^{E}$ | Externally Applied Heave Damping | $B_{77}^{E}$ | PTO Damping |
| $C_{33}^{E}$ | Externally Applied Heave Stiffness | $C_{77}^{E}$ | PTO Stiffness |

Hydrodynamic and hydrostatic coefficients, plus the wave period, $T$, and device mass, $M_{33}$, are computed by the frequency domain model (Section 3.6) for input to the time domain model. The relevant parameters are listed in Table 3.8.

Table 3.8: Hydrodynamic and hydrostatic coefficients

| Parameter | Description | Parameter | Description |
|---|---|---|---|
| $T$ | Wave Period | $M_{33}$ | Device Mass |
| $Mod_{33}$ | Modulus of Haskinds Exciting Force in Heave | $Mod_{77}$ | Modulus of Haskinds Exciting Force for Clam Mode |
| $\sigma_{33}$ | Argument of Haskinds Exciting Force in Heave | $\sigma_{77}$ | Argument of Haskinds Exciting Force for Clam Mode |
| $Mod_{33}$ | Modulus of Haskinds Exciting Force in Heave | $Mod_{77}$ | Modulus of Haskinds Exciting Force for Clam Mode |
| $A_{33}$ | Heave Added Mass | $B_{33}$ | Heave Damping |
| $A_{77}$ | Clam Added Mass | $B_{77}$ | Clam (Added) Damping |
| $A_{37}$ | Cross Coupled (3,7) Added Mass | $B_{37}$ | Cross Coupled (3,7) Damping |
| $A_{73}$ | Cross Coupled (7,3) Added Mass | $B_{73}$ | Cross Coupled (7,3) Damping |
| $C_{33}$ | Heave Hydrostatic Coefficient | $C_{37}$ | Cross Coupled (3,7) Hydrostatic Coefficient |
| $C_{77}$ | Clam Hydrostatic Coefficient | $C_{73}$ | Cross Coupled (7,3) Hydrostatic Coefficient |

The time domain model computes the following parameters in preparation for their use in the equations of motion (3.52 and 3.53) – see Table 3.9.

Table 3.9: Parameters for use in equations of motion

| | | |
|---|---|---|
| Body mass + heave Added Mass: | $m_{33} = M_{33} + A_{33}$ | (3.36) |
| Hydrodynamic damping + externally applied heave damping | $b_{33} = B_{33} + B_{33}^{E}$ | (3.37) |
| Hydrostatic stiffness + externally applied heave stiffness | $c_{33} = C_{33} + C_{33}^{E}$ | (3.38) |
| Hydrodynamic added mass for Clam mode (mode 7) | $m_{77} = A_{77}$ | (3.39) |
| Clam hydrodynamic damping + externally applied Clam mode damping (= PTO damping) | $b_{77} = B_{77} + B_{77}^{E}$ | (3.40) |
| Clam hydrostatic stiffness + externally applied Clam mode stiffness (= PTO stiffness) | $c_{77} = C_{77} + C_{77}^{E}$ | (3.41) |
| Cross Coupled (3,7) Added Mass | $m_{37} = A_{37}$ | (3.42) |
| Cross Coupled (3,7) Damping | $b_{37} = B_{37}$ | (3.43) |
| Cross Coupled (3,7) Hydrostatic Coefficient (= hydrostatic stiffness) | $c_{37} = C_{37}$ | (3.44) |
| Cross Coupled (7,3) Added Mass | $m_{73} = A_{73}$ | (3.45) |
| Cross Coupled (7,3) Damping | $b_{73} = B_{73}$ | (3.46) |
| Cross Coupled (7,3) Hydrostatic Coefficient (= hydrostatic stiffness | $c_{73} = C_{73}$ | (3.47) |

### 3.11.3 *Integration engine*

The inputs to the Integration Engine are the second derivatives $\ddot{\delta}_3$ and $\ddot{\delta}_7$ of the heave and Clam displacements, respectively. These are then integrated with respect to time, $t$, as follows:

Heave velocity, $$\dot{\delta}_3 = \int \ddot{\delta}_3 dt \quad (3.48)$$

Heave position, $$\delta_3 = \int \dot{\delta}_3 \, dt \quad (3.49)$$

Clam velocity, $$\dot{\delta}_7 = \int \ddot{\delta}_7 \, dt \quad (3.50)$$

Clam position, $$\delta_7 = \int \dot{\delta}_7 \, dt \quad (3.51)$$

### 3.11.4 *Equations of motion*

Equation 3.52 is the equation of motion for heave acceleration, $\ddot{\delta}_3$ , while equation 3.53 computes Clam (=PTO) acceleration, $\ddot{\delta}_7$ .

$$\ddot{\delta}_3 = \frac{X_3 - \{b_{33}\dot{\delta}_3 + c_{33}\delta_3 + m_{37}\ddot{\delta}_7 + b_{37}\dot{\delta}_7 + c_{37}\delta_7\}}{m_{33}} \quad (3.52)$$

$$\ddot{\delta}_7 = \frac{X_7 - \{b_{77}\dot{\delta}_7 + c_{77}\delta_7 + m_{73}\ddot{\delta}_3 + b_{73}\dot{\delta}_3 + c_{73}\delta_3\}}{m_{77}} \quad (3.53)$$

### 3.11.5 *Coulomb friction*

The time domain model contains a nonlinear feature that is relevant to the PTO for the wave tank model – namely Coulomb Damping Force, $F_{CD}$. A value for Coulomb Friction Force $F_{CF}$ is input; and the following logic determines the Coulomb Damping Force:

PTO ram moving, i.e. $\dot{\delta}_7 \neq 0$ , then $F_{CD} = F_{CF}$ (3.54)

PTO ram stationary, i.e. $\dot{\delta}_7 = 0$ , then $F_{CD}$ equals the force on the ram – up to $F_{CF}$ (3.55)

PTO ram stationary, i.e. $\dot{\delta}_7 = 0$ , and the force on the ram is greater than $F_{CF}$ , then $F_{CD} = F_{CF}$ (3.56)

### 3.11.6 *Wave generation and excitation*

This block computes the wave forces, $X_3$ and $X_7$ that excite the model in the Heave and in the Clam modes respectively.

***Regular seas***

In regular seas the wave elevation, $w$, in the vertical plane is given by equation

$$w = a.\cos\omega t \tag{3.57}$$

where $a$ is the wave amplitude, $\omega$ is the radian frequency and *t* is time.

Thus: $X_3 = a\{Mod_{33}.cos(\omega t + \sigma_{33})\}$, and (3.58)

$$X_7 = a\{Mod_{77}.cos(\omega t + \sigma_{77})\}. \tag{3.59}$$

Note that positive values of the arguments, $\sigma_{33}$ and$\sigma_{77}$, denote a phase lag.

***Random seas – an approximate method***

An approximate method has been devised by the writer to cater for random seas. The wave input is represented by a data file of wave position, $w$, versus time, $t$.

Where the input is sinusoidal, the method is mathematically identical to that for monochromatic seas – as would be expected – and this is the starting point for the concept.

The mathematical model first computes the differential of the wave position with respect to time, i.e. $\dot{w}$, and then uses it, together with the wave position, $w$, to compute $X_3$ and $X_7$, as follows.

As an alternative to equation 3.58, $X_3$ may be expressed in terms of its real and imaginary parts, as in equation3.60 :

$$X_3 = a\big(\{ReX_3\}cos(\omega t) + \{ImX_3\}sin(\omega t)\big)\ . \tag{3.60}$$

For sinusoidal motion $w = a.\cos\omega t$ and $\dot{w} = -a.\omega.sin(\omega t)$ . (3.61)

Substituting for $sin(\omega t)$ and $cos(\omega t)$ in equation 3.60 , gives

$$X_3 = w\{ReX_3\} + \frac{\dot{w}\{ImX_3\}}{\omega}, \quad (3.62)$$

where: $\{ReX_3\} = Mod_{33}.cos(\sigma_{33})$ and $\{ImX_3\} = Mod_{33}.sin(\sigma_{33})$. (3.63)

Equations 3.62 and 3.63 are implemented in the time domain model.

### 3.11.7 *Use of Convolution Integral*

Where random seas are concerned a mathematically correct method of simulating the behaviour of the device in the time domain involves the use of convolution integrals. The means of achieving this in the time domain model is currently being researched, but has as yet not been fully implemented.

The method is based on work carried out at NTNU Trondheim, Norway (Kurniawan et al., 2011), (Hals, 2010) and the National University of Ireland, Maynooth (Nolan, 2006).

To illustrate the method consider the equation of motion for a single degree of freedom heaving buoy (from Kurniawan et al., 2011):

$$\mathrm{F_e(t)} = [\mathrm{m_m} + \mathrm{m}(\infty)]\dot{\mathrm{u}}(\mathrm{t}) + \mathrm{k(t)} * u(\mathrm{t}) + (\mathrm{S_b} + \mathrm{S})\mathrm{s(t)} + \mathrm{R_q u(t)|u(t)|} \quad (3.64)$$

where:

$F_e(t) =$ Excitation force

$\dot{u}(t) =$ Body vertical acceleration

$u(t) =$ Body vertical velocity

$s(t) =$ Body vertical position

$m_m =$ Mass of body

$m(\infty) =$ Body added mass as wave frequency tends to infinity (i.e. at zero wave period)

$k(t) =$ Radiation Impulse Response Function (IRF)

$S_b =$ Hydrostatic stiffness

$S =$ Externally applied stiffness

$R_q =$ Quadratic damping coefficient

$(t)$ denotes parameter is a function of time, $t$ .

$*$ represents convolution

The excitation force is computed by the following equation (Nolan, 2006):

$$F_e(t) = f(t) * \eta(t) = \int_{-\infty}^{\infty} \eta(\tau) f(t-\tau) d\tau \qquad (3.65)$$

where:

$F_e(t) =$ Excitation force

$f(t) =$ Excitation Impulse Response Function (IRF)

$\eta(t) =$ Wave Position (in relation to mean)

$\tau =$ Time before current time.

$*$ represents convolution

The Excitation Impulse Response Function (IRF) is given by the following equation:

$$f(t) = \frac{1}{\pi}\int_0^{\infty} Re\{F_e(\omega)\}\cos(\omega t) d\varpi - \frac{1}{\pi}\int_0^{\infty} Im\{F_e(\omega)\}\cos(\omega t) d\varpi \qquad (3.66)$$

where $Re\{F_e(\omega)\}$ is the real part of the Excitation Force in the frequency domain and $Im\{F_e(\omega)\}$ is its corresponding Imaginary part. $\omega$ is the wave radian frequency.

The Radiation Impulse Response Function (IRF) may be calculated by either of the two following equations (Kurniawan et al., 2011):

$$k(t) = \frac{2}{\pi}\int_0^{\infty} R(\omega)\cos(\omega t) d\varpi \qquad (3.67)$$

where $R(\omega)$is the radiation damping,

**OR:**

$$k(t) = -\frac{2}{\pi}\int_0^{\infty} \omega[m(\omega) - m(\infty)]\sin(\omega t) d\omega \qquad (3.68)$$

where $m(\omega)$ is the hydrodynamic added mass and $m(\infty)$ is its value as the wave frequency tends to infinity.

Implementing the method in the time domain model entails building arrays that hold the IRF data sets. Also required are arrays that hold values of body velocity and Clam/PTO velocity at past instants in time. However for the Excitation force an array is needed that holds values of wave position, both for past AND future instants in time. The calculation of the Radiation force requires a knowledge of the past velocity profile and the system is said to be “causal”. On the other hand the calculation of the Excitation force requires knowledge of past and future values of wave position and is said to be “non-causal”. For a modelling study and in the wave tank this is not too much of a problem, but in the open sea some method of predicting the future behaviour of the waves is needed.

At the time of writing the time domain model is being adapted to include “convolution”, as an option. The arrays holding the IRFs have been constructed and built into the model. The model still has to be tested and compared with results from the existing model for a sinusoidal wave input; when near perfect agreement should be expected. The calculation of the Exciting force is possibly the most difficult feature, and is currently being implemented. This entails the multiplication of two arrays – the Excitation IRF and the arrays holding wave position data. The result has been compared with earlier regular wave computations and good agreement has been found. The computation has shown itself to be most efficient with model computational speed similar to that of the simpler models that do not employ the convolution integral. It has been found unnecessary to consider data that is more than 6.5 seconds away from current time.

# 4 Wave Tank Trials and Analysis

## 4.1 Introduction

The aim of practical testing in the wave tank is to validate theory and thus support performance predictions. Both regular and random waves have been employed. No testing in extreme waves has been carried out, since the focus of the testing has been to establish the WEC's energy capture potential – large waves would simply have swamped and possibly damaged the model.

## 4.2 Test facilities at Plymouth

The very successful programme of testing has been carried out in the ocean wave basin at the Coastal, Ocean And Sediment Transport (COAST) laboratory housed in University of Plymouth's Marine Building, The COAST laboratory provides physical model testing with combined waves, currents and wind at scales appropriate for device testing, array testing, environmental modelling and coastal engineering. There is the capability to generate short and long-crested waves in combination with currents at any relative direction, sediment dynamics, tidal effects and wind. Model testing may be carried out in a flume (2 off), a sediment basin or the ocean wave basin. There is a 35m flume and a 20m flume with the capability of being tilted. The inclusion of current circulation in the flumes allow tidal as well as wave energy to be tested. The Coastal Basin allows sediment transport and coastal structures to be studied at scale in a controlled environment – it is 15.5m long by 10m wide with a maximum operating depth of 0.5m. Waves up to 0.32 m in height can be generated together with superimposed cross flow of up to 0.5m/s via five individually controlled pumps. The Ocean Wave Basin is 35m long by 15.5m wide with a moveable floor that allows different operating depths of up to 3m. Unidirectional and directional wave fields, regular waves, wave spectra and currents in three dimensions can be produced.. A maximum wave height of 0.9m at 0.4 Hz is possible. However, across a wave frequency range of 0.166 Hz – 1 Hz a wave height of 0.2m is possible. Wave synthesising software allows long and short-crested spectral sea states to be generated as well as special wave effects. Oblique waves can be generated up to 40° from normal.

The wave tank testing was carried out in the ocean wave basin at Plymouth University on the Mark IIa and Mark IIb wave tank models. Previously a short period of ad-hoc testing had been carried out on the Mark I model in a flume, but this yielded little useful data.

The data collected in each trial, included:

- Wave position data, as measured by resistance wave gauges,
- Model position data, captured by the Qualysis system, and
- Load cell data for PTO, measured by commercial standard load cells and captured by LabView.

The data were analysed in a straightforward manner using a linked series of spreadsheets. At each wave period, data was generated and copied into pages of a spreadsheet – one page for each of the three types of data listed above. For the majority of runs a time window some 31 seconds into the test was chosen for the purpose of making the measurements and calculating the various parameters reported later in this section. Whereas it is felt that the data were sufficient to enable an understanding of Clam's dynamics and power capturing potential, no absolute figure for the numerical accuracy of such predictions can be made.

Two sets of trials were carried out – the first with the Mark IIa model and the second with the Mark IIb_1 and Mark IIb_2 models. During the analysis of the first set there was a clear mismatch between the predicted behaviour of the WEC and its actual behaviour, particularly in respect of the phase relationship between the wave input and the Clam response. This proved to be due to the hydrostatic coefficients being incorrectly calculated by the NEWMODES function within the WAMIT suite of programs, as discussed in Section 3.4. Corrected coefficients have been used in the analysis presented in the sections that follow.

In general each trial consists of 8 runs, covering the range 0.6 s to 2 s at model scale which is equivalent to 4.24 s to 14.14 s at full size. The wave periods were chosen to cover the

range of wave periods to be found at sites of moderate wave energy, where the annual mean wave power is of the order of 20 kW per metre of wave front, the scale factor being 1:50. As these were tests on a new concept the aim was to cover a wide range of wave periods rather than concentrating on a specific condition. This influenced the choice of wave periods and their spacing in order to complete the trials within the time available. The wave height was chosen to be the minimum that would yield useful information and that would be more applicable to the linear theory and assumption of zero viscosity on which the WAMIT method of analysis depends. Thus the majority of the trials employed a regular wave input of either 20 mm or 40 mm amplitude, equivalent to 1m or 2 m amplitude at full scale. The larger figure of 40 mm was employed during the first set of trials in order to overcome friction in the model PTO. Modifications to the model, as discussed in 2.8.1, successfully reduced the PTO friction for the second set of trials and allowed testing to be carried out with a wave amplitude of 20 mm.

All trials were carried out in a water depth of 2 m, which equates to 100 m at full scale. This depth was chosen for practical purposes including the wave tank mooring geometry rather than relating to any particular geographical location.

## 4.3 Test setup for trials of Mark IIa model

The first set of trials employed the Mark IIa model, and as has been mentioned in Section 4.1, the friction level in the model PTO was higher than expected, resulting in the need to increase the amplitude of the wave input to 40 mm – except for the Trial described in Section 4.5.2 where Clam action was prevented and the wave amplitude in this case was 20 mm.

The Qualysis system was set up in such a way that each Clam side was a separate body, as was the main structure – three bodies in all. The origin of the axis system for each Clam side was chosen to be its interface with the PTO ram, thus enabling the length of the ram to be easily calculated.

Stops were incorporated into the model to limit the movement of the Clam sides relative to the main body in order to avoid the chance of damaging the PTO rams.

Initially the mooring lines followed the scheme indicated by Figure 4.1. However during initial trials the pitching motion of the model was found to be unacceptably large. In consequence the attachment point of the lateral mooring line was raised to a position close to the underside of the main body, as shown in Figure 4.2. This was only partially successful and additional mooring lines were then added to further reduce the amplitude of the pitch motion, as shown in Figure 4.3.

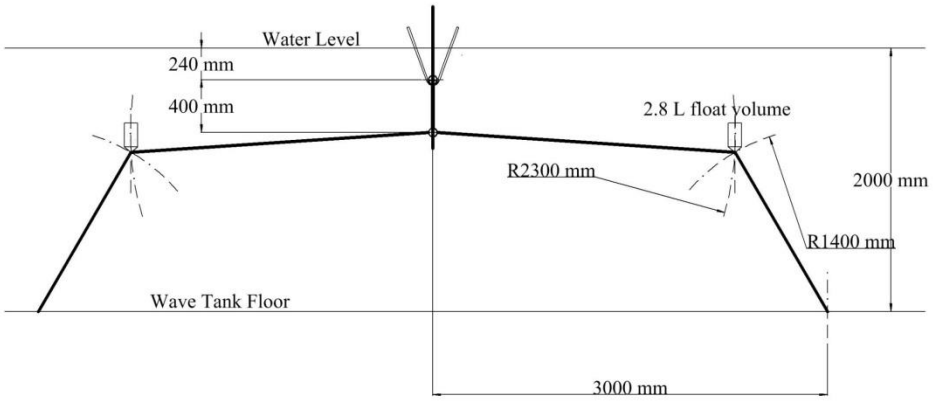


Figure 4.1: Initial Mooring Geometry for the First set of trials

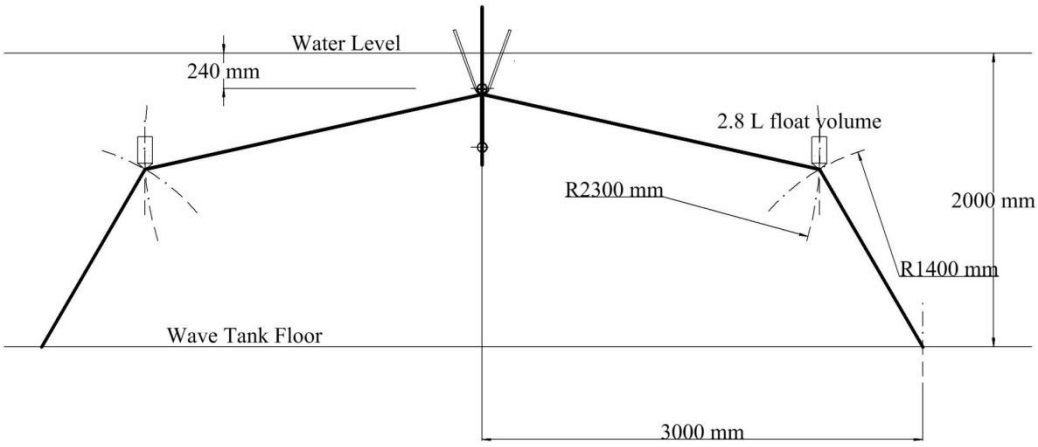


Figure 4.2: First Modification to the Mooring Geometry for the First set of trials

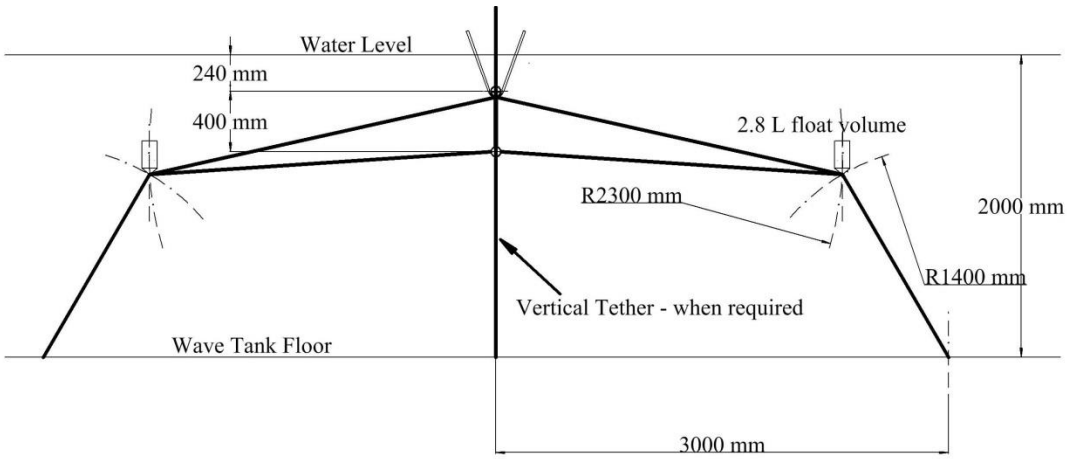


Figure 4.3: Final Modification to the Mooring Geometry for the First set of trials

A further problem was encountered – one that had been anticipated (see Section 3.2.2), but which proved more intractable than expected.

It was found that the wave tank model Clam sides either opened or closed fully and it proved difficult to adjust the pressure in the reservoir (and hence the PTO ram force) to achieve a stable situation in which the Clam sides were partially open at equilibrium and then moved in and out under wave excitation. The explanation for this behaviour lies in the fact that at low values of PTO stiffness the device becomes unstable in heave, since as the device sinks lower in the water the Clam closes due to the increased water pressure. This reduces the buoyancy and the device sinks further and the Clam remains closed. The reverse situation applies when the device rises in the water, resulting in the Clam opening and the device rising further.

A stable configuration was achieved by reducing the air volume in the reservoir and thus increasing the PTO stiffness. It is worth noting that, theoretically, this problem should not apply when the device is fixed in heave. However the vertical tethers employed to restrain the device in heave still allowed some vertical movement due to their flexibility. The vertical motion when restrained was indeed small, but nevertheless did not prevent the undesirable behaviour as described.

## 4.4 Test setup for trials of Mark IIb model

The second set of trials employed the Mark IIb wave tank model, as described in Section 2.8. The friction levels in the PTO were much lower than in the first set of trials, since the air pressure in the PTO reservoir and the consequential load carried by the PTO ram, were much reduced. This enabled the input wave amplitude to be reduced to 20 mm, equating to 1 m at full scale.

The Qualysis system set up was different from that of the first set, as it was felt that the layout of wave gauges (shown in Figure 4.5) was such that a clear view of all the necessary model-mounted targets might not be possible. Accordingly the main structure formed the one body with additional targets on each Clam side. Knowledge of the hinge positions allowed the positions of the Clam sides to be calculated and hence the PTO displacement.

Contrary to the practice employed in the first set of trials the movement of the Clam was not limited by stops, although under certain combinations of Clam action and body pitching, the relative movement of the Clam sides and the main structure was limited by the attachment of the bag to the main structure.

Heave motion was to be prevented. This allowed the mooring system to be considerably simplified, consisting of a direct connection to the floor of the wave tank. The two primary attachments were at the junctions of the keel support with the main body. Each line was in fact a double line with the two strands passing either side of the keel – the idea being to reduce the pitch motion of the device, as shown in Figure 4.4.

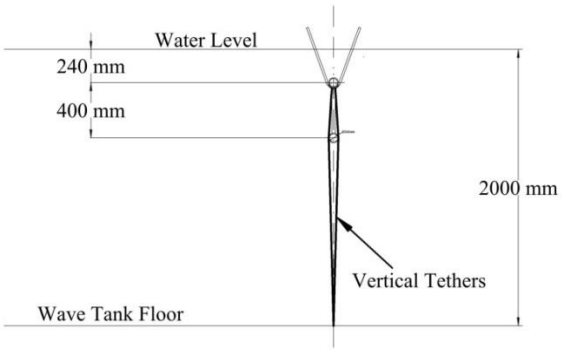


Figure 4.4: Mooring Geometry for Second set of trials

The 12 wave gauges were set out as shown in Figure 4.5. This enabled the angled waves to be recorded without changing the set up, so that testing could progress immediately from straight ahead to angled waves without delay.

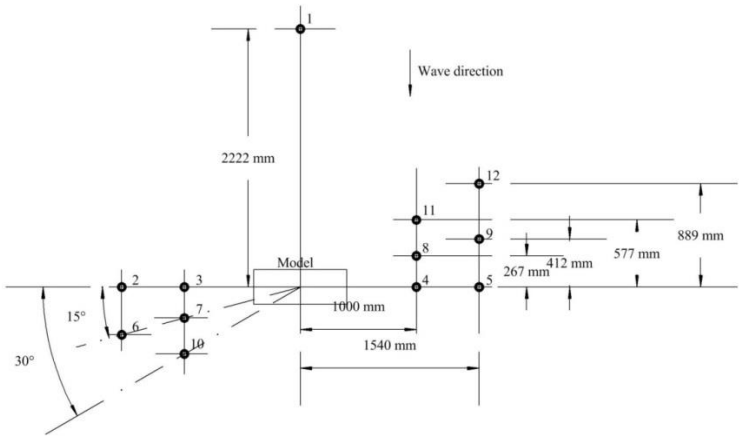


Figure 4.5: Plan View of Wave Gauge Positions for Second set of trials

The usual practice for tests carried out at Plymouth is first to record wave data at the model's position, but with the model absent, and then to carry out the tests with the same wave tank settings with the model present. In this way the theoretically correct wave input is known. However, for the tests carried out here, readings were obtained from the wave gauges that were in line – during testing with the model in position. This approach may be criticised from the point of view of accuracy since such readings would include components that arise from reflections and diffractions of the wave due to the presence of the model. However, by comparing the measurements of wave gauges that were in line with the wave crest there was little difference between them, see Figure 4.6, Figure 4.7 and Figure 4.8 Thus within the present context this approach is believed to be justified.

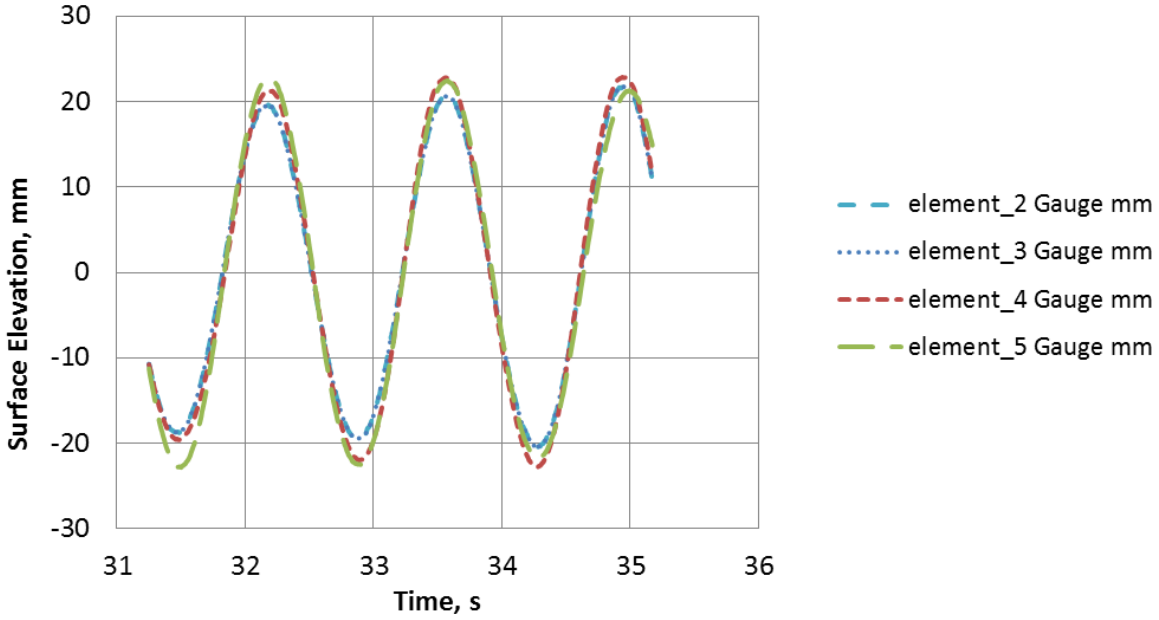


Figure 4.6: Wave gauge readings for a wave incident angle of 0° - trial 7

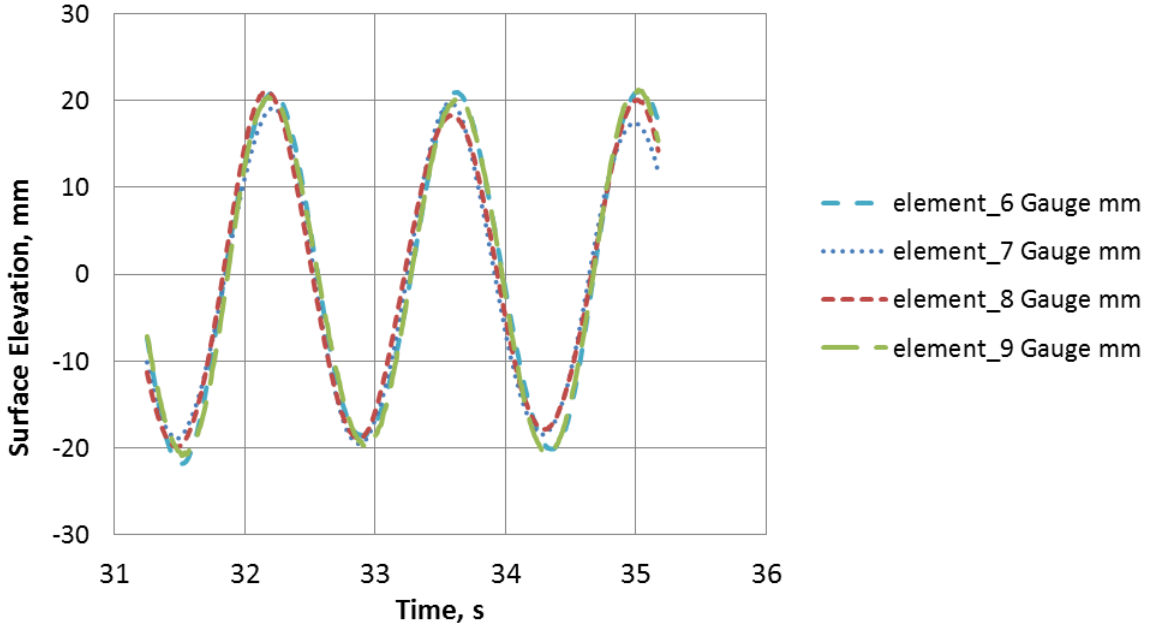


Figure 4.7: Wave gauge readings for a wave incident angle of 15° - trial 7

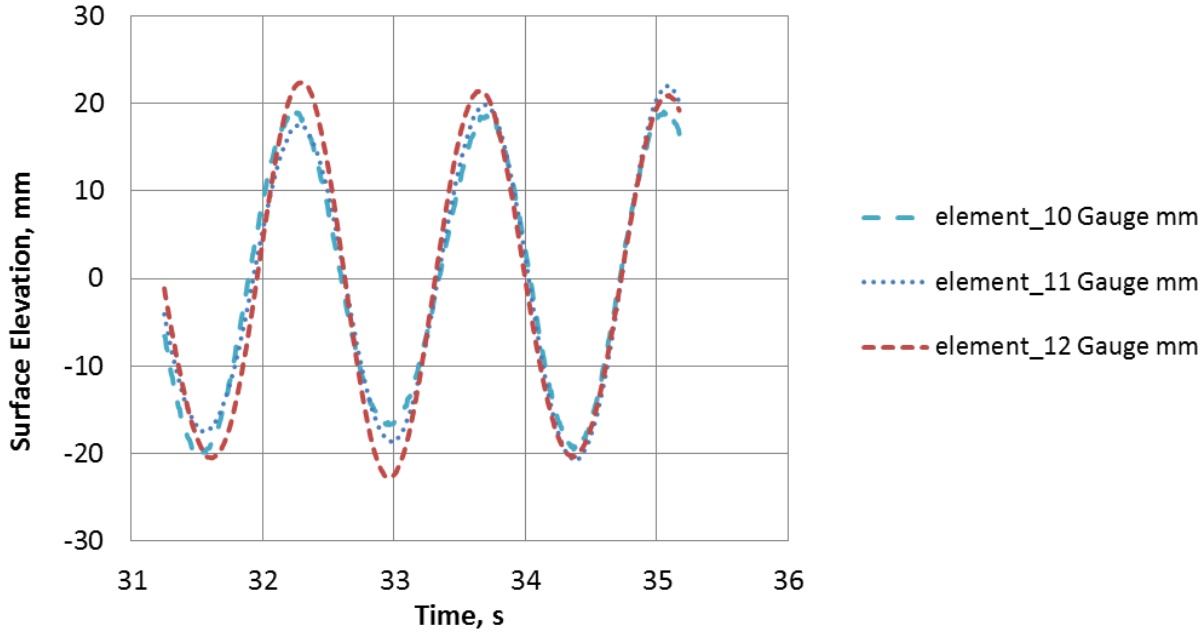


Figure 4.8: Wave gauge readings for a wave incident angle of 30° - trial 7

## 4.5 Trials programme

The trials programme was aimed at validating the theory outlined in Chapter 3, in order to support the design choices and performance predictions for the full scale device described in Chapter 5.

The analysis has been carried out using a number of linked applications. A standardised spreadsheet was devised, into which the raw data from each run was input. Each trial consisted of 8 runs as described in Section 4.1. A master spreadsheet then took the data from these 8 spreadsheets in order to produce plots, such as for Power Capture, RAOs, phase relationships etc.

Theoretical predictions were generated using the programs discussed in Chapter 3. The Mathcad frequency domain model provided the hydrodynamic coefficients and other data for input to the time domain model. This latter model then simulated the dynamic behaviour of the device, taking into account the effect of PTO friction (see Section 3.11.5) in order to provide data for comparison with the practical results.

The full set of trials is indicated by the two tables contained in Appendix B. A subset of these has been selected for detailed analysis as indicated by Table 4.1, and has been renumbered in a logical sequence that follows the steps taken to improve the power capture performance of the device. Thus Trial 1 examined the behaviour of the Mark IIa model (described in Section 2.7) as a floating rigid body to verify that the heave resonance was as expected, while Trials 2 and 3 employed floating and heave restrained configurations respectively. These latter two trials demonstrated that the device behaviour was in line with expectations although friction in the PTO was detrimental to the power capture performance. Trial 3 provided a practical demonstration of the benefit of restricting heave motion.

For trials 4 to 7 the moorings were reconfigured in order to prevent heave motion, and were carried out using the Mark IIb model as described in Section 2.8. Trial 4 employed coil springs and in this configuration it proved impossible to achieve a sufficiently low value of PTO stiffness. Nevertheless the dynamic behaviour of the model was in line with theoretical predictions. Trials 5 through to 7 employed the constant force springs and were able to demonstrate the performance of the device when PTO stiffness and damping values were more in line with those suggested by theory. The results clearly show the benefit of reducing PTO stiffness. Trial 5 used a low value of PTO damping with the aim of demonstrating good power capture at short wave periods. Predictably the Clam amplitude at the longer periods was excessive, limited only by the available PTO stroke. Trials 6 and 7 employed PTO stiffness and damping closer to the ideal.

The performance of the device depends on the PTO stiffness and damping as well as the mooring geometry and internal friction. After having presented the results of the trials the influence of these parameters on the performance of the device is discussed in 0.

For ease in discriminating measured data from calculated predictions, the latter are shown by solid lines in Figure 4.9 through to Figure 4.26. Although such data is continuous, values have been computed only at the points shown.

Table 4.1: Trials selected for detailed analysis

| Wave Tank Trials | | | | Parameter values used in mathematical analysis | | | | | Appendix B trial ref |
|---|---|---|---|---|---|---|---|---|---|
| Trial Number | Wave Tank Model | Description | Damping orifice diameter | Heave damping, MNs/m | Heave stiffness, MN/m | PTO damping, MNs/m | PTO stiffness, MN/m | PTO Friction at Full Scale, MN | PTO Friction at Model Scale, N | |
| 1 | Mark IIa | Floating, fixed Clam angle | N/A | 1 | 0.6 | 40 | 400 | N/A | N/A | D |
| 2 | Mark IIa | Floating, | 3 mm (2 off) | 1.5 | 0.6 | 1.268 | 2.221 | 3.0 | 24 | Q |
| 3 | Mark IIa | Fixed in Heave | 2.5 mm | 2 | 20 | 1.6 | 1.11 | 1.5 | 12 | R |
| 4 | Mark IIb | Fixed in Heave, Coil springs | 3 mm | 10,000 | 10,000 | 1.0 | 2.375 | 0.375 | 3 | 8 |
| 5 | Mark IIb | Fixed in Heave, Constant force springs | 5 mm | 10,000 | 10,000 | 0.148 | 0.068 | 0.75 | 6 | 1,2 &3 |
| 6 | Mark IIb | Fixed in Heave, Constant force springs | 3 mm | 10,000 | 10,000 | 1.395 | 0.074 | 0.375 | 3 | 15 |
| 7 | Mark IIb | Fixed in Heave, Constant force springs | 2.5 mm | 10,000 | 10,000 | 1.8 | 0.074 | 0.25 | 2 | 17 to 21 |

### 4.5.1 *Trial 1 - Floating, Rigid body*

For this trial the Clam mode was inhibited by replacing the PTO with a fixed length prop, the objective being to validate the theoretical model in this simple configuration, i.e. to determine the heave resonance and to see whether the PTO loads conformed to theory. High values of PTO damping and stiffness (Table 4.1) were input to the time domain model to effectively prevent Clam motion – even higher values resulted in model instability and were not therefore used. The chosen values of Heave damping and stiffness provided a match with the measured resonant peak RAO. The Response Amplification Operator, or RAO, is the ratio of the amplitude of the output parameter, heave or PTO displacement, to the wave input amplitude. See Equation 3.28 for its mathematical definition.

Figure 4.9 shows the comparison between predicted and measured heave response in terms of RAO and phase lag for a wave input amplitude of 20 mm. As can be seen from the RAO plot, the measured response is generally in line with expectations and the resonant peak is consistent with theory. However at the longer wave periods the RAO falls to unity faster than theory would suggest, possibly due to drag effects causing the device to move with the motion of the waves. The measured phase lag at the longer wave periods shows the heave motion leading the waves. At very long wave periods a floating body will simply rise and fall with the waves, with zero phase lag. Thus the calculated values of phase approach zero as the wave period increases, as shown by the continuous curve of Figure 4.9.

The measured values of Figure 4.9 however, show a phase lead approaching 20° which is difficult to explain. Two causes for this behaviour have been investigated. Firstly, and most likely, there could have been a timing error in the wave data, due possibly to a problem with the synchronisation signal within the data gathering system. A second cause could be a positional effect due to the model not being in line with the wave gauges. Of these two possibilities the first has been investigated by the laboratory staff and no fault has been found and the second cause requires a positional error that is not seen on the relevant video recordings. The discrepancy between measured and predicted phase is

seen in virtually every trial and does appear to be the result of a data collection timing issue. However, since all the positional data for the wave tank model is provided by a single system (Qualysis) the problem does not affect the conclusions reached.

Figure 4.10 shows the amplitude of the load in the PTO (or rather the fixed length prop) compared with that predicted by theory. Again it can be seen that the agreement becomes less good at the longer wave periods.

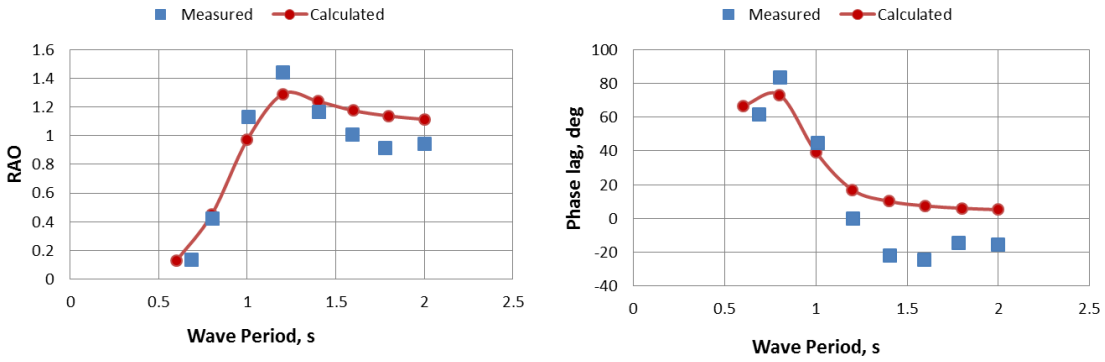


Figure 4.9: Heave RAO and Phase, Fixed Clam, Trial 1

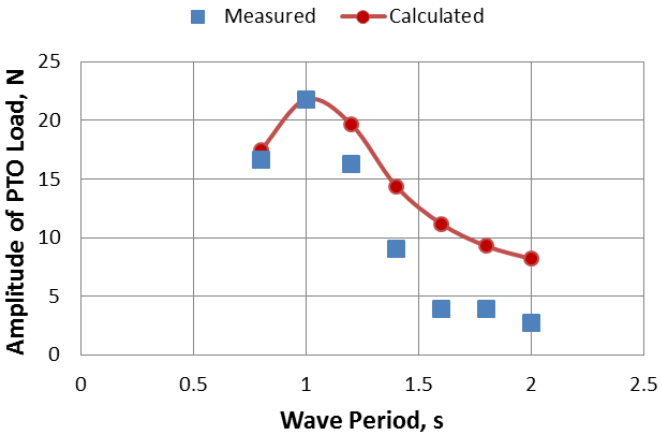


Figure 4.10: Amplitude of PTO Load, Fixed Clam, Trial 1

### 4.5.2 *Trial 2 - Floating Clam*

For this trial the Clam sides were allowed to move and the two PTOs were placed in position. The values of PTO damping and stiffness were chosen from the point of view of ensuring effective power capture, Table 4.1. Also shown is the value of Coulomb Friction, which, being undesirably high, considerably affected the performance of the device. Nevertheless agreement between the theoretical predictions and trial results served to validate the analysis and provide confidence in the mathematical modelling. The wave amplitude for this trial was 40 mm which is equivalent to 2 m at full scale. This is an increase from the desirable amplitude of 20 mm and was necessary in order to overcome the friction in the PTO.

In matching the calculated heave response to the observed behaviour, the heave damping used in the time domain model was increased from that of trial 1 but the heave stiffness was the same (see Table 4.1). PTO damping and stiffness were calculated from knowledge of the characteristics of the orifice and the coil springs, while the Coulomb Friction level in the PTO was chosen to provide a match between the calculated and observed response of the device. Figure 4.11 shows the comparison between calculated and measured heave response while Figure 4.12 shows the comparison between calculated and measured PTO response. As can be seen from Figure 4.12 the match with the PTO RAO is not good. However, if the heave damping and PTO friction values are chosen in order to provide a better match with the measured PTO RAO and PTO load, then the power capture is over-estimated.

Figure 4.13 shows the measured PTO load compared with calculated values and again the match is not good. Figure 4.14 shows the power capture as a function of wave period, at both model and full scales (for the same basic data).

To fully understand the behaviour of the floating device, more test and analysis work would be needed. The mathematical model would require the inclusion of viscous drag on the

body of the WEC - clearly one of the next steps in the investigation. However, the behaviour of the device was generally in line with expectations.

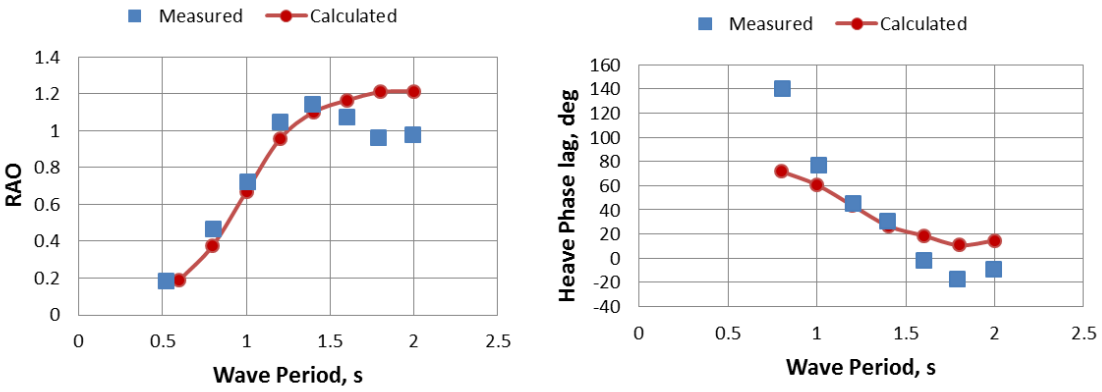


Figure 4.11: Heave RAO and Phase, Trial 2

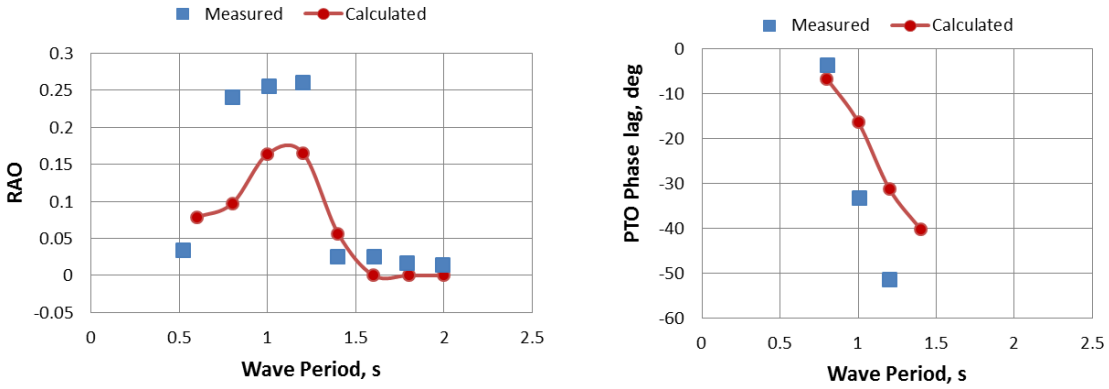


Figure 4.12: RAO and Phase for PTO, Trial 2

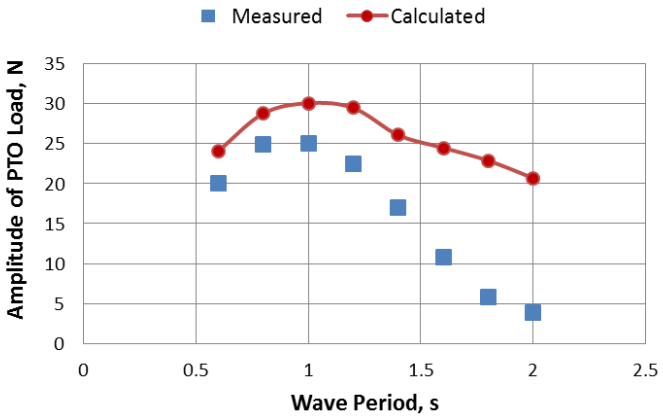


Figure 4.13: Load in Model PTO, Trial 2

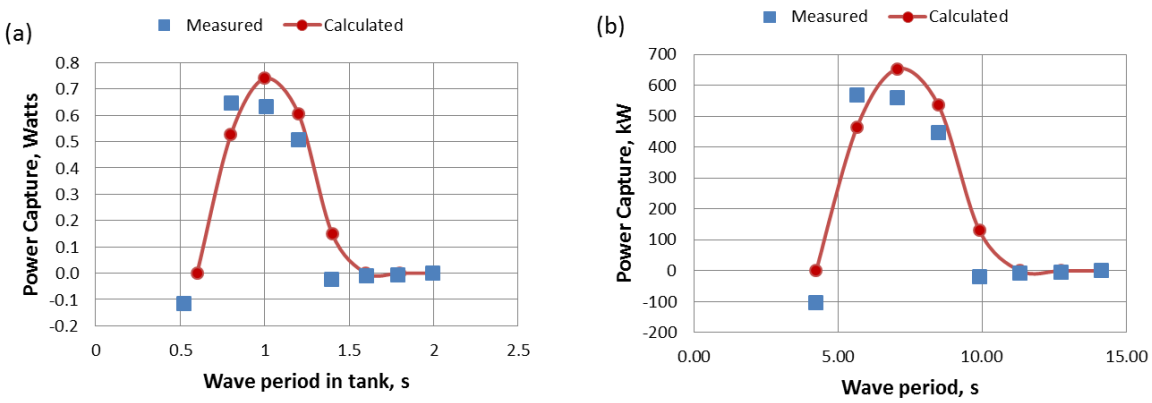


Figure 4.14: Power Capture, Trial 2, (a) model scale, (b) full scale

### 4.5.3 *Trial 3 - No heave, 40 mm wave input*

Trial 3 was the carried out on the final day of the first set of trials. One of the PTOs was leaking and was therefore removed, as was one of the two coil springs. The air pressure in the one remaining PTO air reservoirs was increased to a level necessary to keep the Clam sides apart – and to counteract the load of the tension spring.

The device was considerably lightened in order that the heave movement could be more effectively reduced by using the model's buoyancy to keep the vertical tethers taut. The total mass in this configuration was 24.3 kg, which compares with its 43 kg displacement.

The heave damping and stiffness were chosen in order to provide a match with the observed heave response, since although the aim was to prevent heave motion this was not entirely possible owing to the flexibility of the mooring lines. Table 4.1 shows the resulting estimated values of PTO Damping, Stiffness and Coulomb Friction.

As in the earlier trials the wave amplitude was 40 mm.

Figure 4.15 shows the comparison between calculated and measured heave response while Figure 4.16 shows the comparison between calculated and measured PTO response.

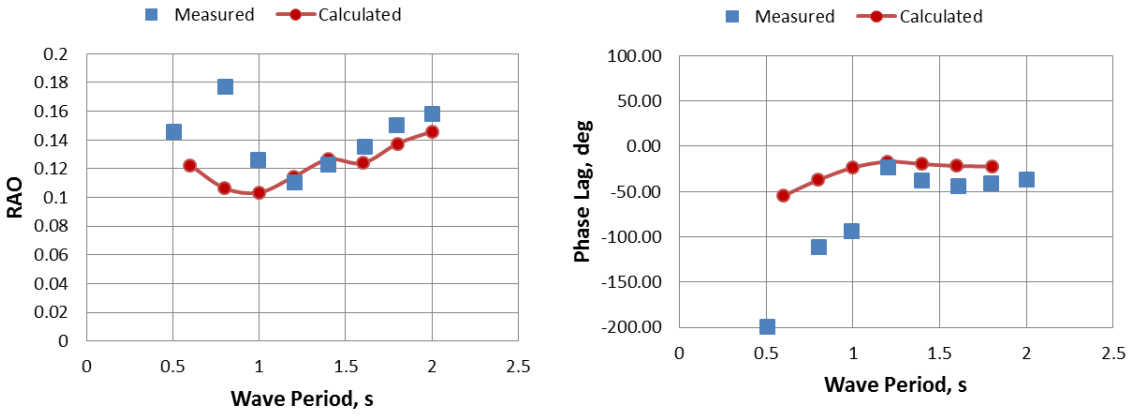


Figure 4.15: Heave RAO and Phase, Trial 3

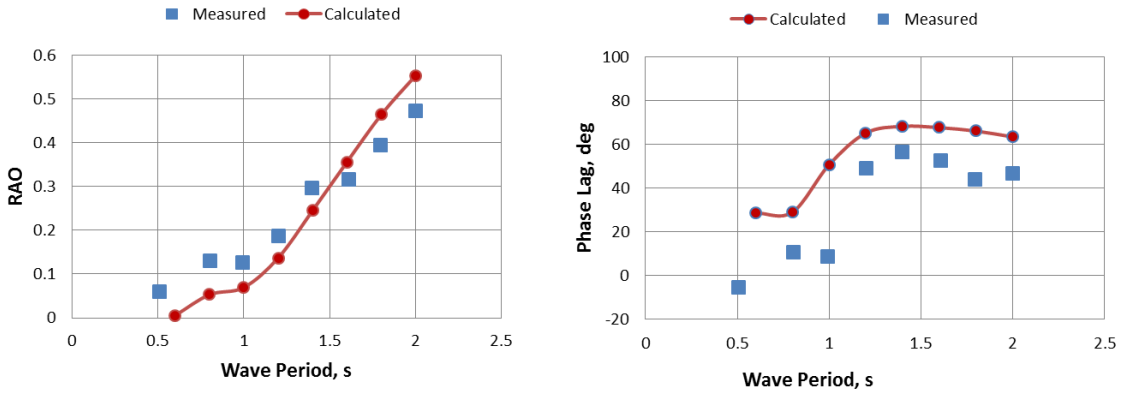


Figure 4.16: PTO RAO and Phase Lag, Trial 3

Figure 4.17 shows the power capture as a function of wave period, at both model and full scales, while the PTO load is shown in Figure 4.18 – good agreement can be seen..

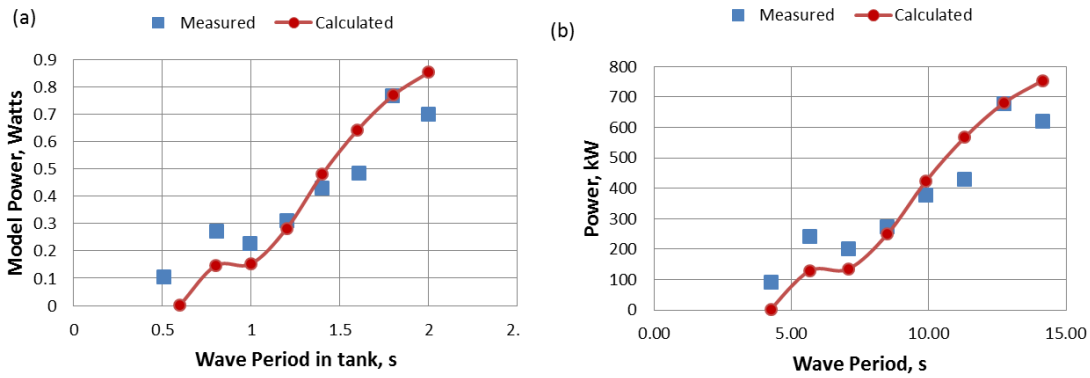


Figure 4.17: Power Capture, Trial 3, (a) model scale, (b) full scale

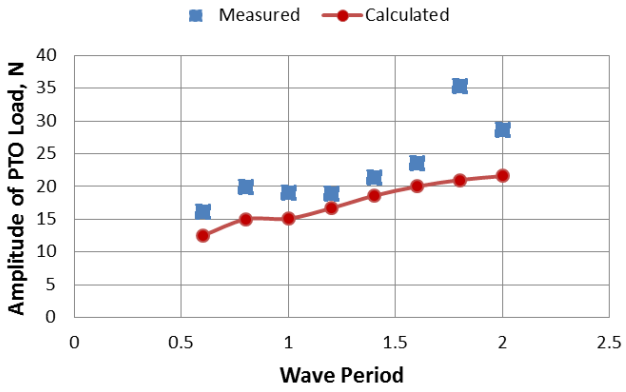


Figure 4.18: Load in Model PTO, Trial 3

### 4.5.4 *Trial 4 – No Heave, 20 mm wave input, coil spring*

The configuration adopted for this trial - and the remaining trials – was the use of one PTO assembly designed to provide the desired level of damping with the majority of the PTO stiffness being provided by steel springs – either conventional coil springs or the special constant force springs. As for trial 3, the device was lightened in order to provide excess buoyancy so as to maintain the mooring lines in tension and thus restrict heave motion.

Table 4.1 shows the estimated values of PTO Damping, Stiffness and Coulomb Friction. The PTO stiffness was far from ideal but was the lowest value that could be achieved from an arrangement where the springs had to support the hydrostatic pressure on the Clam sides and also meet the necessary stroke length.

The heave damping and stiffness chosen for mathematical modelling were such that they effectively prevented heave. The wave amplitude was 20 mm. Figure 4.19 shows the comparison between calculated and measured PTO/Clam response and PTO Load.

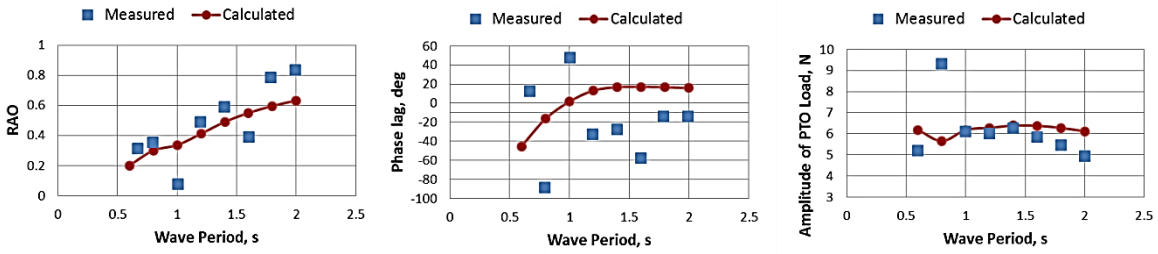


Figure 4.19: RAO, Phase Lag and Load Amplitude in Model PTO, Trial 4

Calculated versus measured power capture is shown in Figure 4.20. Here it can be seen that the power capture is poor, as compared with the potential levels of power capture indicated by the "½ power in 40m wave front" line. This is due to the PTO stiffness being so far from ideal (as explained above). However there is general agreement between the calculated and measured data.

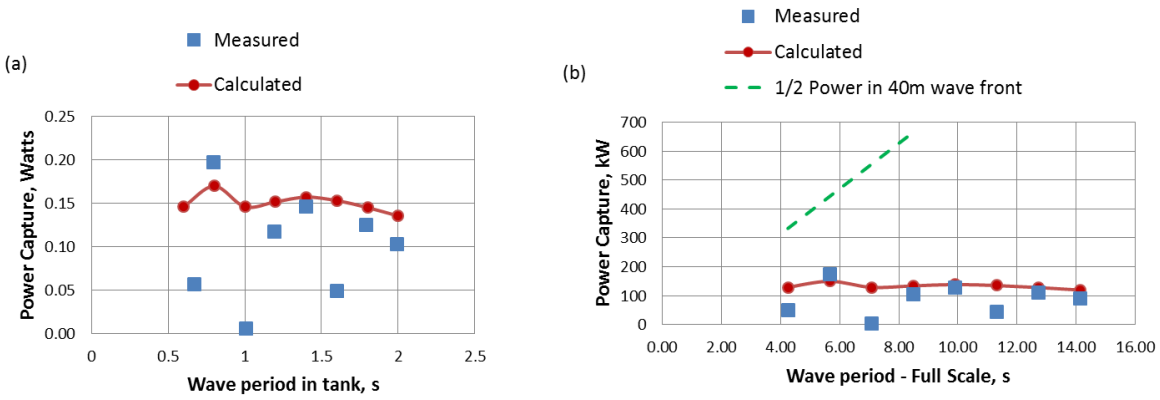


Figure 4.20: Power Capture, Trial 4, (a) model scale, (b) full scale

### 4.5.5 *Trial 5 – 20mm wave, constant force spring, 5 mm orifice*

The configuration adopted for this trial used the PTO assembly that was designed to provide the desired level of damping with the majority of the PTO stiffness being provided by steel springs – either conventional coil springs or special constant force springs. In this case the constant force springs were used. The device was lightened in order that its buoyancy would maintain the mooring lines in tension and thus restrict heave motion.

At wave periods greater than 1.2 s, the PTO movement exceeded the capability of the device. Consequently for Trial 5 the testing was restricted to wave periods between 0.6 and 1.2 seconds.

Table 4.1 shows the resulting estimated values of PTO Damping, Stiffness and Coulomb Friction for trial 5. The PTO stiffness was a practical minimum and was due solely to the

compressibility of the air in the reservoir, while the level of PTO damping arose from the use of a 5 mm diameter damping orifice. The wave amplitude was 20 mm.

Figure 4.21 shows the comparison between calculated and measured PTO/Clam response and PTO Load. As in previous trials the PTO lag was significantly less than calculated. Calculated versus measured power capture is shown in Figure 4.22. Here it can be seen that the power capture is in line with calculated levels – and is of the expected form, including the "kink" at a model period of 1 sec. The "1/2 Power in 40m wave front" line is added for comparative purposes; representing as it does, the best that can reasonably be expected from the device.

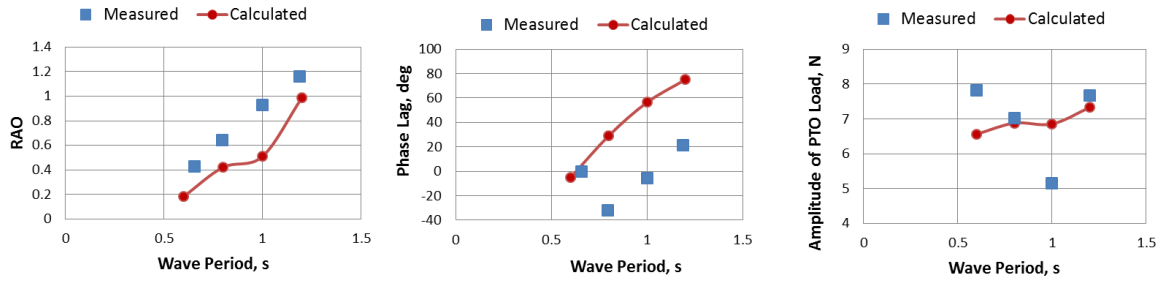


Figure 4.21: RAO, Phase Lag and Load Amplitude in Model PTO, Trial 5

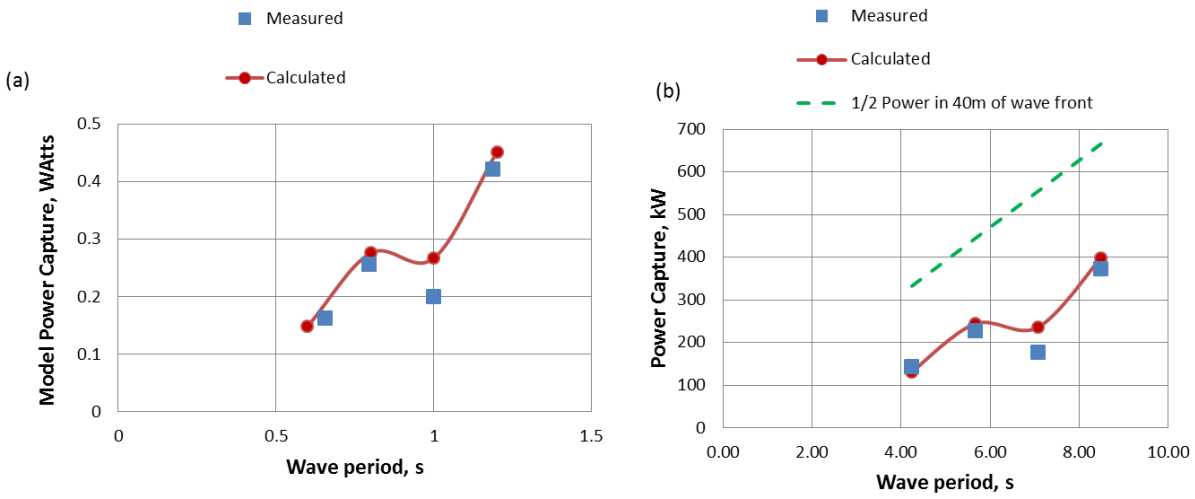


Figure 4.22: Power Capture, Trial 5, (a) model scale, (b) full scale

### 4.5.6 *Trial 6 – 20mm wave, constant force spring, 3 mm orifice*

The setup for Trial 6 was the same as for Trial 5, excepting only that the PTO damping was increased, by reducing the damping orifice diameter to 3 mm from the Trial 5 size of 5 mm. This allowed the testing to be carried out over the full range of wave periods.

Table 4.1 shows the resulting estimated values of PTO Damping, Stiffness and Coulomb Friction for trial 6.

Figure 4.23 shows the comparison between calculated and measured PTO response and PTO Load. As in previous trials the PTO lag was significantly less than calculated.

Calculated versus measured power capture is shown in Figure 4.24. Here it can be seen that the power capture is in line with calculated levels – and is of the expected form, including the "kink" at a model period of 1 sec.

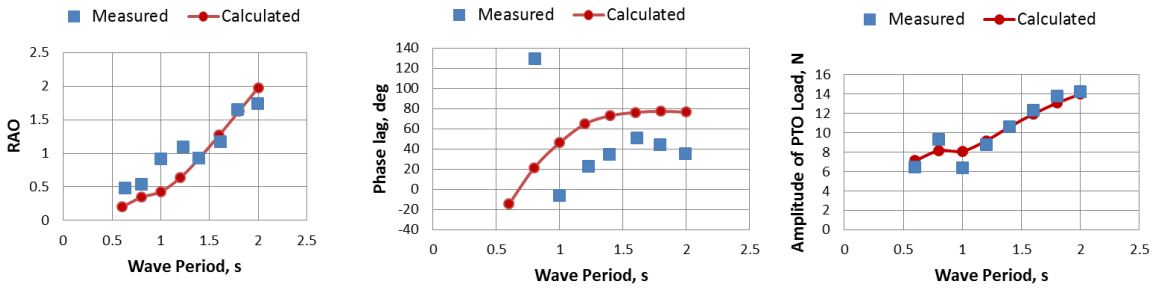


Figure 4.23: RAO, Phase Lag and Load Amplitude in Model PTO, Trial 6, (a) model scale, (b) full scale

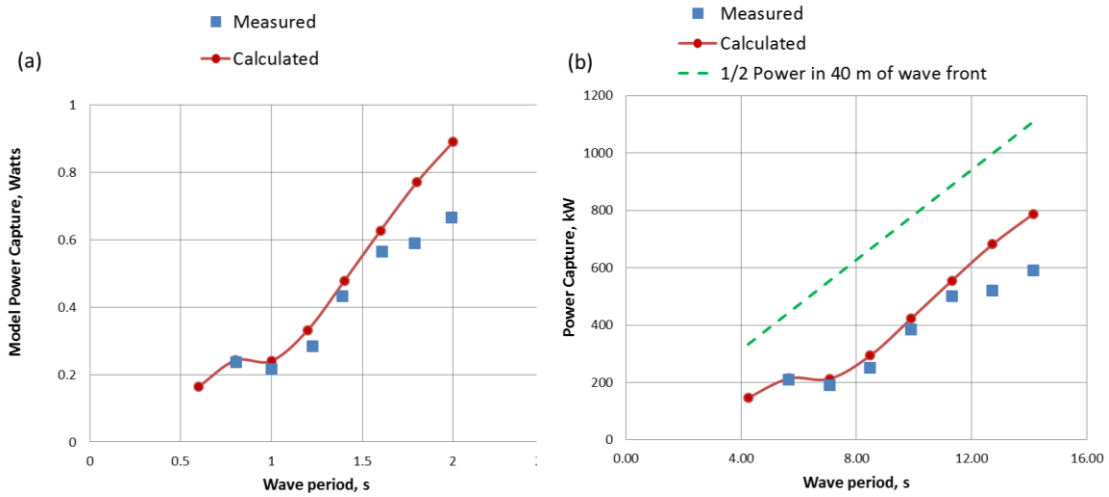


Figure 4.24: Power Capture, Trial 6, (a) model scale, (b) full scale

### 4.5.7 *Trial 7 – 20mm wave, constant force spring, 2.5 mm orifice*

Trial 7 employed the same setup as the previous two trials, except that the PTO damping was further increased by reducing the orifice size to 2.5 mm – see Table 4.1 for the estimated values of PTO Damping, Stiffness and Coulomb Friction. The increase in PTO damping had the effect of increasing the power capture at the longest wave period.

Figure 4.25 shows the comparison between calculated and measured PTO response and PTO Load. As in previous trials the PTO lag was significantly less than calculated. As compared with previous trials, Trial 7 provided the best match between test data and calculated values.

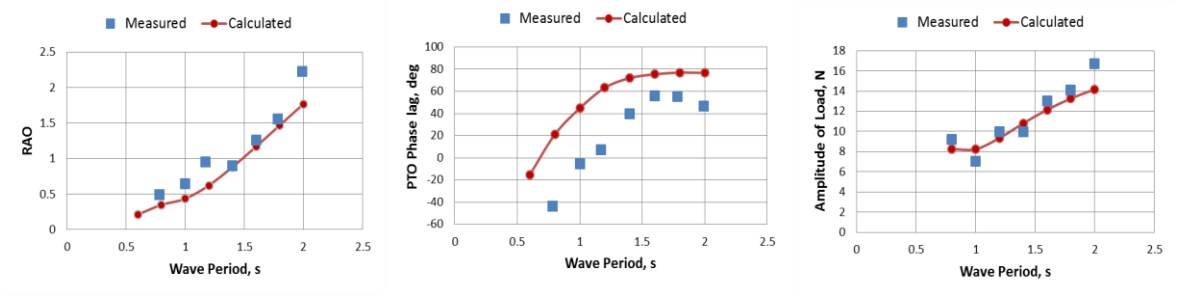


Figure 4.25: RAO, Phase Lag and Load Amplitude in Model PTO, Trial 7

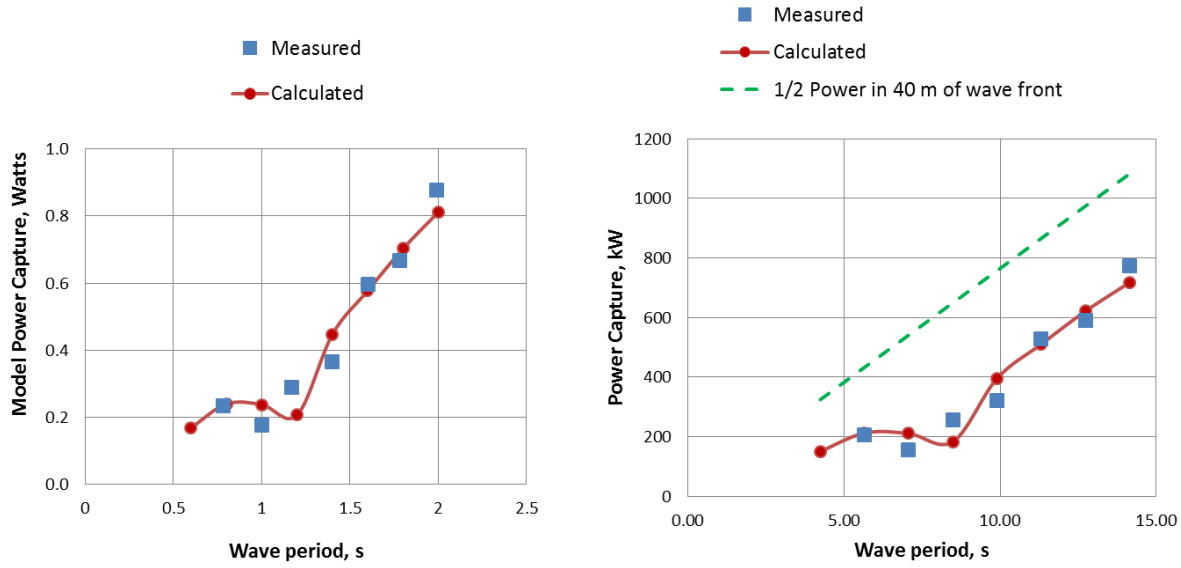


Figure 4.26: Power Capture, Trial 7, (a) model scale, (b) full scale

### 4.5.8 *Variation of power capture with wave input angle*

Two ad-hoc investigations were carried out, looking at the effect of varying the angle of incidence of the incoming wave. The first involved the model configured as for Trial 5, i.e. with the 5 mm orifice.

The angled waves were produced by appropriate changes to the wave tank control input data files. The readings from the wave gauges confirmed that the demanded incident wave angles and wave amplitudes had been achieved, as shown in Section 4.4.

The result of this investigation is shown in Figure 4.27, which shows a reduction in power capture as the incident angle is increased. It should be noted that the longer wave periods could not be investigated due to stroke limitations of the PTO.

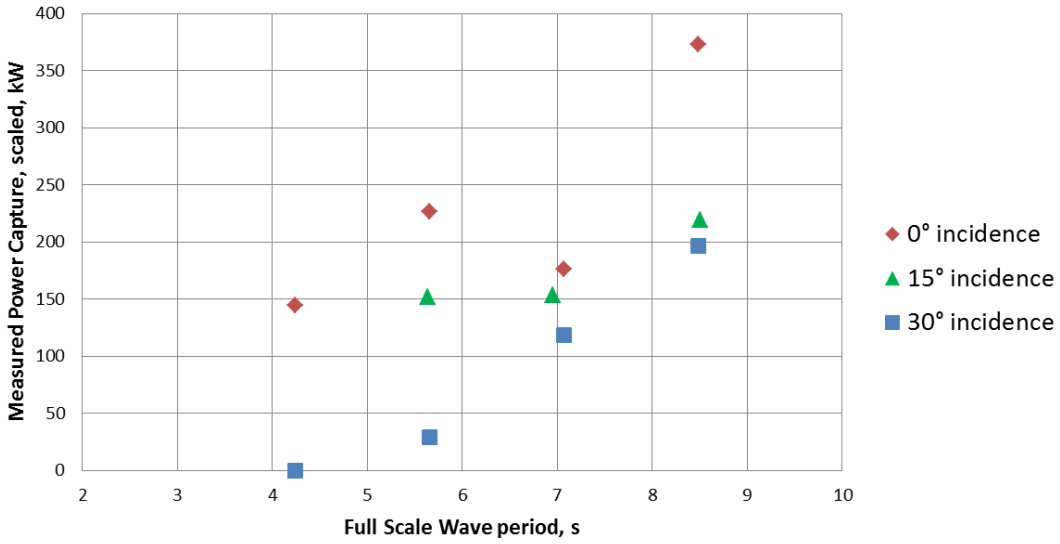


Figure 4.27: Power Capture variation with wave angle; model configured as for Trial 5

The second set of runs was carried out with the model configured as for Trial 7, i.e. with the 2.5 mm orifice. The results are shown in

Figure 4.28.

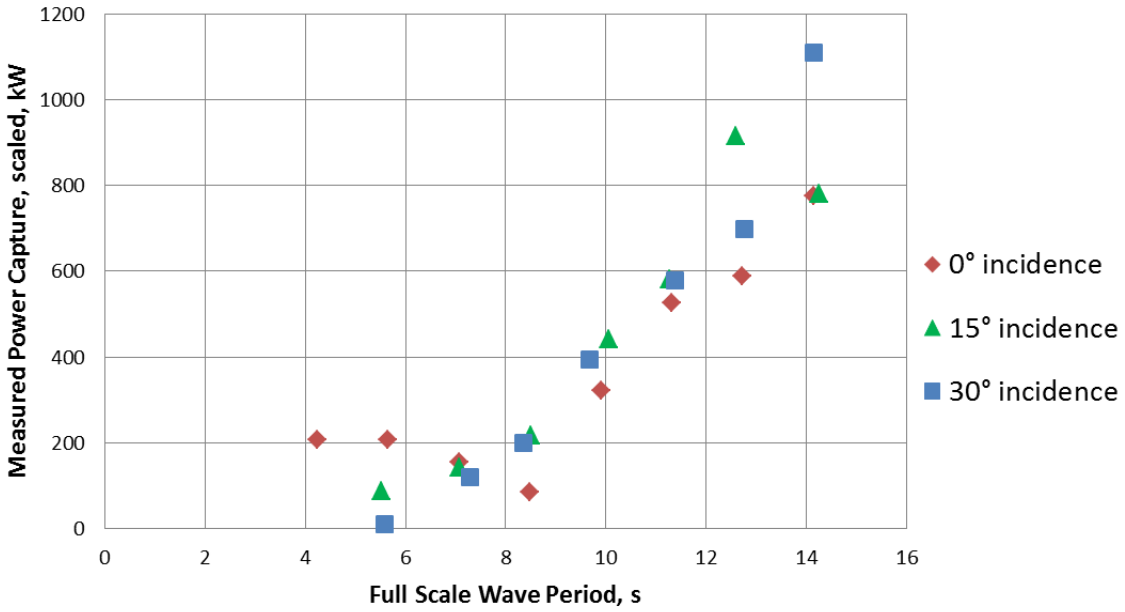


Figure 4.28: Power Capture variation with wave angle; model configured as for Trial 7

Interestingly the device captures more power from the angled waves than those at zero incidence, at least at the longer wave periods. The converse is true for the short period waves.

No explanation is offered for this finding, due to both a lack of time to investigate and also the need for a more extensive investigation, which should be one of the topics for future work, both experimentally and theoretically. It is suggested that the present analysis methodology is followed in the future. WAMIT, for example allows wave incidence angle to be specified by the data input file.

### 4.5.9 *Time domain modelling – Trial 7*

Figure 4.29 shows a 4 seconds "clip" from Run 5 of Trial 7, i.e. a nominal input wave amplitude of 20 mm and a period of 1.4 seconds. Mean removal has been applied to each of the data series. Figure 4.30 shows the corresponding plots generated by the time domain model, using an equivalent sine wave input - see Section 3.11.6 for the mathematical methods employed.

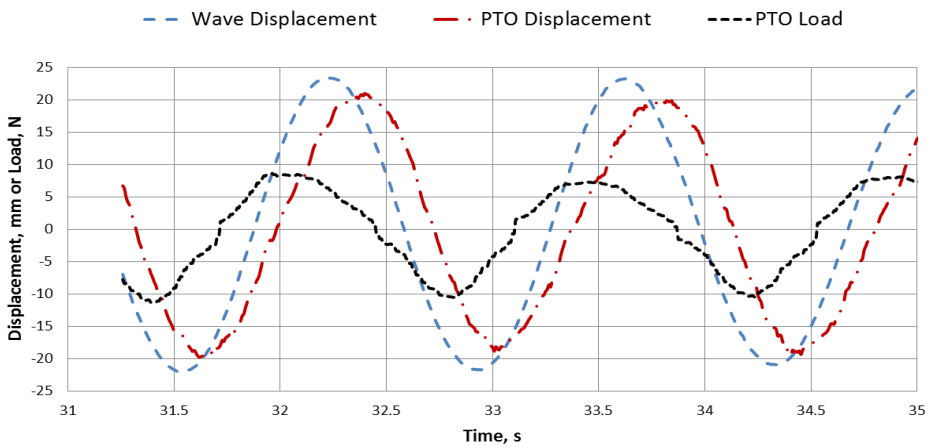


Figure 4.29: Wave Tank Data - Trial 7, Run 5

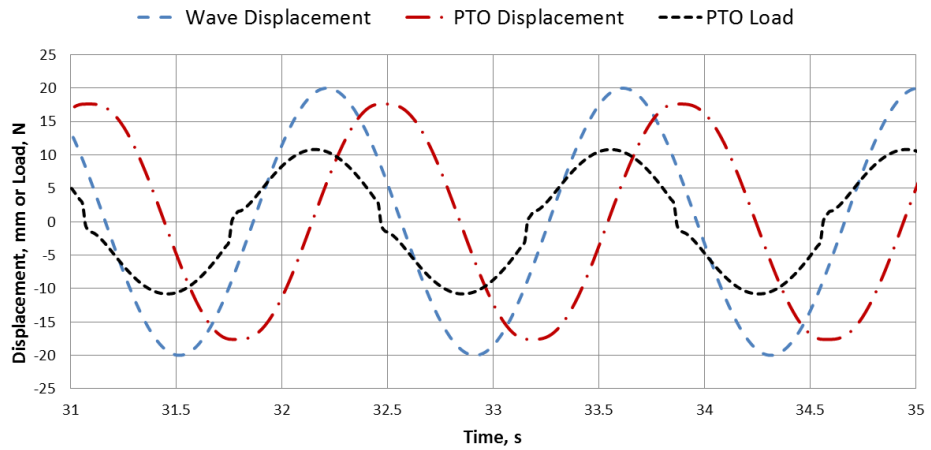


Figure 4.30: Time domain model simulation - Trial 7, Run 5

As can be seen, there is good general agreement between the measured and calculated system behaviour. In particular the calculated PTO Load plot has the same characteristic shape as the measured data.

However, to get a better measure of the comparison between measured and calculated data, a further two plots are included, namely Figure 4.31 and Figure 4.32. Good agreement can be seen and the timing mismatch in Figure 4.31 is most likely to be caused by a timing error in logging the wave data.

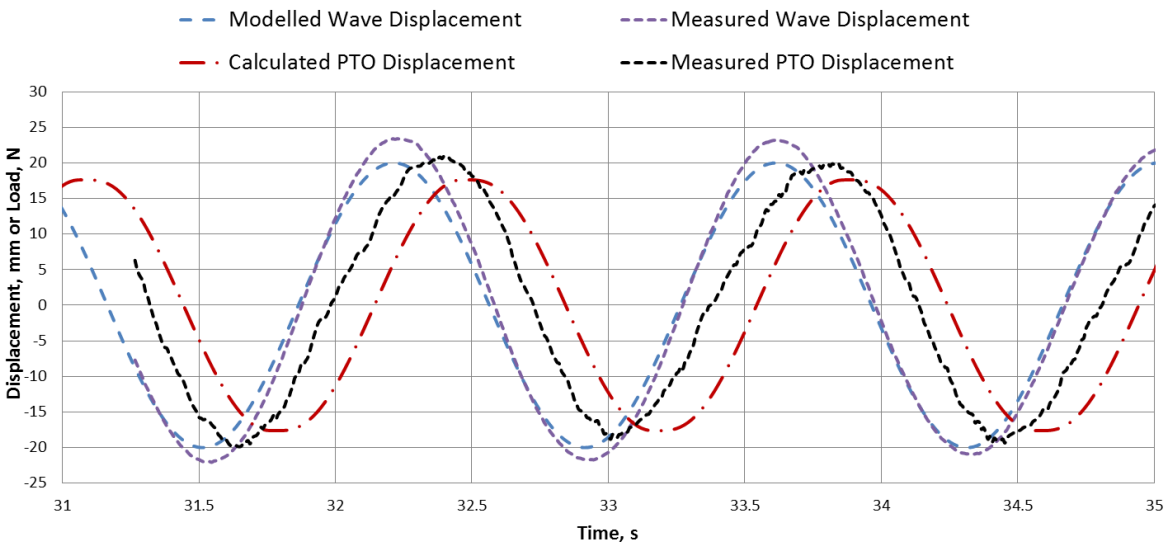


Figure 4.31: Comparison between Calculated and Measured PTO Displacement - Trial 7, Run 5

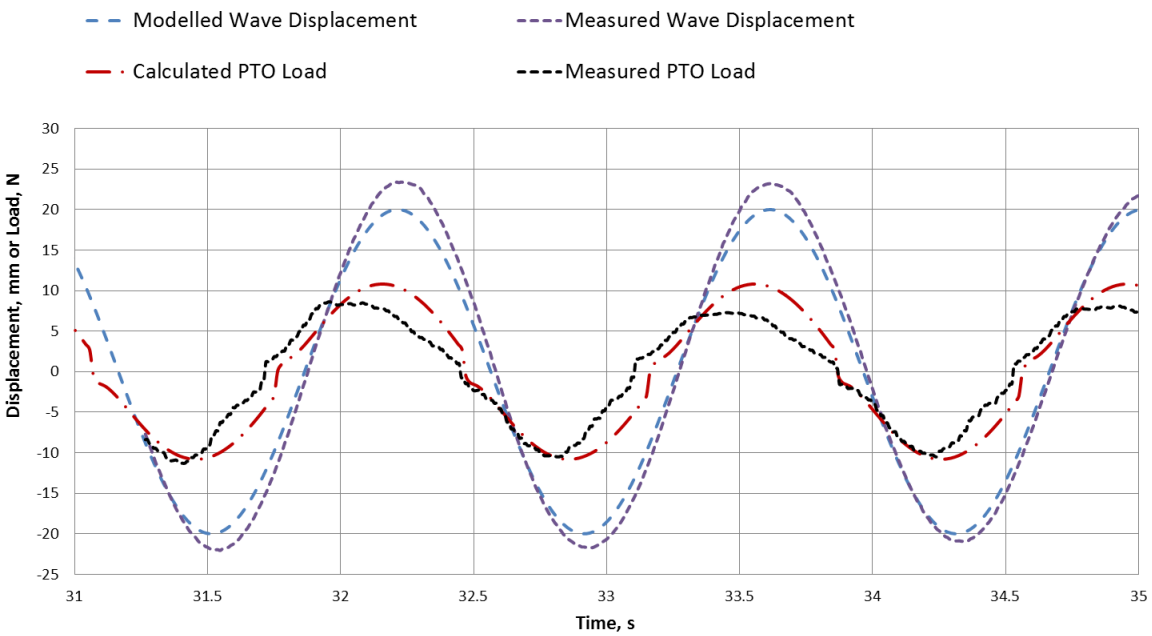


Figure 4.32: Comparison between Calculated and Measured PTO Load - Trial 7, Run 5

### 4.5.10 *Performance in random seas*

A test was carried out with the same physical model as for Trial 7. The angle of wave incidence was 0° and the wave tank was programmed to deliver a Pierson-Moskowitz spectrum with the parameters given in column 2 of Table 4.2. Column 3 gives the full scale values – obtained by appropriately scaling the values in column 2 (scaling factors listed in Appendix A). PM2 is the arbitrarily chosen name for the wave tank settings of this test.

In order to provide confidence in the data it was decided to analyse the measured wave data from the test using a method that included a Fast Fourier Transform function within the Mathcad toolbox - the 4$^{th}$ column of Table 4.2 gives the results. Figure 4.33 shows the Power Spectral Density, $PSD_j$, compared with the spectrum used in the frequency domain analysis, $S_j$, with the measured value of Tz as input - see equation 1.11. $Period_j$ is the wave period in seconds, while 'j' is an index used in the calculation.

Comparing the column 4 data of Table 4.2 with that of column 3, it appears that the parameter, Ts, used in the wave tank set up is the Zero Crossing Period, rather than the Significant Period – the usual interpretation of the symbol, Ts.

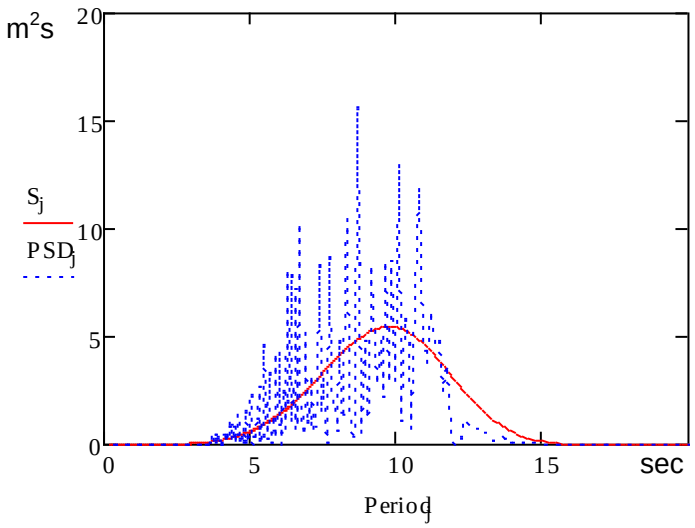


Figure 4.33: Measured PSD for Trial 20 compared with smooth spectrum used for analysis

Table 4.2: Random Sea, PM2

| Parameter | Value at model scale | Full scale value | Measured value (full scale) |
|---|---|---|---|
| Significant Height, Hs | 48 mm | 2.4 m | 2.505 m |
| Hsig | 89 mm | 4.45 m | ---- |
| Max Amplitude | 79 mm | 3.95 m | 2.46 m |
| Peak Frequency | 0.9 Hz | 6.36 s | ---- |
| Equivalent Peak Period | 1.111 s | 7.857 s | ---- |
| Ts | 0.920 s | 6.505 s | ---- |
| Energy Period, Te | ---- | ---- | 8.206 s |
| Zero Crossing Period, Tz | ---- | ---- | 6.911 s |

Figure 4.34 shows a 6 seconds “clip” from Trial 20. Mean removal has been applied to each of the data series.

Figure 4.35 shows the corresponding plots generated by the time domain model, using the measured wave data as input - see Section 3.11.6 for the mathematical methods employed.

As can be seen, there is good general agreement between the measured and calculated system behaviour. In particular the calculated PTO Load plot has the same characteristic shape as the measured data. Also it can be seen that in common with every trial, the PTO Position and Load plots show a measured lag that is less than that indicated by the calculated data.

The hydrodynamic data chosen for the mathematical modelling was that appropriate to the computed energy period of 8.206 seconds. It was found that this provided the best match with the measured data in respect of the magnitude of the system responses.

The measured mean power capture was 233 kW when scaled to full size, while the comparable time domain model produced a figure of 232 kW.

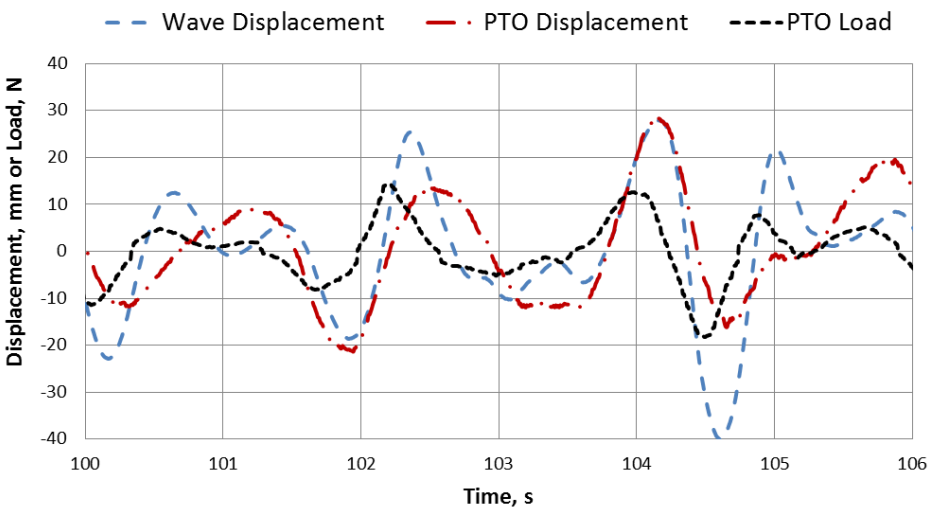


Figure 4.34: Wave Tank Data – Random Seas, PM2

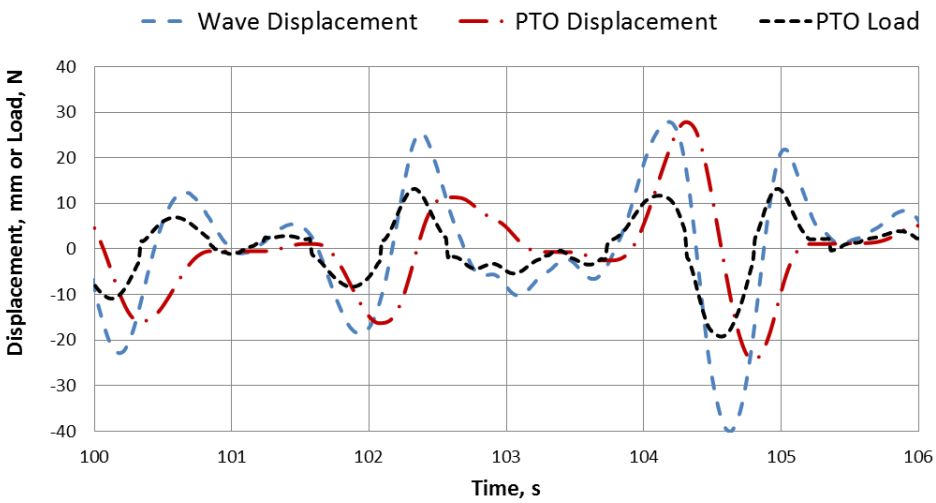


Figure 4.35: Time domain model simulation - Random Seas, PM2

As in the case of the regular wave data, a further two plots are included, namely Figure 4.36 and Figure 4.37. Good agreement can be seen and the timing mismatch can again be detected.

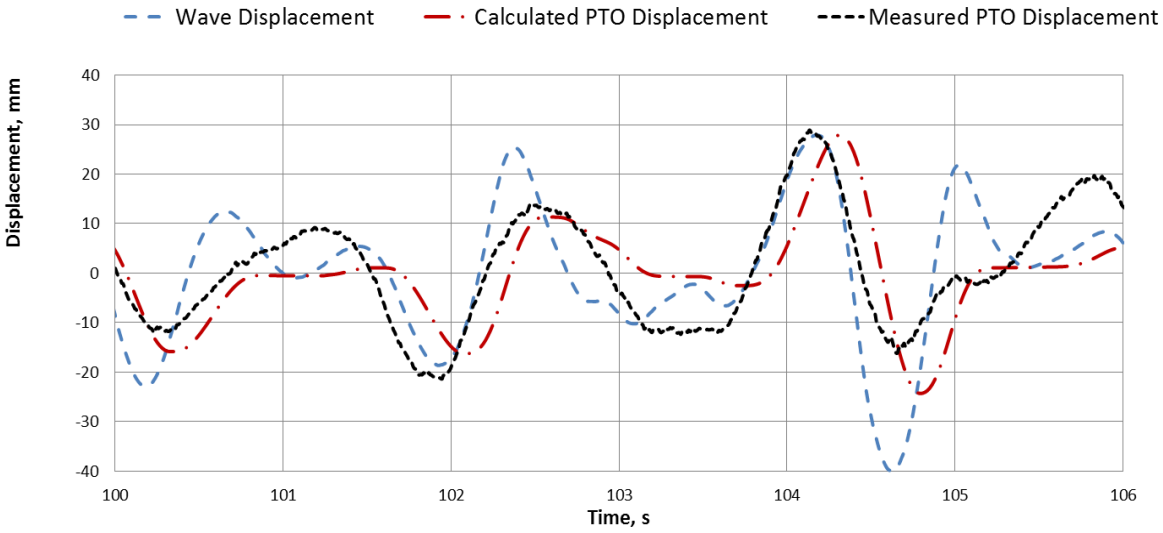


Figure 4.36: Comparison between Calculated and Measured PTO Displacement - Random Seas, PM2

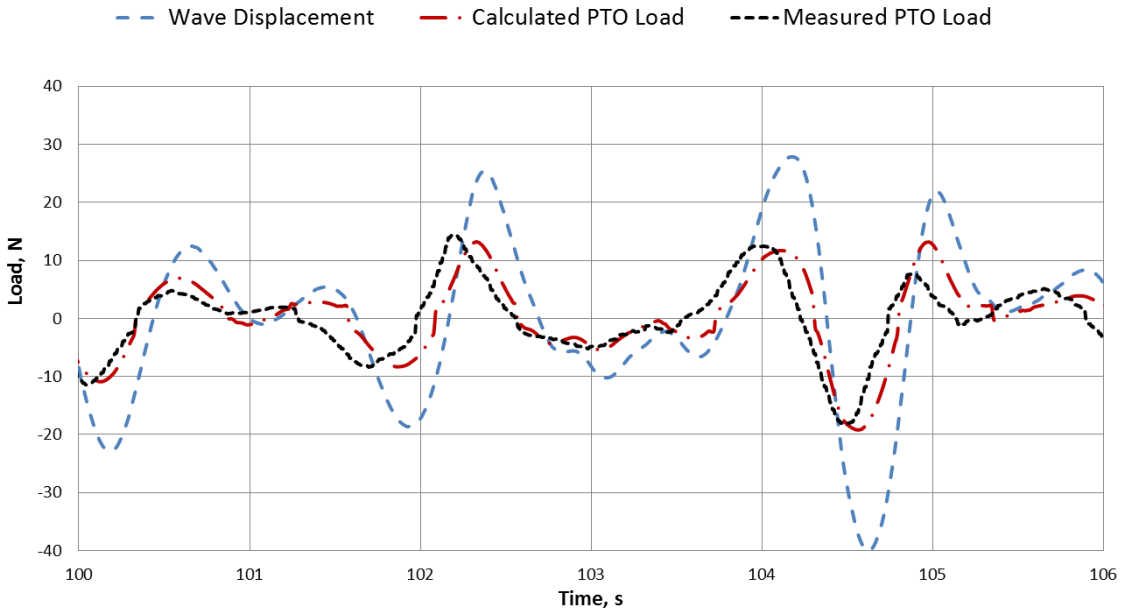


Figure 4.37: Comparison between Calculated and Measured PTO Load - Random Seas, PM2

A further check on the validity of the mathematical modelling was carried out. This entailed using Mathcad to calculate the power capture using the Pierson-Moskowitz spectrum (see Section 3.10 for method) and comparing it with the value calculated by the time domain model using the measured values of Significant Wave Height, Hs, and Energy Period, Te given in Table 4.2 as input. In order to make the comparison, the Coulomb friction in the time domain model was set to zero since the frequency domain model had no provision to allow for friction. The resulting figures were:

- From frequency domain model: 301 kW
- From time domain model simulation: 283 kW

These figures do not show total agreement, but are within 10% of each other which demonstrates the validity of the mathematical modelling. In the future it is hoped to adopt a more mathematically correct method of analysis using a convolution integral approach; and this would naturally be expected to produce a more accurate prediction. However the approximate approach can be seen to give acceptably close results for the purpose of hardware and control system design. With a Coulomb friction value of 2 N (model scale) the time domain model predicted a power capture of 232kW – as reported above.

#### 4.5.11 *Performance in random seas with spread*

As a final test of the performance of the Clam, model was tested with the same specification of wave spectrum as previously – but with a spreading factor of 12. This is the spreading factor that would be appropriate for summer conditions at Wave Hub (Daruvala, 2009). The measured power capture was 198 kW as compared with nominally the same wave input but without spread, of 233 kW – a reduction of 15%.

## 4.6 Discussion of trial results

The aim of the practical testing was to examine the performance across a wide range of operating conditions, rather than looking at just one or two conditions in depth. This aim has been achieved, in that all the plotted curves display a behaviour that compares well with theory – to the extent that the shape of the curves is similar.

In examining the data and the modelling predictions certain questions naturally arise:

- Why does the power capture performance curve display a “kink”?
- Why does the power capture performance curve tend to naturally follow the curve of available wave power across a wide range of wave periods?
- What are the main drivers in determining power capture performance?
- What level of confidence can be put on the performance predictions?
- How does the performance of this device compare with other wave energy converters?

These questions provide the headings that follow:

***Why does the power capture performance curve display a “kink”?***

Referring to the performance data for trial 7 as shown in Figure 4.26, a local minimum in power capture occurs at a wave period of around 8.5 seconds. This characteristic is seen in both the measured and calculated data. The obvious answer to the question is that the hydrodynamic and other physical characteristics of the system are such as to produce this result – and that the mathematical modelling of the system is correct. The hydrodynamic coefficients have been examined in the hope that a simple explanation for the shape of the performance curve might be found. However, there seems to be no single piece of data that provides an explanation and this is a question that could be examined more fully in the future.

***Why does the power capture performance curve tend to naturally follow the curve of available wave power across a wide range of wave periods?***

The conventional wisdom regarding the mechanism of WEC maximum power capture may be captured by the following two statements (Shaw, 1982):

1) The undamped natural frequency should be matched to the forcing frequency of the waves, and
2) The energy extraction damping coefficients should be equal to the sum of the hydrodynamic damping coefficients and viscous damping coefficients due to the motion of the WEC.

In the case of the present device the only mode of interest is mode 7, the Clam or PTO mode. Natural frequency is related to mass and stiffness values, Section 1.5.2 and equation 1.26.

The only movement is that of the Clam sides, and these have negligible mass in relation to the surrounding water. Thus the undamped natural frequency and hence resonant period depend on the hydrodynamic and hydrostatic coefficients alone, as in equation 4.1:

$$\omega_0 = \sqrt{\frac{C_{77}}{A_{77}}} \text{ and thus } T_0 = \frac{2\pi}{\omega_0} \tag{4.1}$$

where $C_{77}$ is the Clam Hydrostatic Coefficient and $A_{77}$ is the Clam Added Mass, $\omega_0$ is the undamped radian frequency and $T_0$ is the undamped resonant period.

Figure 4.38 shows the comparison of the undamped resonant period, calculated using equation 4.1 with the ideal situation of equalling the input wave period. Thus between, say, a 5 s and 13 s period the resonant period of the system provides a reasonable match with the wave input.

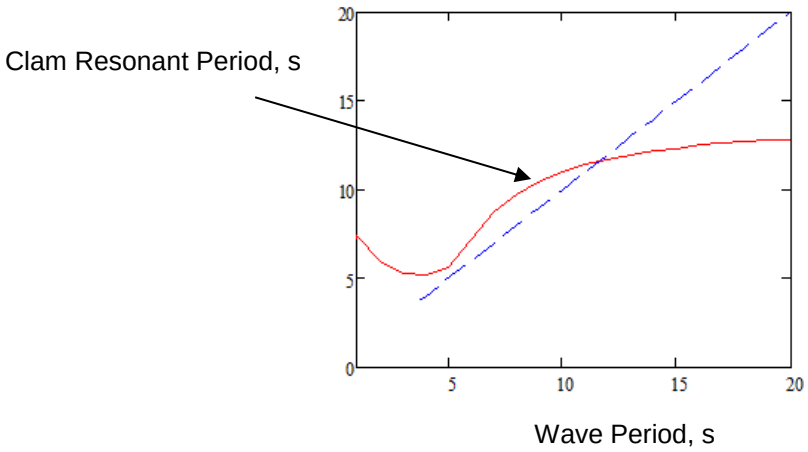


Figure 4.38: Resonant Period of Clam mode

The second requirement for maximum power capture is that the energy extraction damping coefficients should be equal to the sum of the hydrodynamic damping coefficients and viscous damping coefficients due to the motion of the WEC.

The hydrodynamic damping coefficient, $B_{77}$, has the value of 0.0318 MNs/m for a 10 s wave, which is much less than the 1.8 MNs/m for PTO damping that has been found during the practical testing to be a good value to use, (Table 4.1)

If the PTO damping is given the values in the region of 0.03 MNs/m to 0.04 MNs/m, in line with conventional wisdom, the result is good power capture at the resonant period, as would be expected, but much poorer power capture at other wave periods. Also the PTO RAOs are unrealistically large, since the available stroke of the PTO would not be sufficient. It is likely that the increased stroke (if achieved) would result in increased viscous drag, and a consequent reduction in power capture.

Thus the key to the wide band response would appear to lie in the natural ability of the Clam resonance to match the input wave period.

***What are the main drivers in determining power capture performance?***

As has been seen from the test programme and modelling studies reported here, heave damping and stiffness have a marked effect on power capture. Also it appears necessary to prevent heave motion as much as possible. Both practical testing and mathematical modelling indicate that the PTO stiffness should be as low a value as possible. PTO Damping should be chosen on the basis of mathematical modelling simulations. In addition, friction within the WEC should be kept as low as possible. This may be demonstrated by reference to the setup for Trials 6 and 7.

Rows 1 and 4 of Table 4.3 contain the values of friction, stiffness and damping that were considered appropriate for trials 6 and 7, respectively. The resulting calculated power and PTO RAO is also shown, as is the measured power. In the case of trial 6, the comparison between calculated and measured power is not good. In examining the trial data and spreadsheet calculations the explanation for the discrepancy would appear to lie in the fact that the pressure in the air reservoir in trial 6 was too low for this particular wave period, with the consequence that the PTO ram did not remain in sufficiently good contact with the Clam sides throughout the cycle.

Rows 2, 3, 5 and 6 of Table 4.3, show the effect of reducing friction and PTO stiffness whilst maintaining the PTO RAO to a value of 2 or less. To achieve this aim, the PTO damping value of row 3 has been increased from the row 2 value. If however the limitation on PTO RAO is ignored the power capture can be significantly increased, as shown by the data in row 7. In this case the all the available wave power over the 40 m width of the Clam is captured. In practice this would not be possible due to the design limitations on PTO stroke and also the effect of viscous drag that would accompany the increased movement of the Clam sides. However, it is instructive to examine the effect of allowing an increase in PTO stroke and Table 4.4 shows the result of a brief investigation. In this case the PTO damping figure was retained at 0.23 MNs/m and the friction level was increased. Since the friction in the wave tank model is measured by the load cells and contributes to the power

capture measurement, the mathematical model does the same. Hence this strategy is equivalent to employing Coulomb damping in the PTO.

Table 4.3: Effect of PTO stiffness, damping and friction on performance of Clam at 12.73 s period

| Row | Trial | Friction, MN | PTO Stiffness, MN/m | PTO Damping, MNs/m | Calculated Power, kW | Measured Power, kW | Calculated Clam/PTO RAO | Calculated Capture Width, m |
|---|---|---|---|---|---|---|---|---|
| 1 | 6 | 0.375 | 0.074 | 1.395 | 689.5 | 563 | 1.624 | 14.2 |
| 2 | -- | 0.0 | 0.074 | 1.395 | 884 | --- | 2.28 | 18.2 |
| 3 | -- | 0.0 | 0.0 | 1.6 | 810 | --- | 2.038 | 16.6 |
| 4 | 7 | 0.250 | 0.074 | 1.8 | 621 | 615 | 1.468 | 12.8 |
| 5 | -- | 0.0 | 0.074 | 1.8 | 732 | --- | 1.83 | 15.0 |
| 6 | | 0.0 | 0.0 | 1.8 | 740 | --- | 1.84 | 15.2 |
| 7 | -- | 0.0 | 0.0 | 0.23 | 1932 | --- | 8.303 | 39.7 |

Table 4.4: Effect on power capture of increasing Clam RAO - at 12.73 s wave period

| Friction, MN | PTO Stiffness, MN/m | PTO Damping, MNs/m | Calculated Power, kW | Calculated Clam/PTO RAO | Calculated Capture Width, m |
|---|---|---|---|---|---|
| 0.0 | 0.0 | 0.23 | 1932 | 8.303 | 39.7 |
| 0.3 | 0.0 | 0.23 | 1839 | 6.56 | 37.8 |
| 0.6 | 0.0 | 0.23 | 1587 | 4.81 | 32.6 |
| 0.8 | 0.0 | 0.23 | 1332 | 3.57 | 27.4 |
| 1.0 | 0.0 | 0.23 | 1016 | 2.51 | 20.9 |
| 1.083 | 0.0 | 0.23 | 910 | 2.194 | 18.7 |
| 1.125 | 0.0 | 0.23 | 804 | 1.89 | 16.5 |
| 1.2 | 0.0 | 0.23 | 677 | 1.54 | 13.9 |

Figure 4.39 takes values from Table 4.4 to show the relationship between capture width and PTO RAO. By doubling the possible RAO from 2 to 4, the power capture is almost doubled. Thus increasing the allowable PTO stroke should be a design aim.

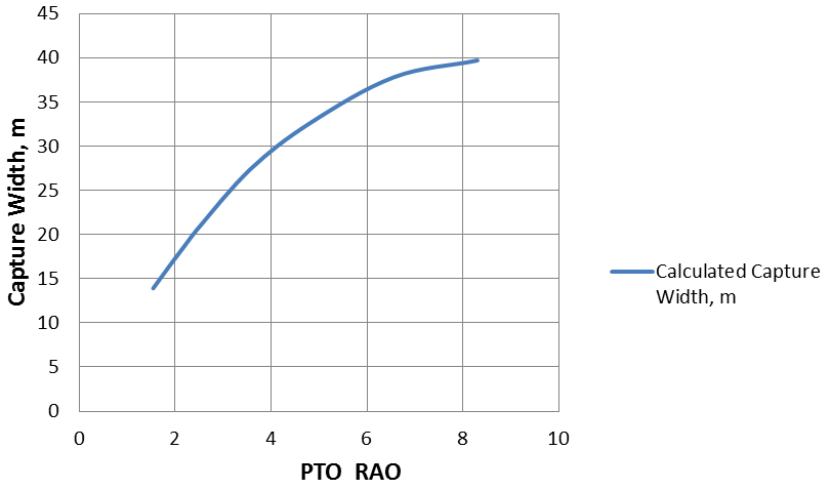


Figure 4.39: Capture width versus PTO RAO

***What level of confidence can be put on the performance predictions?***

It is difficult to answer this question. However, it is not unreasonable to claim that the behaviour of the device in both free floating and heave restrained configurations can be predicted with confidence. The predictions are better and more consistent at the longer wave periods and higher levels of power capture, say above 8 s and 450 kW.

As experience was gained in carrying out the trials, the agreement between predictions and tests improved – as evidenced by the trial 7 results shown in Section 4.5.7. Figure 4.40 compares the measured power capture with the calculated power, and with a ± 10% band around it. Thus using trial 7 as the standard it is reasonable to claim an accuracy of predictions within 10% for wave periods greater than 10 s. For periods less than 10 s the correlation is not as good.

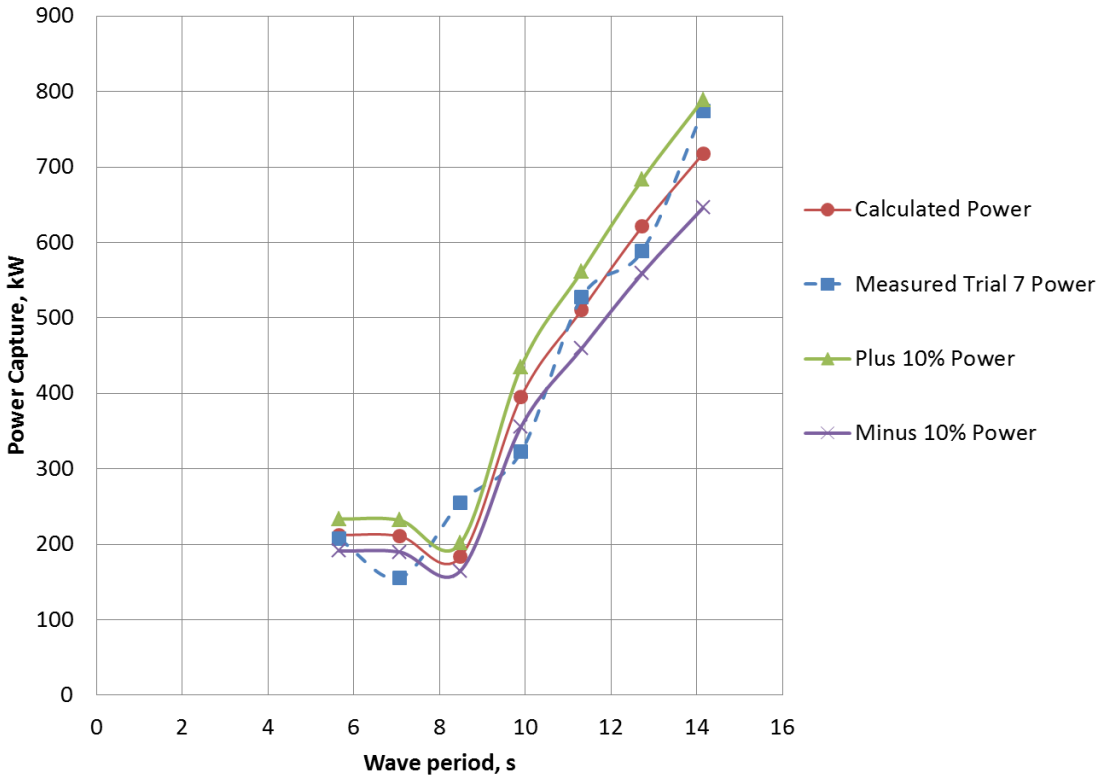


Figure 4.40: Power prediction accuracy

Bearing in mind that these predictions are based on tests in the wave tank, it is worth considering how the performance of a full sized device might compare. Although the calculated predictions ignore viscosity, it would have influenced the practical results of the wave tank testing. Viscous effects do not scale in the same way as the hydrodynamic and inertia loads, so that at full scale they are much less significant. Accordingly the power capture at full size is likely to be greater than the tests suggest.

***How does the performance of this device compare with other wave energy converters?***

To answer this question fully is a research project in itself. However, it is instructive to look at a couple of examples that provide a comparison with the Clam, i.e. SPERBOY™ and Oyster.

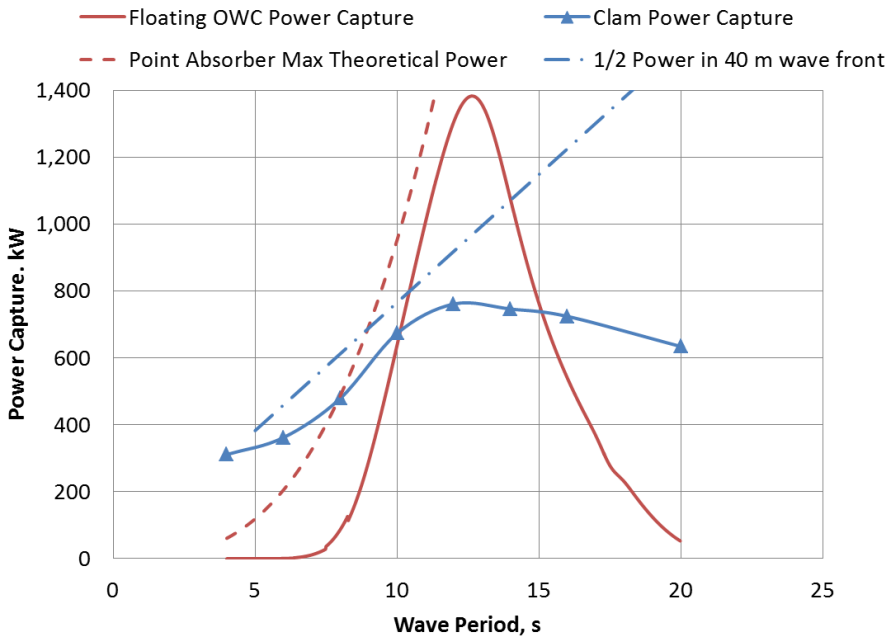


Figure 4.41: Comparison of Clam's Performance with Floating Oscillating Water Column WEC

Figure 4.41 shows the comparison of the Clam with the SPERBOY™ floating Oscillating Water Column (OWC) wave energy converter (Tucker et al., 2010). The power capture data is based on a regular wave input of 1 m amplitude across the range of wave periods shown.

The SPERBOY™ WEC is a Point Absorber designed to operate in the highly energetic wave climate found in the Outer Hebrides where the annual average wave power is of the order of 62 kW per metre of wave front. The chosen location for the study was Benbecula in the Outer Hebrides taken as the WERATLAS (INETI, 2009) data for point Barra. Figure 4.42 describes the location by means of an Annual Average Spectrum that is defined from the individual spectra for a number of wave states weighted by their frequency of occurrence. It can be seen by comparing Figure 4.41 and Figure 4.42 that the

SPERBOY$^{TM}$ WEC has been designed to match the characteristics of the wave resource (Phillips & Rainey, 2005).

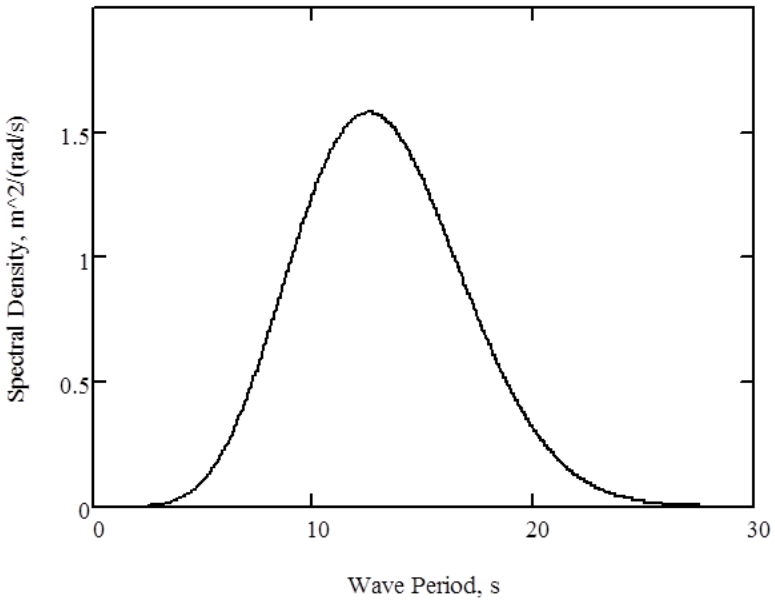


Figure 4.42: "Annual Average" Wave Input Spectrum at Benbecula (Phillips & Rainey, 2005)

The mean annual power capture of SPERBOY$^{TM}$ was calculated, and confirmed by testing, to be 700 kW – prior to considering losses in the PTO. The rating of the PTO maximum power capture was 3 MW. However, to achieve this level of power capture the device had the following characteristics:

- Overall diameter – 40 m
- Column internal diameter – 22 m
- Column length (below waterline) – 70 m
- Overall Mass, including ballast – 17,200 tonnes

Although a point absorber can achieve a capture width much larger than its physical size, the range of wave periods where this applies may be small. It was found that the large size of SPERBOY$^{TM}$ was necessary to achieve a sufficiently large bandwidth.

To match the performance of SPERBOY$^{TM}$ with a Clam-type WEC in the wave climate of Benbecula, it would be necessary to increase its physical size – a not impossible task. However, the advantage that the Clam displays lies in its performance in less energetic locations and hence shorter wave periods.

A device more akin to the Clam is the Oyster WEC – a nearshore oscillating wave surge converter that takes the form of a flap mounted on the sea floor and hinged at its base. The Clam has a number of features in common with Oyster. In particular its physical size is similar - as is its annual power capture, i.e. 200 kW mean power in a wave climate of 19 kW/m, although this relates to Oyster 1 which has a width of 18 m.

Oyster does not follow the conventional wisdom of Section 1.5.2 – it "couples with incoming waves without being highly tuned" (Whittaker et al., 2007) and aims to optimise the wave torque. In common with Oyster, the Clam does not follow conventional wisdom, but there are differences. Oyster is not highly tuned whereas the Clam achieves tuning naturally, as shown by Figure 4.38. At a width of 26 m Oyster 2 operates partly as a point absorber, while studies of a wider device of 50 m width show a power capture of 50% of the incoming wave power, which is in line with Clam experience.

Oyster's energy capture varies with incoming wave direction. Thus the reduction in power capture is approximately proportional to the cosine of the angle of incidence to the power of 2.1 (i.e. roughly "power squared"), such that at 90 degrees to the normal wave direction the energy capture is zero (Whittaker et al., 2007). It is possible that the Clam performs better than Oyster in this respect - see Figure 4.28 which shows little reduction in power capture, at least up to an angle of incidence of 30°.

# 5 Full Scale Design

## 5.1 Introduction

Having completed the programme of analysis and experimentation it may be concluded that the Clam-type wave energy converter (WEC) has good potential. A promising performance regime, that of low or negative PTO stiffness, has been identified,

However, there is a not-inconsiderable amount of work needed to prove the feasibility of the concept at full scale. In the sections that follow a possible way forward is described and the power capture at the Wave Hub test site is estimated.

## 5.2 Main Features of the proposed design concept

Having demonstrated that this Clam-type wave energy converter (WEC) has potential, the question is whether a full scale realization is feasible – one that embodies the features that have been shown to be effective through mathematical modelling and physical model testing.

---

***The remainder of this section, which contained details of a possible full scale device, has been removed due to Copyright restrictions.***

---

## 5.3 Performance prediction

An assessment of the performance of a full size device at the Wave Hub test site has been carried out using data on the annual wave climate, including directionality. The approach that has been adopted is first to assess the device performance for a specific number of wave states and then to curve fit these so that the annual energy capture for any desired wave state can be found by interpolation. With knowledge of the frequency of occurrence of each wave state the annual energy capture (and hence annual mean power capture) may be found by summing the energy capture contribution from each wave state.

A Prototype device would have the facility to change the PTO characteristics in accordance with whatever control philosophy is found to be appropriate. However, for the purpose of

making the present assessment just three parameters are adjusted; namely the PTO stiffness, PTO damping and the wave period that produces the hydrodynamic coefficients for use in the time domain model. Adjustment of this last parameter is a consequence of employing the approximate method of analysis described in Section 3.11.6. Thus this wave period value is adjusted in order to obtain agreement between the calculated power capture predictions of the frequency domain (Mathcad) and time domain (VisSim) models. Then the behaviour of the system in response to non-linear effects such as PTO friction may be assessed by using the time domain model.

For the purpose of the analysis the limit of PTO movement is taken as ± 3 m. Within this limitation, PTO damping and stiffness values that maximise power capture are found by trial and error. In the absence of specific data a nominal figure for Coulomb friction of 50kN has been chosen for the PTO drive system. Furthermore the PTO drive system and associated counter balance system adds inertia to the Clam mode. Thus an additional mass of 1003.2 tonne has been added to mode 7, the PTO/Clam mode.

The random wave input to the time domain model has been taken from a previous study (Phillips, 2003) and scaled for the four chosen wave energy periods.

The effect of wave spreading has been simulated by reducing the modelled input wave amplitude by a factor of 8% for the least energetic seas, i.e. for Hs = 2 m. This factor is reduced to 4% for the more energetic seas, i.e. for Hs = 4 m and 6 m. For the most energetic seas (Hs = 8 m) the input wave amplitude is not reduced. The thinking behind this is that the resulting power capture for the least energetic seas is about 15% - which is in accordance with the reduction of power capture found in the wave tank. The spread of incident wave angles is found to reduce as the wave input increases - hence the reduction in the wave amplitude factor for more energetic seas.

The resulting power capture matrix is given in Table 5.1. Each cell contains predicted power capture in kW for the given sea state. The zeros values are added for the benefit of the interpolation routine.

Table 5.1: Predicted Performance for Full Scale WEC, kW

| Te, s | Hs, m | | | | |
|---|---|---|---|---|---|
| | 0 | 2 | 4 | 6 | 8 |
| 0 | 0 | 0 | 0 | 0 | 0 |
| 4 | 0 | 79 | 375 | 728 | 1471 |
| 8 | 0 | 231 | 646 | 1236 | 1473 |
| 12 | 0 | 244 | 548 | 565 | 874 |
| 16 | 0 | 240 | 366 | 333 | 433 |

The cubic spline interpolation routine provided by Mathcad is then used to give a predicted power capture for any particular sea state within the range covered by Table 5.1. Figure 5.1 shows a surface plot of the interpolated values. To accommodate the interpolation routine the x and y axes values have been scaled in order to provide simple index values (i.e. as Te/4 and Hs/2). The vertical z-axis contains the power capture in kW.

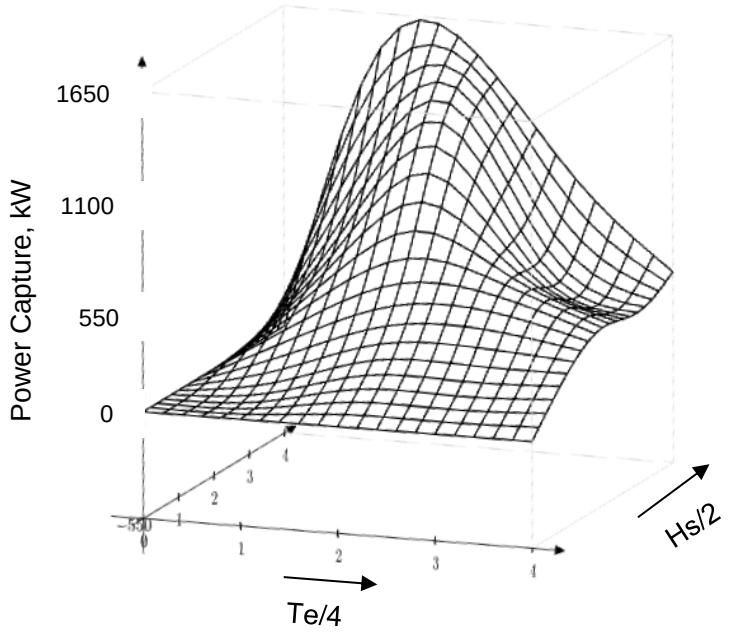


Figure 5.1: Surface Plot of interpolated power capture values

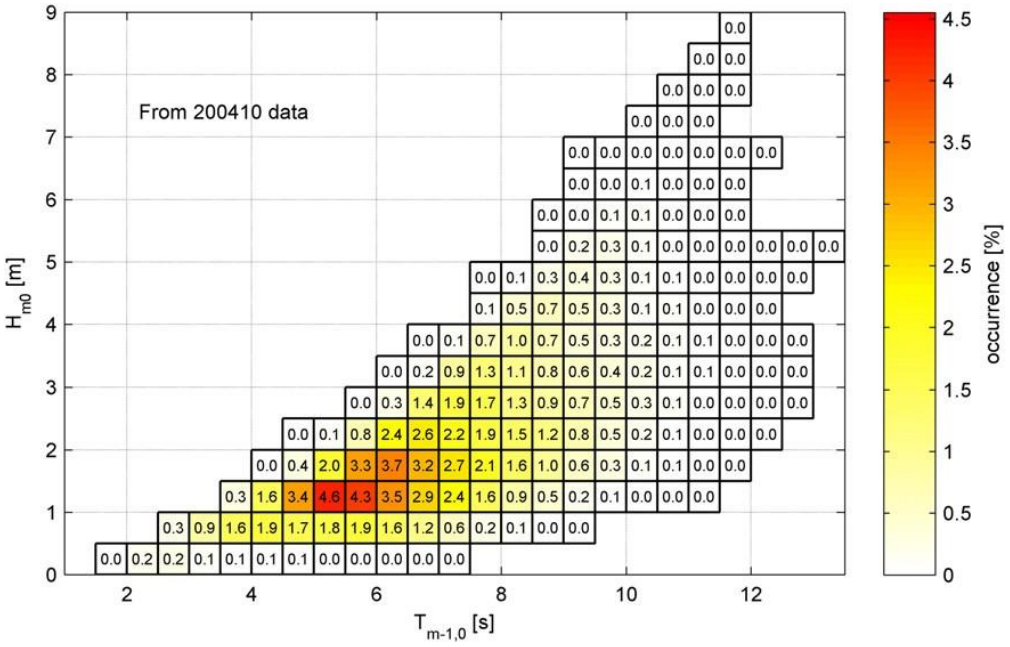


*Figure 5.2: Joint probabilities, $H_{m0}$ (Hs) and $T_{m-1,0}$ (Te) at Wave Hub, locn 1 (Nieuwkoop et al.), 2013)*

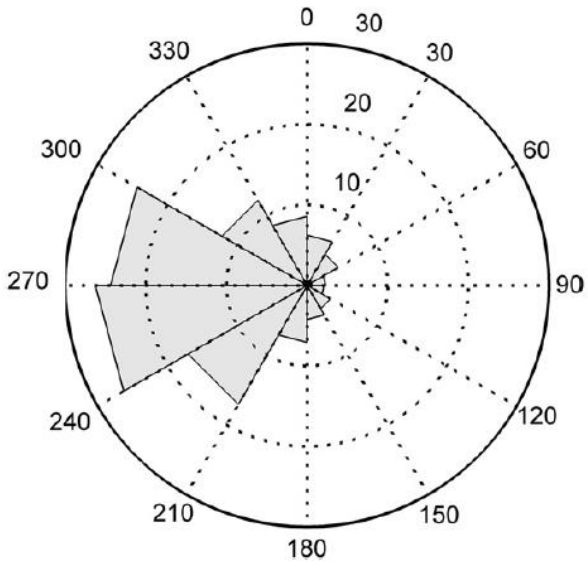


*Figure 5.3, Mean Wave Pwr (kW/m) binned by wave dirn (°N) at Wave Hub (Nieuwkoop et al.), 2013)*

Figure 5.2 shows the joint probability for Significant Wave Height, $H_s$ ( $= H_{m0}$) and Energy Period, $T_e$ ($= T_{m-1,0}$) at location 1. Each square shows probability of occurrence of the particular wave state as a percentage. Where a square shows a figure of zero the probability of that wave state is less than 0.04%. Thus combining this data with the power capture data of Figure 5.1 provides an estimate of the mean annual power capture, as in the spreadsheet of Appendix C. The effect of wave direction is approximated by applying a

factor of 0.7 to wave states with energies below 24 kW/m – based on the data given in Figure 5.3 (Nieuwkoop et al., 2013).

Thus, as can be seen from Appendix C, the mean annual power capture is estimated to be 179.5 kW at Wave Hub location 1, where the available annual wave power is calculated to be 18 kW per metre of wave front. The mean annual wave power incident on the 40 m width of the Clam is thus 700 kW, and a reasonable aim for the WEC would be half of this figure, i.e. 350 kW. The estimate of 179.5 kW is just 51% of 350 kW. Naturally the conversion efficiency of the generator needs to be taken into account, but bearing in mind that the generator is directly driven by the motion of the Clam, an efficiency of 90% or greater is not unreasonable. Thus a reasonable estimate of mean annual power capture in a far from energetic 18 kw/m sea is 157.5 kW, wave to wire.

However there is scope for improving power capture by a suitable choice of control methodology – and by design changes to increase the PTO stroke. In a random sea many of the individual waves cause a PTO motion that is well within the stroke limitations, while other waves result in PTO motion that would exceed the stroke limitation if the control system were not designed to prevent this. A possible way forward is to design the control system to make full use of the available stroke whatever the size of the individual waves.

The key to maximising power capture lies in the way the WEC responds to the wave action, both in a general sense and also on a wave by wave basis. It is believed that the proposed PTO will enable this to be done. By way of explanation consider a regular (sine wave) input. The optimum value of PTO damping depends on the wave period. Thus at each instant in time the force by which the PTO resists the loads put upon it, will vary according to the desired level of damping. Thus a passive method of damping, such as that employed by the wave tank model, is simulated by an active system that can respond to wave period. In random waves the situation is more complex and although the damping may be varied along the lines discussed there is the potential to implement more efficient control strategies – a subject for further research.

# 6 Conclusions and Suggestions for further research

## 6.1 Aim of the research

At the start of the project the research aim was to investigate the mechanism of power capture from sea waves and to optimise the performance of a vee-shaped floating Wave Energy Converter, the Floating Clam, patented by Francis Farley (Farley, 2011d). His patent was based on the use of a pressurised bag (or 'reservoir') to hold the hinged Clam sides apart, so that as they moved under the action of sae waves, air would be pumped into and out of a further air reservoir via a turbine/generator set in order to extract power from the system. A novel feature of the concept was the lengthening of the resonant period in heave resulting from the flexibility of the air bag support of the Clam sides. This was expected to lead to a reduction in the mass (and hence cost) of the Clam as compared with a rigid body.

Further aims were to examine alternative power take-off (PTO) mechanisms and to estimate the cost of energy produced at a sample location, such as Wave Hub.

The theoretical investigations were to be supported by the construction and testing of suitable wave tank models.

## 6.2 Conclusions reached

The research supports the conclusion that the Clam is a feasible device, with development potential. However, the most promising mode of operation is not as originally proposed, since the Clam captures more energy when restrained in heave than when free to move in all axes. Furthermore, practical testing confirmed by mathematical modelling, has led to the conclusion that very low values of PTO flexibility are necessary and this in turn led to the use of constant-force springs in the wave tank model and the pulley plus counterbalance proposal for the full scale device. By good fortune the pulley can be configured to provide a direct drive to the generator, thus enabling an efficient drive with inherently very low friction losses.

In the time available, and due overcoming technical challenges along the way, it has not been possible to complete the research with an estimate of the cost of energy produced. However, a number of achievements may be claimed, and briefly summarised. In respect of the mathematical modelling, the hydrodynamic coefficients have been curve-fitted so that the correct values are available for any particular wave period, and the frequency domain and time domain models are linked in such a way as to automatically use the same hydrodynamic and hydrostatic data. Furthermore, an approximate, but most effective method has been conceived for simulating the behaviour of the Clam in irregular waves, which could be of great use in future control system studies, if speed of computation is an issue. A comprehensive series of wave tank trials has been completed, and included in this achievement is the modification of the wave tank model to achieve very low values of PTO flexibility with negligible mechanical friction in the hinge mechanism. The novel arrangement of wave gauges to facilitate trials of varying incident wave angles can also be regarded as a success.

The wave tank model has demonstrated its robustness and therefore its suitability for use in further test programmes. In particular, it should be possible to embody the design concepts laid out in Chapter 5 directly into the model.

Two problems remain unresolved. The first concerns the discrepancy between calculated and measured phase angles (Section 4.5.1) and the second concerns the calculation of hydrostatic coefficients (see Section 3.4). The phase angle discrepancy points to a more-or-less constant timing error of 0.15 s across all wave periods - indicating an instrumentation problem. However, this is a preliminary finding and should be further investigated. The calculation of hydrostatic coefficients question is unlikely to be resolved – at least in terms of hunting down an error in the commercially supplied software. Fortunately the error does not affect the analysis of the heave-restrained configuration.

In conclusion, at the current stage of research, the mean annual power capture is estimated as 157.5 kW, wave to wire in a far from energetic 18 kw/m mean annual wave climate, but with scope for improvement, including through control system development.

## 6.3 Suggestions for further research and development

A number of possible topics for study are discussed below. Some topics lie clearly in the academic arena while others, such as the design and costing studies, would involve a commercial input.

Mathematical modelling in the time domain should be improved through the use of 'convolution' in order to provide a more reliable prediction of WEC behaviour in irregular seas. The modelling should include the PTO control system and non-linear effects, such as friction, with allowance for skin friction and other body drag effects. The mathematical models would include simulation of the control system and the control system real world inputs. In fact the Clam lends itself to both theoretical and practical studies of a range of control philosophies including reactive and latching control (see Section 1.5.4). The theoretical methods and tools which have been used in the present work could be applied to such a study, albeit with the updates just described. Practical work could be based on further use of the wave tank model to confirm the theoretical analysis. The model PTO could take the form of a capstan drive and stepper motor, such that with a suitable electronic control system all possible control philosophies could be tested.

Investigations into the effect of changes to basic geometrical parameters, such as overall size, width and clam angle should be carried out. Knowledge of the effect of such changes on energy capture would then provide data to assist in matching the device to specific wave climates. In order to make a more definitive prediction of energy capture in real seas a detailed knowledge of the real sea spectra at locations of interest, such as at Wave Hub would be needed. Where assessments are supported by physical model testing, it would be necessary to reproduce these spectra in the wave tank. Employing standard spectra, such a Pierson-Moskowitz is unlikely to be sufficient. The performance of the Clam when deployed in an array should also be investigated.

A design study of the full sized WEC is clearly a necessary part of the process of estimating the cost of generated electricity. Certain aspects of the design require more attention than others, such as the flexible membrane, the capstan drive and the hinge. However,

although employing less innovative technology, the structure, the electrical machine and associated control systems, all present significant design challenges. Integral with this activity would be a survival assessment, with particular emphasis on the device behaviour in very large waves. Having chosen the site and settled on a suitable design for the Clam; the cost of manufacture, deployment, maintenance and decommissioning could be estimated. These costs, together with knowledge of the design life, annual energy capture, electricity distribution costs and the interest costs of financing the project, need to be taken into account when calculating the cost of generated electricity.

# References


AeroHydro (2012) *MultiSurf*. [Online] Available at: http://www.aerohydro.com/products/marine/multisurf.htm.

Anon (2016) *Wave Energy Prize*. [Online] Available at: http://waveenergyprize.org/teams.

AWS (2012) *AWS Ocean Energy*. [Online] Available at: http://www.awsocean.com.

Babarit A and Clément AH (2005) Optimal Latching Control of a Wave Energy Converter. In: *6th European Wave and Tidal Energy Conference*. Glasgow, UK. 19–26.

Barber NF and Ghey G (1969) *Water Waves*. London: Wykeham Publications

Bawden T (2015) *Wind Power now UK's chapest source of electricity*. [Online] Available at: http://www.independent.co.uk/environment/wind-power-now-the-cheapest-source-of-electricity-but-the-government-continues-to-resist-onshore-a6685326.html.

Bellamy NW (1985) *The Circular Sea Clam Wave Energy Converter*. Coventry, England

Cahill B and Lewis AW (2014) Wave period ratios and the calculation of wave power. *The 2nd Marine Energy Technology Symposium*, 1–10.

Cahill BG and Lewis AW (2011) Wave Energy Resource Characterization of the Atlantic Marine Energy Test Site. In: *9th European Wave and Tidal Energy Conferenceth*. Southampton, UK. 1–8.

Carbon Trust (2011) Accelerating Marine Energy. *Current*. 103 (July), 1–64. Available at: http://www.carbontrust.co.uk/emerging-technologies/current-focus-areas/marine-energy-accelerator/pages/default.aspx.

Carbon Trust (2016) *Carbon Trust Marine Renewables Proving Fund*. [Online] Available at: https://www.carbontrust.com/client-services/technology/innovation/marine-renewables-proving-fund/ (accessed 12/04/16).

Carbon Trust (2006) Future Marine Energy. *Development*, 36. Available at: http://www.carbontrust.co.uk/Publications/pages/PublicationDetail.aspx?id=CTC601.

Chaplin JR, Heller V, Farley FJM, Hearn GE and Rainey RCT (2012) Laboratory testing the Anaconda. *Philosophical transactions. Series A, Mathematical, physical, and engineering sciences*. 370 (1959), 403–24. Available at: http://www.ncbi.nlm.nih.gov/pubmed/22184668 (accessed 01/09/12).

Cornett AM (2008) A global wave energy resource assessment J. S. Chung ed. *Renewable Energy*. 1 (6), 1–9.

Craik ADD (2005) George Gabriel Stokes on Water Wave Theory. *Annual Review of Fluid Mechanics*. 37 (1), 23–42. Available at: http://www.annualreviews.org/doi/abs/10.1146/annurev.fluid.37.061903.175836 (accessed 13/03/12).

Daruvala J (2009) *Sw Wave Hub - Metocean Design Basis*. Liphook, Hants, UK Available at: www.metoc.co.uk.

Dawson JK (1979) Wave Energy, Energy Paper No 42. *HMSO*.

Dean RG and Dalrymple RA (1991) *Water Wave Mechanics for Engineers and Scientists*. World Scientific Publishing Co. Pte. Ltd

DoE UK (1985) *Wave Energy : the Department of Energy's R & D programme 1974-1983: ETSU report; R26*. ETSU for the Department of Energy

Falcão AF de O (2005) Modelling and Control of Oscillating-Body Wave Energy Converters with Hydraulic Power Take-Off and Gas Accumulator. In: *6th European Wave and Tidal Energy Conference*. Glasgow UK. 113–120.

Falcão AF de O (2007) Phase control through load control of oscillating-body wave energy converters with hydraulic PTO system. In: *7th European Wave and Tidal Energy Conference*. Porto, Portugal. 1–10.

Falnes J (2002) *Ocean waves and oscillating systems: linear interactions including wave-energy extraction*. Cambridge: Cambridge University Press

Falnes J (2005) *Principles for capture of energy from ocean waves. Phase control and optimum oscillation.* Norway

Farley FJM (2010) *A new wave energy converter - the distensible buoy*. Le Bar-sur-Loup

Farley FJM (2011a) clamsim8a - Excel Spreadsheet.

Farley FJM (2012) Opening remarks and the power spectrum of ocean waves. In: *Philosophical transactions. Series A, Mathematical, physical, and engineering sciences*. 203–7. Available at: http://www.ncbi.nlm.nih.gov/pubmed/22184658 (accessed 21/07/12).

Farley FJM (2011b) *The conical free-floating clam*. Southampton, UK

Farley FJM (2011c) *The free floating clam*. Southampton, UK

Farley FJM (2011d) The free floating clam - a new wave energy converter. In: *9th European Wave and Tidal Energy Conference*. Southampton, UK. 1–4.

Farley FJM, Rainey RCT and Chaplin JR (2012) Rubber tubes in the sea. *Philosophical transactions. Series A, Mathematical, physical, and engineering sciences*. 370 (1959), 381–402. Available at: http://www.ncbi.nlm.nih.gov/pubmed/22184667 (accessed 07/09/12).

Filianoti, P U of RC and Camporeale, S M PU of B (2005) A linearized model for estimating the performance of sea wave energy converters (REWEC). In: *6th European Wave and Tidal Energy Conference*. Glasgow UK. 125–132. Available at: http://scholar.google.com/scholar?hl=en&btnG=Search&q=intitle:A+linearized+model+for+estimating+the+performance+of+Wave+Energy+Converters+(REWEC)#0 (accessed 03/08/12).

Francis JRD (1962) *A Textbook of Fluid Mechanics* (2nd edition). London: Edward Arnold

Freeman K (2011) *Modelling and control of an oscillating water column wave energy converter for maximum power capture*. Plymouth. UK.

Gato LMC, Justino PAP and Falcão AF de O (2005) Optimization of power take-off equipment for an oscillating-water column wave energy plant. In: *6th European Wave and Tidal Energy Conference*. Glasgow UK. 155–162.

Hals J (2010) *Modelling and phase control of wave-energy converters*. Norwegian University of Science and Technology, Trondheim.

Hartman HL (1992) *SME Mining Engineering Handbook* (2nd edition). Society for Mining, Metallurgy, and Exploration

Henry A (2010) Advances in the design of the Oyster wave energy converter. In: *Marine Renewable and Offshore Wind Energy*. London: RINA. 42 slides.

Holmes B, Nielsen K and Barrett S (2007) Wave Energy Development & Evaluation Protocol.

Iglesias G and Carballo R (2011) Wave Resource Characterization and WEC Selection – a Comprehensive Methodology Applied to NW Spain. In: *9th European Wave and Tidal Energy Conference*. Southampton, UK. 1–8.

INETI (2009) *WERATLAS EUROPEAN WAVE ENERGY ATLAS*. [Online] Available at: http://users.ntua.gr/mathan/pdf/WERATLAS.pdf (accessed 01/01/16).

Joubert JR, Niekerk JL Van, Reinecke J and Meyer I (2013) *Wave Energy Converters ( WECs ) October 2013* Available at: http://www.crses.sun.ac.za/files/technologies/ocean/WECs_2013_list.pdf.

Kurniawan A, Hals J and Moan T (2011) Assessment of Time-Domain Models of Wave Energy Conversion Systems. *Proceedings of the 9th European Wave and Tidal Energy Conference*, 12. Available at: http://www.ntnu.edu/documents/174596/8a074f75-91a3-490f-9770-bf3f661db05f.

Mackay EBL (2011) Modelling and Description of Omnidirectional Wave Spectra. In: *9th European Wave and Tidal Energy Conference*. Southampton, UK.

Maplesoft (2014) *Maple*. [Online] Available at: http://www.maplesoft.com/ (accessed 21/10/14).

Margheritini L, Frigaard P and Stratigaki V (2011) Characterization of Wave Climate at Hanstholm Location with Focus on the Ratio between Average and Extreme Waves Heights. In: *9th European Wave and Tidal Energy Conference*. Southampton, UK.

Mathworks (2014) *MATLAB*. [Online] Available at: http://www.mathworks.co.uk/products/matlab/ (accessed 22/10/14).

McIver P (2002) Hydrodynamics technical advice for generic wave model. Report 1: General aspects of wave-energy device modelling. In: Loughborough. 1–20.

Mei CC (2012) Hydrodynamic principles of wave power extraction. *Philosophical transactions. Series A, Mathematical, physical, and engineering sciences*. 370 (1959), 208–34. Available at: http://www.ncbi.nlm.nih.gov/pubmed/22184659 (accessed 08/08/12).

Newman J (1994) Wave effects on deformable bodies. *Applied Ocean Research*. 16 (1), 47–59. Available at: http://www.sciencedirect.com/science/article/pii/0141118794900132 (accessed 07/09/12).

Newman JN (1977) *Marine hydrodynamics*. Cambridge, Massachusetts: The MIT Press

Nieuwkoop JCC Van, Smith HCM, Smith GH and Johanning L (2013) Wave resource assessment along the Cornish coast ( UK ) from a 23-year hindcast dataset validated against buoy measurements. *Renewable Energy*. 58, 1–14. Available at: http://dx.doi.org/10.1016/j.renene.2013.02.033.

Nolan GA (2006) *Modelling and Optimisation of a Heaving Buoy Wave Energy Converter for Potable Water Production*. National University of Ireland, Maynooth.

Phillips JW (2003) Sperboy Dynamic Modelling , Including comparison with wave tank and seagoing trials. In: *5th European Wave and Tidal Energy Conference*. Cork, Ireland. 370–377.

Phillips JW (2008) Why is Wave Power so Difficult? In: *The Bristol Scientific Club*. Bristol: Bristol Scientific Club. 46 slides.

Phillips JW and Rainey RCT (2005) Sperboy Design Evolution. In: *Wave Power - Moving Towards Commercial Viability*. London: IMechE. 1–12.

Pierson WJJ and Moskowitz L (1964) A proposed spectral form for fully developed wind seas based on the similarity theory of S. A. Kitaigorodskii. *J. Geophys. Research, 69 (24)*, 5181–5190.

PTC (2014) *Mathcad*. [Online] Available at: http://www.ptc.com/product/mathcad (accessed 21/10/14).

Ransley EJ (2015) *Survivability of Wave Energy Concerter and Mooring Coupled System using CFD*. University of Plymouth. Available at: https://pearl.plymouth.ac.uk/handle/10026.1/3503.

Reeve D, Pan S, Magar V and Simmonds D (2011) Impact of Climate Change on Wave Energy Generation near the Wave Hub , Cornwall , UK. In: *9th European Wave and Tidal Energy Conference*. Southampton, UK. 1–6.

Sarpkaya T and Isaacson M (1981) *Mechanics of forces on offshore structures*. New York: Van Nostrand Reinhold Company Inc.

Saulnier J-BMG, Maisondieu C, Ashton IGC and Smith GH (2011) Wave Hub Test Facility : Sea State Directional Analysis from an Array of 4 Measurement Buoys. In: *9th European Wave and Tidal Energy Conference*. Southampton, UK. 1–10.

Saulnier J-BMG, Prevosto M and Maisondieu C (2011) Refinements of sea state statistics for marine renewables: A case study from simultaneous buoy measurements in Portugal. *Renewable Energy*. 36 (11), 2853–2865. Available at: http://dx.doi.org/10.1016/j.renene.2011.04.015.

Schwarzenbach J and Gill KF (1992) *System Modelling and Control* (3rd edition). Leeds University: Edward Arnold

Shaw R (1982) *Wave energy: a design challenge*. Chichester: Ellis Horwood Ltd, Halstead Press

Skinner NA and Scott M (2010) Development of a Reactive Hydraulic Modulator (RHM). In: *Marine Renewable and Offshore Wind Energy*. London: RINA. 1–10.

South West of England Regional Development Agency (2004) Seapower SW Review WAVE DATA PRESENTATION.

Stokes GG (1847) On the Theory of Oscillating Waves. *Transactions, Cambridge Philosophical Society*. I, No. 197.

Torkel B-L and Falnes J (2005) Investigation of a phase-controlled wave-power buoy. In: *6th European Wave and Tidal Energy Conference*. Glasgow, UK. 47–50.

Tucker A, Pemberton JM, Swift-Hook DT, Swift-Hook JM and Phillips JW (2010) LAMINATED REINFORCED CONCRETE TECHNOLOGY FOR THE SPERBOY WAVE ENERGY CONVERTER. In: *Marine Renewable and Offshore Wind Energy*. The Royal Institution of Naval Architects, London, UK.

Universiteit Ghent (2016) *MILDwave web page*. [Online] Available at: http://www.ugent.be/ea/civil-engineering/en/research/coastal-bridges-roads/coastal-engineering/infrastructure-services/mildwave (accessed 18/04/16).

Visual Solutions (2014) *VisSim*. [Online] Available at: http://www.vissim.com/ (accessed 22/10/14).

WAMDI Group T (1988) The WAM model - A third generation ocean wave prediction model. *Journal of Physical Oceanography*. 18 (12), 1775–1810.

WAMIT (2012) *WAMIT User Manual, Version 7*. [Online] Available at: http://www.wamit.com/manual.htm.

Wave Hub Ltd (2016) *Wave Hub Web Site*. [Online] Available at: http://www.wavehub.co.uk/ (accessed 01/09/16).

WES (2016a) *Search for novel wave energy converters results in £2.25m award to technology innovators*. [Online] Available at: http://www.hie.co.uk/growth-sectors/energy/wave-energy-scotland/news-and-events/news/search-for-novel-wave-energy-converters-results-in--2-25m-award--to-technology-innovators.html.

WES (2016b) *Wave Energy Scotland*. [Online] Available at: http://www.hi-energy.org.uk/renewables/wave-energy.htm (accessed 12/04/16).

Whittaker T, Collier D, Folley M, Osterried M and Henry A (2007) The development of Oyster - A shallow water surging wave energy converter . *7th European Wave and Tidal Energy Conference*.

Whittaker T and Folley M (2012) Nearshore oscillating wave surge converters and the development of Oyster. *Philosophical transactions. Series A, Mathematical, physical, and engineering sciences*. 370 (1959), 345–64. Available at: http://www.ncbi.nlm.nih.gov/pubmed/22184665 (accessed 08/08/12).

Wilson C (2010) Choosing your history: Wave energy development in the UK. *History and Policy*, 1–5. Available at: http://www.historyandpolicy.org/opinion-articles/articles/choosing-your-history-wave-energy-development-in-the-uk.

Wyatt LR (2011) Using HF radar to measure the directionality of the wave energy resource. In: *9th European Wave and Tidal Energy Conference*. Southampton, UK.

# Appendix A: Scaling Factors

Table A.1: Scaling Factors

| Quantity | Typical Unit | Scale factor | Factor when s = 50 |
|---|---|---|---|
| Length | $m$ | $s$ | 50 |
| Volume | $m^3$ | $s^3$ | 125000 |
| Density | $\frac{kg}{m^3}$ | 1 | 1 |
| Mass | $kg$ | $s^3$ | 125000 |
| Force | $N$ | $s^3$ | 125000 |
| Time | $sec$ | $\sqrt{s}$ | 7.07107 |
| Velocity | $\frac{m}{sec}$ | $\sqrt{s}$ | 7.07107 |
| Pressure | $\frac{N}{m^2} = Pa$ | $s$ | 50 |
| Flow | $\frac{m^3}{sec}$ | $s^{2.5}$ | 17678 |
| Damping | $\frac{N.sec}{m}$ | $s^{2.5}$ | 17678 |
| Stiffness | $\frac{N}{m}$ | $s^2$ | 2500 |
| Power | $\frac{N.sec}{m}$ = Watts | $s^{3.5}$ | 883883 |

# Appendix B: WAMIT modelling

## B.1 General

The WAMIT modelling is most conveniently described by presenting the model input and output files and explaining their significant features. Sufficient detail is given to enable the reader to reproduce the analysis if desired.

## B.2 Model Control Files

Four files are used to control the calculation, i.e.:

- The Filenames list, fnames.wam
- The first Configuration file, config.wam, and
- The second Configuration file, *.cfg
- The Potential Control file, *.pot

The model name was chosen to be “tank”. The contents of these files is as follows:

fnames.wam:
Tank.cfg
Tank.pot
Tank.frc

config.wam:
! generic configuration file: config.wam
RAMGBMAX=0.5
NCPU=1
USERID_PATH=\wamitv7 (directory for *.exe, *.dll, and userid.wam)
LICENSE_PATH=\wamitv7\license

Tank.cfg
! Wave Tank Model: Tank.cfg -- With Clam action
ILOWHI=0 (Use lower order method)
IALTFRC=2 (Force Control File (FRC) – Specifies Alternative Form 2)
ipltdat=5 (Output file tank_pan.dat written – value of 5 more relevant when higher order solution used)
maxscr=1024 (assign a maximum block of 1024*1024 RAM for scratch LHS)
ISOR=1 (omit ISOR in POT file, include source formulation)
ISOLVE=0 (use iterative solver)
ISCATT=0 (solve for total diffraction potential, not scattering)
IQUAD=0 (omit IQUAD in POT file, use single-node quadrature)
ILOG=1 (omit ILOG in POT file, integrate log singularity)
IDIAG=0 (omit IDIAG in POT file, panel length based on area)
IRR=0 (omit IRR in POT file, no irregular-frequency removal)
MONITR=0 (do not write FORCE output data to monitor)
NUMHDR=1 (write headers to numeric output files)
IGENMDS=150 (if 150 - points to Wave Tank Model, Lower Order subroutine in newmodes.f)
NEWMDS=1 (if 1 then ONE generalised mode)
Tank.pot
Wave Tank Model: Tank.pot, w=40m, ILOWHI=0, IRR=0

-1.0 HBOT (Infinite water depth)
0 0 IRAD, IDIFF (See note[i])
15 NPER (array PER follows) (No. of values of wave period to be solved)
2.0 3.0 4.0 5.0 6.0 7.0 8.0 9.0 10.0 12.0 14.0 16.0 32.0 100.0 500.0 PER (List of wave periods)
1 NBETA (array BETA follows) (No. of wave headings to be solved)
0. BETA (Direction of wave heading)
1 NBODY (Number of bodies in the analysis)
Tank.gdf (Name of geometric data file for body)
0.0 0.0 0.0 0.0 XBODY(1-4) (offset of bodies local axes from global axes)
0 0 1 0 0 0 IMODE(1-6) (heave solution only)

Note[i]: The value of 0 for IRAD and IDIFF ensures that the radiation and diffraction hydrodynamics are solved just for the modes specified by IMODE – in this case just for the heave motion.

## B.3 Geometry definition

The geometric data file Tank.out is a large text file, only the first few lines of which are shown here. For the generalized mode method to be successful using NEWMODES, the length parameter ULEN must be 1 m. GRAV is the acceleration due to gravity in $m/s^2$.

NEQN is effectively the number of simultaneous equations to be solved, i.e. the number of unknowns. In the lower order panel method used here it is simply the number of panels – which equates to the number of lines of data in the file.

The first 12 lines of geometric data are shown; each line gives the panel vertices for one panel. Note that the coordinates in the actual file are given to 6 decimal places – shortened here for space reasons.

Tank.gdf

Wave Tank Model: Tank.gdf, w=40m, ILOWHI=0, IRR=0

1.000000 9.806650 ULEN, GRAV

0 0 ISX, ISY

1824 NEQN

| | | | | | | | | | | | |
|---|---|---|---|---|---|---|---|---|---|---|---|
| 2.74 | 1.00 | -11.78 | 2.74 | 0.00 | -11.78 | 2.35 | 0.00 | -12.86 | 2.35 | 1.00 | -12.86 |
| 3.13 | 1.00 | -10.71 | 3.13 | 0.00 | -10.71 | 2.74 | 0.00 | -11.78 | 2.74 | 1.00 | -11.78 |
| 3.52 | 1.00 | -9.64 | 3.52 | 0.00 | -9.64 | 3.13 | 0.00 | -10.71 | 3.13 | 1.00 | -10.71 |
| 3.91 | 1.00 | -8.57 | 3.91 | 0.00 | -8.57 | 3.52 | 0.00 | -9.64 | 3.52 | 1.00 | -9.64 |
| 4.30 | 1.00 | -7.50 | 4.30 | 0.00 | -7.50 | 3.91 | 0.00 | -8.57 | 3.91 | 1.00 | -8.57 |
| 4.69 | 1.00 | -6.43 | 4.69 | 0.00 | -6.43 | 4.30 | 0.00 | -7.50 | 4.30 | 1.00 | -7.50 |
| 5.08 | 1.00 | -5.36 | 5.08 | 0.00 | -5.36 | 4.69 | 0.00 | -6.43 | 4.69 | 1.00 | -6.43 |
| 5.47 | 1.00 | -4.29 | 5.47 | 0.00 | -4.29 | 5.08 | 0.00 | -5.36 | 5.08 | 1.00 | -5.36 |
| 5.86 | 1.00 | -3.21 | 5.86 | 0.00 | -3.21 | 5.47 | 0.00 | -4.29 | 5.47 | 1.00 | -4.29 |
| 6.25 | 1.00 | -2.14 | 6.25 | 0.00 | -2.14 | 5.86 | 0.00 | -3.21 | 5.86 | 1.00 | -3.21 |
| 6.64 | 1.00 | -1.07 | 6.64 | 0.00 | -1.07 | 6.25 | 0.00 | -2.14 | 6.25 | 1.00 | -2.14 |
| 7.03 | 1.00 | 0.00 | 7.03 | 0.00 | 0.00 | 6.64 | 0.00 | -1.07 | 6.64 | 1.00 | -1.07 |
| X1 | Y1 | Z1 | X2 | Y2 | Z2 | X3 | Y3 | Z3 | X4 | Y4 | Z4 |

## B.4 Force Control file

The format of the Force Control File is in accordance with “Alternative form 2”, since IALTFRC=2 in the control file, Tank.cfg. The chosen IOPTN options control the evaluation and output of the following quantities:

| | |
|---|---|
| Added-mass and damping coefficients | output file: Tank.1 |
| Exciting forces from Haskind relations | output file: Tank.2 |
| Exciting forces from diffraction potential | output file: Tank.3 |
| Motions of body (response amplitude operator) | output file: Tank.4 |

The total mass of the device is 5423.11 tonne and the figures for rotary inertia are based on arbitrarily chosen values of radius of inertia, k , as follows:

Rotation about x-axis (roll): $k_{xx}$= 5 m thus inertia, $I_{xx}$= 1.35577e8 kg m$^2$
Rotation about y-axis (pitch): $k_{yy}$= 5 m thus inertia, $I_{yy}$= 1.35577e8 kg m$^2$
Rotation about x-axis (roll): $k_{zz}$= 4 m thus inertia, $I_{zz}$= 8.67697e7 kg m$^2$

It needs to be pointed out that these inertia values are not correct, but were chosen during the de-bugging exercise when comparing the WAMIT and AQWA models. This does not affect the validity of the analyses in this document which consider the heave motion alone. However, realistic inertia values were used in the design calculations to assess the stability and resonant periods in roll, pitch and yaw of the wave tank model. The damping and stiffness values are those for mode 7, the Clam PTO. Thus in this example the PTO damping is 4e5 Ns/m and its stiffness is 1.5e6 N/m .

**Tank.frc**

```
Wave Tank Model: Tank.frc, w=40m, ILOWHI=0, IRR=0
 1   1   1   1  0   0   0   0   0  IOPTN(1-9)
1000.0                            RHO   (Density of water – fresh water, as in wave tank)
0.0   0.0   -12.0          XCG YCG ZCG   (C of G is 12 m below waterline)
1                                 IMASS


 5.42311e6 .0000000  .0000000  .0000000  .0000000  .0000000  .0000000
 .0000000  5.42311e6 .0000000  .0000000  .0000000  .0000000  .0000000
 .0000000   .0000000 5.42311e6 .0000000  .0000000  .0000000  .0000000
 .0000000   .0000000  .0000000 1.35577e8 .0000000  .0000000  .0000000
 .0000000   .0000000  .0000000  .0000000 1.35577e8 .0000000  .0000000
 .0000000   .0000000  .0000000  .0000000  .0000000 8.67697e7 .0000000
 .0000000   .0000000  .0000000  .0000000  .0000000 .0000000  .0000000 EXMASS (7x7)
1                               IDAMP


 .0000000  .0000000  .0000000  .0000000  .0000000  .0000000  .0000000
 .0000000  .0000000  .0000000  .0000000  .0000000  .0000000  .0000000
 .0000000  .0000000  .0000000  .0000000  .0000000  .0000000  .0000000
 .0000000  .0000000  .0000000  .0000000  .0000000  .0000000  .0000000
 .0000000  .0000000  .0000000  .0000000  .0000000  .0000000  .0000000
 .0000000  .0000000  .0000000  .0000000  .0000000  .0000000  .0000000
 .0000000  .0000000   0.00000  .0000000  .0000000  .0000000  4.0e5    EXDAMP (7x7)
1                               ISTIF


 .0000000  .0000000  .0000000  .0000000  .0000000  .0000000  .0000000
 .0000000  .0000000  .0000000  .0000000  .0000000  .0000000  .0000000
 .0000000  .0000000  .0000000  .0000000  .0000000  .0000000  .0000000
 .0000000  .0000000  .0000000  .0000000  .0000000  .0000000  .0000000
 .0000000  .0000000  .0000000  .0000000  .0000000  .0000000  .0000000
 .0000000  .0000000  .0000000  .0000000  .0000000  .0000000  .0000000
 .0000000  .0000000  .0000000  .0000000  .0000000  .0000000  1.5e6    EXSTIF (7x7)

 0                    NBETAH   (No. of Haskind wave headings, see note below)
 0                    NFIELD    (No. of points in fluid domain to analyse wave elevation etc.)
```

Note: The user guide says: “The Haskind wave headings may be introduced in the Force Control File as an option, to enable evaluations to be made of the Haskind exciting forces

(Option 2) and body motions in waves (Option 4) at heading angles not included in the Potential Control File". However, the Tank.pot file does specify a wave heading of 0°.

## B.5 NEWMODES data file

This file contains geometric data that is input by the specially written FORTRAN subroutine Newmodes.f that calculates VELH ZDISP, see Section 3.4. The length data is in metres and the angles are degrees.

Tank_GeomData.dat

GeomData.DAT for Wave Tank Model
12.0 13.0 20.0 40.0 2.0 2.5 (HWATER, HPTO, THETA1, THETA2, ALENGTH, BLENGTH)

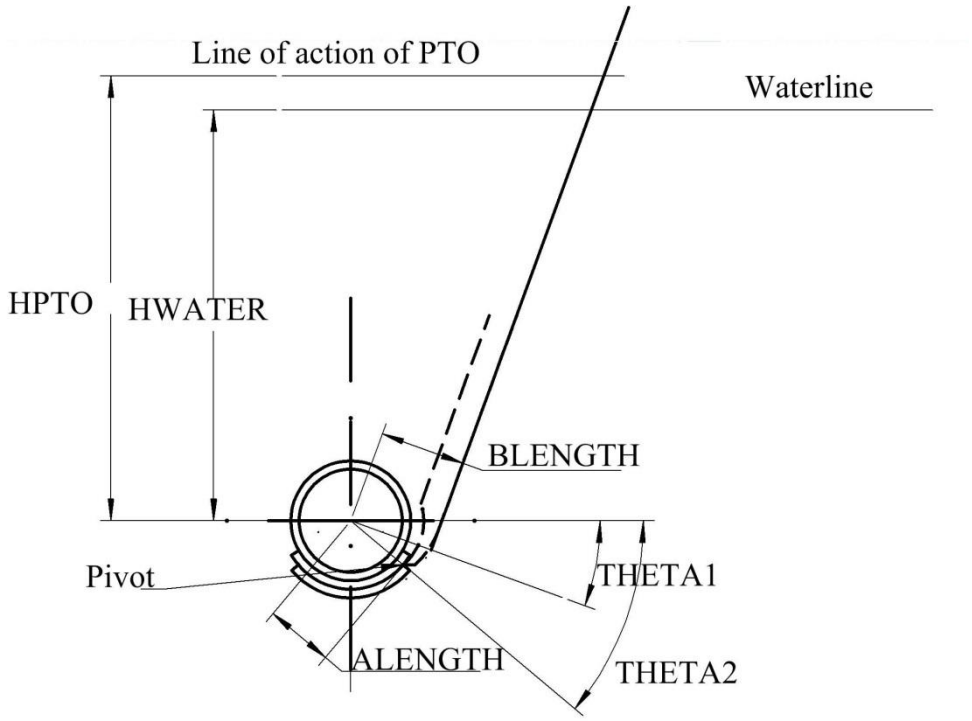


Figure B.1: Input parameters for Newmodes.f

## B.6 Output from WAMIT model

WAMIT produces a number of output files in line with the control data in Tank.cfg and Tank.pot, see Section B.2. The main output file that is always written (and which contains most of the data of interest) is Tank.out. Also the file, wamitlog.txt contains information on the progress of the computation and useful data should the run not be completed.

# Appendix C: Trials carried out

Table C.1: First Set of Trials

| Trial | Title | Test Day | Wave Amplitude | Heave restrained? | Orifice Dia. | Remarks | No. of PTOs |
|---|---|---|---|---|---|---|---|
| A | Floating_5mm_20mm | Fri | 20 mm | No | 5 mm | | 2 |
| B | Floating_5mm_30mm | Fri | 30 mm | No | 5 mm | | 2 |
| C | Fixed_5mm_20mm | Fri | 20 mm | Yes | 5 mm | Runs 7 & 8 used 40 mm wave | 2 |
| D | Semi_rigid_20mm | Mon | 20 mm | No | - | Used rigid bar in place of PTO | 0 |
| E | Rigid_20mm | Mon | 20 mm | No | - | Used rigid bar in place of PTO | 0 |
| F | Rigid_PM | Mon | - | No | - | Used rigid bar in place of PTO | 0 |
| G | Springs_20mm Floating | Mon | 20 mm | No | 5 mm | | 2 |
| H | Springs_noheave_20mm | Mon | 20 mm | Yes | 5 mm | | 2 |
| I | Springs_noheave_20mm | Tues | 20 mm | Yes | 5 mm | | 2 |
| J | Springs_noheave_40mm | Tues | 40 mm | Yes | 5 mm | | 2 |
| K | Springs_heave_40mm | Tues | 40 mm | No | 5 mm | | 2 |
| L | Springs_heave_40mm_3 mm_orifice | Tues | 40 mm | No | 3 mm | | 2 |
| M | Springs_noheave_40mm_ 3mm_orifice | Tues | 40 mm | Yes | 3 mm | | 2 |
| N | Strong_Springs_heave_4 0mm_3mm_orifice | Tues | 40 mm | No | 3 mm | | 2 |
| O | Strong_Springs_noheave _40mm_3mm_orifice | Tues | 40 mm | Yes | 3 mm | | 2 |
| P | Springs_noheave_40mm_ 3mm_orifice_rpt | Wed | 40 mm | Yes | 3 mm | | 2 |
| Q | Springs_heave_40mm_3 mm_orifice_rpt | Wed | 40 mm | No | 3 mm | | 2 |

| | | | | | | | |
|---|---|---|---|---|---|---|---|
| R | FinalConfig_noheave_40 mm_wave_2_5mm_orifice | Wed | 40 mm | Yes | 2.5 mm | | 1 |
| S | FinalConfigP_M_noheave _40mm_wave_2_5mm_o | Wed | 40 mm | Yes | 2.5 mm | | 1 |
| T | Heave Response in Still Water | Wed | N/A | N/A | - | 3 configs – Clam open, closed and central | - |

Table C.2: Second Set of Trials

| Trial | Title | Test Day | Wave Amplitude, mm | Wave Direction | Orifice Dia., mm | Spring Type | Remarks |
|---|---|---|---|---|---|---|---|
| 1, 1R | Const_5mm_20mm | Wed | 20 | 0° | 5 | C F | Nomenclature:<br>R – repeat<br>C F – Constant Force Spring<br>Coil – Coil spring: force varies linearly with displacement<br>PM – Pierson-Moskowitz wave spectrum<br>All wave inputs are regular except where PM is indicated |
| 2, 2R | Const_5mm_20mm_ 15deg | Wed | 20 | 15° | 5 | C F | |
| 3,3R | Const_5mm_20mm_ 30deg | Wed | 20 | 30° | 5 | C F | |
| 4,4R | Const_5mm_Run PM2 | Wed | N/A | 0° | 5 | C F | |
| 5, 5R | CoilSpring_5mm_20 mm | Wed | 20 | 0° | 5 | Coil | |
| 6 | CoilSpring_5mm_ RunPM2 | Wed | N/A | 0° | 5 | Coil | |
| 7 | CoilSpring_3mm_ 20mm | Thurs | 20 | 0° | 3 | Coil | |
| 8 | CoilSpring_3mm_ 20mm | Thurs | 20 | 0° | 3 | Coil | |
| 9 | CoilSpring_3mm_20 mm_Run2 | Thurs | 20 | 0° | 3 | Coil | |

| | | | | | | | |
|---|---|---|---|---|---|---|---|
| 10 | CoilSpring_3mm_20 mm_15deg | Thurs | 20 | 15° | 3 | Coil | |
| 11 | CoilSpring_3mm_20 mm_30deg | Thurs | 20 | 30° | 3 | Coil | |
| 12 | CoilSpring_3mm_ 20mm _RunPM2 | Thurs | N/A | 0° | 3 | Coil | |
| 13 | CoilSpring_3mm_ 20mm_RunPM2_ Spread | Thurs | N/A | 0° | 3 | Coil | |
| 14 | CoilSpring_3mm_ 30mm | Thurs | 30 | 0° | 3 | Coil | |
| 15, 15R | Const_3mm_20mm | Thurs | 20 | 0° | 3 | C F | |
| 16A,B,C | Const_3mm_20mm_ 15deg | Fri | 20 | 15° | 3 | C F | |
| 17 | Const_2_5mm_ 20mm | Fri | 20 | 0° | 2.5 | C F | |
| 18 | Const_2_5mm_ 20mm_15deg | Fri | 20 | 15° | 2.5 | C F | |
| 19 | Const_2_5mm_ 20mm_30deg | Fri | 20 | 30° | 2.5 | C F | |
| 20 | Const_2_5mm_ RunPM2 | Fri | N/A | 0° | 2.5 | C F | |
| 21 | Const_2_5mm_Run PM2_Spread | Fri | N/A | 0° | 2.5 | C F | |

# Appendix D: Power Capture at Wave Hub

Table D.1: Clam Power Capture

| Bin | Hs, m | Te, s | Energy in Sea, kW/m of Wave front | Occurrence, % | Annual, Power, kW | Clam Power, kW | Factor for wave direction | Annual Energy Capture, kW |
|---|---|---|---|---|---|---|---|---|
| 1 | 0.5 | 2.25 | 0.3 | 0.2 | 0.00055 | 0.00 | 0.7 | 0.0000 |
| 2 | 0.5 | 2.75 | 0.3 | 0.2 | 0.00067 | 0.00 | 0.7 | 0.0000 |
| 3 | 0.5 | 3.25 | 0.4 | 0.1 | 0.00040 | 0.55 | 0.7 | 0.0004 |
| 4 | 0.5 | 3.75 | 0.5 | 0.1 | 0.00046 | 3.52 | 0.7 | 0.0025 |
| 5 | 0.5 | 4.25 | 0.5 | 0.1 | 0.00052 | 7.70 | 0.7 | 0.0054 |
| 6 | 0.5 | 4.75 | 0.6 | 0.1 | 0.00058 | 13.01 | 0.7 | 0.0091 |
| 7 | 0.75 | 2.75 | 0.8 | 0.3 | 0.00228 | 0.00 | 0.7 | 0.0000 |
| 8 | 0.75 | 3.25 | 0.9 | 0.9 | 0.00807 | 2.50 | 0.7 | 0.0158 |
| 9 | 0.75 | 3.75 | 1.0 | 1.6 | 0.01655 | 7.04 | 0.7 | 0.0789 |
| 10 | 0.75 | 4.25 | 1.2 | 1.9 | 0.02227 | 13.34 | 0.7 | 0.1774 |
| 11 | 0.75 | 4.75 | 1.3 | 1.7 | 0.02227 | 21.25 | 0.7 | 0.2529 |
| 12 | 0.75 | 5.25 | 1.4 | 1.8 | 0.02606 | 30.28 | 0.7 | 0.3815 |
| 13 | 0.75 | 5.75 | 1.6 | 1.9 | 0.03013 | 39.91 | 0.7 | 0.5308 |
| 14 | 0.75 | 6.25 | 1.7 | 1.6 | 0.02758 | 49.62 | 0.7 | 0.5558 |
| 15 | 0.75 | 6.75 | 1.9 | 1.2 | 0.02234 | 58.90 | 0.7 | 0.4948 |
| 16 | 0.75 | 7.25 | 2.0 | 0.6 | 0.01200 | 67.23 | 0.7 | 0.2824 |
| 17 | 0.75 | 7.75 | 2.1 | 0.2 | 0.00427 | 74.09 | 0.7 | 0.1037 |
| 18 | 0.75 | 8.25 | 2.3 | 0.1 | 0.00228 | 78.98 | 0.7 | 0.0553 |
| 19 | 1.25 | 3.75 | 2.9 | 0.3 | 0.00862 | 21.19 | 0.7 | 0.0445 |
| 20 | 1.25 | 4.25 | 3.3 | 1.6 | 0.05209 | 31.74 | 0.7 | 0.3555 |
| 21 | 1.25 | 4.75 | 3.6 | 3.4 | 0.12372 | 44.63 | 0.7 | 1.0622 |
| 22 | 1.25 | 5.25 | 4.0 | 4.6 | 0.18500 | 59.10 | 0.7 | 1.9031 |
| 23 | 1.25 | 5.75 | 4.4 | 4.3 | 0.18941 | 74.39 | 0.7 | 2.2392 |
| 24 | 1.25 | 6.25 | 4.8 | 3.5 | 0.16757 | 89.73 | 0.7 | 2.1985 |

| | | | | | | | | |
|---|---|---|---|---|---|---|---|---|
| 25 | 1.25 | 6.75 | 5.2 | 2.9 | 0.14995 | 104.3 | 0.7 | 2.1185 |
| 26 | 1.25 | 7.25 | 5.6 | 2.4 | 0.13329 | 117.5 | 0.7 | 1.9741 |
| 27 | 1.25 | 7.75 | 5.9 | 1.6 | 0.09499 | 128.4 | 0.7 | 1.4381 |
| 28 | 1.25 | 8.25 | 6.3 | 1 | 0.06320 | 136.3 | 0.7 | 0.9542 |
| 29 | 1.25 | 8.75 | 6.7 | 0.6 | 0.04022 | 141.1 | 0.7 | 0.5928 |
| 30 | 1.25 | 9.25 | 7.1 | 0.3 | 0.02126 | 143.4 | 0.7 | 0.3012 |
| 31 | 1.25 | 9.75 | 7.5 | 0.1 | 0.00747 | 143.7 | 0.7 | 0.1006 |
| 32 | 1.75 | 4.75 | 7.1 | 0.4 | 0.02853 | 81.84 | 0.7 | 0.2291 |
| 33 | 1.75 | 5.25 | 7.9 | 2 | 0.15765 | 100.8 | 0.7 | 1.4123 |
| 34 | 1.75 | 5.75 | 8.6 | 3.3 | 0.28490 | 120.6 | 0.7 | 2.7879 |
| 35 | 1.75 | 6.25 | 9.4 | 3.7 | 0.34721 | 140.3 | 0.7 | 3.6360 |
| 36 | 1.75 | 6.75 | 10.1 | 3.2 | 0.32431 | 159.1 | 0.7 | 3.5640 |
| 37 | 1.75 | 7.25 | 10.9 | 2.7 | 0.29391 | 175.9 | 0.7 | 3.3258 |
| 38 | 1.75 | 7.75 | 11.6 | 2.1 | 0.24436 | 190.1 | 0.7 | 2.7945 |
| 39 | 1.75 | 8.25 | 12.4 | 1.6 | 0.19819 | 200.6 | 0.7 | 2.2475 |
| 40 | 1.75 | 8.75 | 13.1 | 1 | 0.13138 | 207.5 | 0.7 | 1.4528 |
| 41 | 1.75 | 9.25 | 13.9 | 0.6 | 0.08333 | 211.3 | 0.7 | 0.8875 |
| 42 | 1.75 | 9.75 | 14.6 | 0.3 | 0.04392 | 212.6 | 0.7 | 0.4465 |
| 43 | 1.75 | 10.3 | 15.4 | 0.1 | 0.01539 | 212.1 | 0.7 | 0.1485 |
| 44 | 1.75 | 10.8 | 16.1 | 0.1 | 0.01614 | 210.3 | 0.7 | 0.1473 |
| 45 | 2.25 | 5.25 | 13.0 | 0.1 | 0.01303 | 160.6 | 0.7 | 0.1124 |
| 46 | 2.25 | 5.75 | 14.3 | 0.8 | 0.11417 | 183.3 | 0.7 | 1.0269 |
| 47 | 2.25 | 6.25 | 15.5 | 2.4 | 0.37230 | 205.7 | 0.7 | 3.4559 |
| 48 | 2.25 | 6.75 | 16.8 | 2.6 | 0.43559 | 226.8 | 0.7 | 4.1278 |
| 49 | 2.25 | 7.25 | 18.0 | 2.2 | 0.39588 | 245.8 | 0.7 | 3.7865 |
| 50 | 2.25 | 7.75 | 19.2 | 1.9 | 0.36547 | 262.1 | 0.7 | 3.4866 |
| 51 | 2.25 | 8.25 | 20.5 | 1.5 | 0.30715 | 274.8 | 0.7 | 2.8860 |
| 52 | 2.25 | 8.75 | 21.7 | 1.2 | 0.26061 | 283.8 | 0.7 | 2.3845 |
| 53 | 2.25 | 9.25 | 23.0 | 0.8 | 0.18367 | 289.6 | 0.7 | 1.6221 |
| 54 | 2.25 | 9.75 | 24.2 | 0.3 | 0.07260 | 292.7 | 1.0 | 0.8782 |
| 55 | 2.25 | 10.3 | 25.4 | 0.1 | 0.02544 | 293.6 | 1.0 | 0.2936 |

| | | | | | | | | |
|---|---|---|---|---|---|---|---|---|
| 56 | 2.25 | 10.8 | 26.7 | 0.1 | 0.02668 | 292.7 | 1.0 | 0.2928 |
| 57 | 2.75 | 6.25 | 23.17 | 0.3 | 0.06952 | 287.6 | 0.7 | 0.6041 |
| 58 | 2.75 | 6.75 | 25.0 | 1.4 | 0.35037 | 301.0 | 1.0 | 4.2143 |
| 59 | 2.75 | 7.25 | 26.9 | 1.9 | 0.51073 | 330.2 | 1.0 | 6.2734 |
| 60 | 2.75 | 7.75 | 28.7 | 1.7 | 0.48849 | 347.5 | 1.0 | 5.9084 |
| 61 | 2.75 | 8.25 | 30.6 | 1.3 | 0.39765 | 361.5 | 1.0 | 4.7005 |
| 62 | 2.75 | 8.75 | 32.4 | 0.9 | 0.29198 | 372.1 | 1.0 | 3.3491 |
| 63 | 2.75 | 9.25 | 34.3 | 0.7 | 0.24007 | 379.4 | 1.0 | 2.6563 |
| 64 | 2.75 | 9.75 | 36.1 | 0.5 | 0.18075 | 383.9 | 1.0 | 1.9197 |
| 65 | 2.75 | 10.3 | 38.0 | 0.3 | 0.11401 | 385.8 | 1.0 | 1.1575 |
| 66 | 2.75 | 10.8 | 39.9 | 0.1 | 0.03986 | 385.4 | 1.0 | 0.3854 |
| 67 | 3.25 | 6.75 | 35.0 | 0.2 | 0.06991 | 410.2 | 1.0 | 0.8205 |
| 68 | 3.25 | 7.25 | 37.5 | 0.9 | 0.33790 | 431.5 | 1.0 | 3.8835 |
| 69 | 3.25 | 7.75 | 40.1 | 1.3 | 0.52173 | 449.3 | 1.0 | 5.8421 |
| 70 | 3.25 | 8.25 | 42.7 | 1.1 | 0.46995 | 463.4 | 1.0 | 5.0976 |
| 71 | 3.25 | 8.75 | 45.3 | 0.8 | 0.36249 | 473.5 | 1.0 | 3.7879 |
| 72 | 3.25 | 9.25 | 47.9 | 0.6 | 0.28741 | 479.8 | 1.0 | 2.8791 |
| 73 | 3.25 | 9.75 | 50.5 | 0.4 | 0.20196 | 482.8 | 1.0 | 1.9312 |
| 74 | 3.25 | 10.3 | 53.1 | 0.2 | 0.10616 | 482.6 | 1.0 | 0.9652 |
| 75 | 3.25 | 10.8 | 55.7 | 0.1 | 0.05567 | 479.5 | 1.0 | 0.4796 |
| 76 | 3.25 | 11.3 | 58.3 | 0.1 | 0.05826 | 473.9 | 1.0 | 0.4740 |
| 77 | 3.75 | 7.25 | 50.0 | 0.1 | 0.04998 | 552.4 | 1.0 | 0.5525 |
| 78 | 3.75 | 7.75 | 53.4 | 0.7 | 0.37402 | 570.7 | 1.0 | 3.9952 |
| 79 | 3.75 | 8.25 | 56.9 | 1 | 0.56879 | 582.9 | 1.0 | 5.8297 |
| 80 | 3.75 | 8.75 | 60.3 | 0.7 | 0.42228 | 589.1 | 1.0 | 4.1239 |
| 81 | 3.75 | 9.25 | 63.8 | 0.5 | 0.31887 | 589.8 | 1.0 | 2.9493 |
| 82 | 3.75 | 9.75 | 67.2 | 0.3 | 0.20166 | 585.8 | 1.0 | 1.7575 |
| 83 | 3.75 | 10.3 | 70.7 | 0.2 | 0.14134 | 577.7 | 1.0 | 1.1554 |
| 84 | 3.75 | 10.8 | 74.1 | 0.1 | 0.07412 | 566.1 | 1.0 | 0.5662 |
| 85 | 3.75 | 11.3 | 77.6 | 0.1 | 0.07756 | 551.9 | 1.0 | 0.5519 |
| 86 | 4.25 | 7.75 | 68.6 | 0.1 | 0.06863 | 714.2 | 1.0 | 0.7143 |

| | | | | | | | | |
|---|---|---|---|---|---|---|---|---|
| 87 | 4.25 | 8.25 | 73.1 | 0.5 | 0.36529 | 722.4 | 1.0 | 3.6123 |
| 88 | 4.25 | 8.75 | 77.5 | 0.7 | 0.54240 | 719.9 | 1.0 | 5.0395 |
| 89 | 4.25 | 9.25 | 81.9 | 0.5 | 0.40957 | 708.3 | 1.0 | 3.5418 |
| 90 | 4.25 | 9.75 | 86.3 | 0.3 | 0.25902 | 689.4 | 1.0 | 2.0684 |
| 91 | 4.25 | 10.3 | 90.8 | 0.1 | 0.09077 | 664.9 | 1.0 | 0.6650 |
| 92 | 4.25 | 10.8 | 95.2 | 0.1 | 0.09520 | 636.5 | 1.0 | 0.6366 |
| 93 | 4.75 | 8.25 | 91.3 | 0.1 | 0.09126 | 875.6 | 1.0 | 0.8756 |
| 94 | 4.75 | 8.75 | 96.8 | 0.3 | 0.29037 | 860.2 | 1.0 | 2.5806 |
| 95 | 4.75 | 9.25 | 102.3 | 0.4 | 0.40928 | 830.6 | 1.0 | 3.3226 |
| 96 | 4.75 | 9.75 | 107.9 | 0.3 | 0.32356 | 790.2 | 1.0 | 2.3708 |
| 97 | 4.75 | 10.3 | 113.4 | 0.1 | 0.11338 | 742.3 | 1.0 | 0.7424 |
| 98 | 4.75 | 10.8 | 118.9 | 0.1 | 0.11891 | 690.2 | 1.0 | 0.6903 |
| 99 | 5.25 | 9.25 | 125.0 | 0.2 | 0.24999 | 948.4 | 1.0 | 1.8969 |
| 100 | 5.25 | 9.75 | 131.8 | 0.3 | 0.39526 | 884.9 | 1.0 | 2.6547 |
| 101 | 5.25 | 10.3 | 138.5 | 0.1 | 0.13851 | 812.0 | 1.0 | 0.8121 |
| 102 | 5.75 | 9.75 | 158.0 | 0.1 | 0.15804 | 970.0 | 1.0 | 0.9700 |
| 103 | 5.75 | 10.3 | 166.1 | 0.1 | 0.16615 | 876.3 | 1.0 | 0.8763 |
| 104 | 6.25 | 10.3 | 196.3 | 0.1 | 0.19630 | 937.4 | 1.0 | 0.9375 |
| | | | Total %: | 99.3 | 18.0 | | | 179.5 |
| | | | | | Annual Power, kW/m | | | Mean Annual Power Capture, kW |